ICJ

THE INDIAN CONCRETE JOURNAL

Published by ACC Limited

ICJ Since 1927

Volume 95 • Number 6 • June 2021 • Pages 58 • ₹ 175

CONCRETE 3D PRINTED HOUSE

THE INDIAN CONCRETE JOURNAL

Volume 95 • Number 6 • June 2021 • Pages 58

ISSN (Digital) : 0019-4565

Founded in 1927

Published by ACC Limited, L.B. Shastri Road, Near Teen Haath Naka, Thane (West) 400 604.

This is a Scopus® indexed journal.

Cover image source:
Mr V. S. Adithya, Founder, Tvasta Manufacturing Solutions Pvt Ltd.

Cover

The cover-page carries a picture of a "Concrete 3D Printed House" constructed employing an automated manufacturing method used for constructing three-dimensional real-life structure at all realizable scales. The house was developed with catalytic funding support from Habitat for Humanity's Terwilliger Center for Innovation in Shelter and in collaboration with Indian Institute of Technology (IIT) Madras.

PART I : FEATURES

PART II : TECHNICAL PAPERS

CIRCULATION OFFICE: The Indian Concrete Journal, ACC Limited. L.B. Shastri Road, Near Teen Haath Naka, Next to Eternity Mall, Thane (West) 400 604, Maharashtra, INDIA.
Website: http://www.icjonline.com; e-mail: info@icjonline.com, editor@icjonline.com

Dear Colleagues,

The Indian Concrete Journal (ICJ) is pleased to issue its current edition to the readership. As the infrastructure projects around the world are developing continuously, the need for new innovative materials to satisfy the increasing demand is rising. Concrete, as the most versatile material used in structural applications, has been improved throughout the last decades with the help of different types of fibers, which not only enhance the mechanical properties of concrete, but also contribute to the global sustainability. In the current issue of the ICJ, five papers, which deal with novel developments in concrete industry and rehabilitation of bridges towards more resilient infrastructures, have been published.

The first article has proposed an alternative strategy for rehabilitation of box-girder bridge decks without long disruption of traffic, which is usually necessitated by conventional construction. The proposed technique of rehabilitation has relied upon strengthening the bridge deck with near surface mounted (NSM) fiber-reinforced polymer (FRP) strips as additional reinforcement on the overhang region of the bridge deck. The purpose for such strengthening was to enable the placement of sound/ noise barriers without extensive modification of the existing structure. The experimental test has simulated the load pattern from the addition of the sound barrier wall, and assessed the failure mode and the adequacy for carrying the additional loads. The findings have demonstrated that the capacity of the strengthened section was significantly higher than the demand. Furthermore, the achieved final failure was ductile rather than sudden/brittle, based on which the proposed technique for rehabilitation was found efficient and cost-effective. The second article has investigated on the performance of sintered fly ash lightweight aggregated concrete, whose findings resulted in the formulation of Indian Standard IS: 9142 (Part-2) 2018. The experimental program has dealt with the characterization of the investigated material (i.e., evaluation of micro-structural, mechanical, and durability properties) and its suitability for application in structures. The results have indicated the suitability of using fly ash lightweight aggregate in structural concrete, which is not prone to wearing. However, the study has highlighted the need for establishment of various more stringent structural design codal provisions as compared to those recommended for normal weight aggregate concrete members. The third article has presented a novel cavity wall panel system, using textile-reinforced concrete (TRC)-cold form steel, for fast-track construction, which is becoming the need of the day. Several advantages of the proposed panel were stated such as: easy erection on site, less labor demand, fast-track construction, better thermal/ acoustic insulation, and more strength-to-weight ratio as compared to conventional masonry walls. The developed system consisted of a pre-fabricated TRC skin material and a profiled cold form steel sheet as a core material, both connected together using self-tapping screws integrated within the system. The experimental results have demonstrated the possible potential of TRC, integrated with cold form steel sheets, for load-bearing applications, rather than the limitation to non-load-bearing applications, which was found in the past studies. The fourth article has reported details of study carried out to investigate the fracture energy of fiber-reinforced rubcrete made using steel/ polypropylene fibers with partial replacement of fine aggregate with crumb rubber. The experimental work included three-point bending tests on beam samples cast from four different concrete mixes with/ without fibers/ rubber. A notable improvement in ductility was observed with steel fiber-reinforced rubcrete, which makes it suitable for application in structures that require significant energy absorption. Furthermore, it was concluded that the use of fiber-reinforced rubcrete results in limiting the exploitation of fine aggregates, and thus helps to ensure responsible utilization of precious natural resources. The last article has discussed the combined effect of high fiber content and constant dosage of polymer on properties of so called polymer-modified fiber-reinforced high-strength concrete. The experimental work has resulted in a considerable improvement in compressive, flexural, and shear strength, as well as ductility and toughness of concrete owing to the synergistic effect of polymer and fiber.

Thus, we are glad to issue this edition of the ICJ dealing with innovative technologies that could benefit the concrete industry as well as infrastructure resilience. The topics covered in this edition are of a great significance and will be useful for structural engineers towards making more developments in construction technology. Thank you.

Vasant Matsagar
Editor-in-Chief

ICJ - EDITORIAL BOARD

We are pleased to announce the Editorial Team of the Indian Concrete Journal (ICJ). We thank our Editorial Team for graciously accepting our request to extend their exemplary support to accelerate our vision of enabling the construction value chain with information on the latest research and applications through the ICJ.

Congratulations to the winners!

To enrich the contribution and to honour the contributors of outstanding merit, the ICJ Best Paper Awards were launched starting 2020. All papers published from January to December 2020 were considered for this annual award. Applying the key criteria of novel concept and well-documented paper, of the 92 published papers, the top fifteen papers were shortlisted. These selected top fifteen papers were further evaluated by an independent jury panel consisting of three faculty members from academia with vast research experience and association with reputed international journals.

The jury panel carefully evaluated these shortlisted papers in categories such as : i) Numerical analysis ii) Experimental research iii) Experiments and model development and iv) Review papers.

We are pleased to share with you top three ICJ Best Paper Awards - 2020 winners:

1st

Authors




DAMAN K. PANESAR
University of Toronto, Canada

KARINA E. SETO
University of Toronto, Canada

CAMERON J. CHURCHILL
McMaster University, Canada

RUNXIAO ZHANG
University of Toronto, Canada

Title: **Life cycle assessment and environmental disturbance indicators to evaluate the sustainability of concrete mix designs**

Published in February 2020 edition.

Read full paper on our website: https://icjonline.com/award1

2nd

Authors


KOMATHI MURUGAN
Indian Institute of Technology (IIT) Madras, India

AMLAN K. SENGUPTA
Indian Institute of Technology (IIT) Madras, India

Title: **Performance of high-strength concrete as jacket material in strengthening applications**

Published in May 2020 edition.

Read full paper on our website: https://icjonline.com/award2

3rd

Authors




PREETHY MARY ARULANANDAM
National Institute of Technology (NIT) Puducherry, India

S. B. SINGH
Birla Institute of Technology and Science (BITS) Pilani, India

TOSHIYUKI KANAKUBO
University of Tsukuba, Japan

MADAPPA V. R. SIVASUBRAMANIAN
National Institute of Technology (NIT) Puducherry, India

Title : **Behavior of engineered cementitious composite structural elements – A review**

Published in June 2020 edition.

Read full paper on our website: https://icjonline.com/award3

We congratulate the winners and thank our jury panel who took time off their busy schedule to carefully evaluate each contribution and select the top three ICJ Best Papers - 2020. We also thank Dr Radhakrishna Pillai who has been instrumental in conceptualizing and instituting the ICJ Best Paper Awards.

We have made all these papers open access and available for our readers to read them online. Please visit our website to read these and many other open access papers.

RILEM UPDATE

The International Union of Laboratories and Experts in Construction Materials, Systems and Structures

New RILEM State-of-the-Art Report

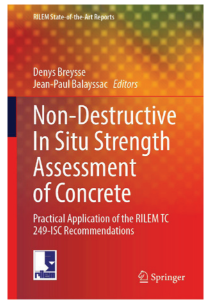

A new State-of-the-Art report is now available: *Non-destructive in situ strength assessment of concrete - Practical Application of the RILEM TC 249-ISC Recommendations*, Edited by Denys Breysse and Jean-Paul Balayssac. You can purchase the hardcopy or ebook on the Springer website: bit.ly/3xWV2cr. The unedited electronic version is available for FREE on the RILEM website: bit.ly/3erkXkK.

Online Doctoral Courses at the 75th RILEM Annual Week

The RILEM Educational Advisory Committee (EAC) has established 5 online doctoral courses to be given at the 75th RILEM Annual Week in September this year. These courses target those individuals currently enrolled in a doctoral program willing to enhance their training and knowledge on:

1) HYDRATION AND MICROSTRUCTURAL CHARACTERIZATION OF CEMENTITIOUS SYSTEMS
2) STEEL CORROSION; THEORY, PREVENTION, AND REPAIR
3) ULTRA-HIGH PERFORMANCE CONCRETE
4) ALKALI-ACTIVATED MATERIALS
5) DURABILITY OF REINFORCED CONCRETE.

Postdoc fellows and early-career researchers are also encouraged to attend. Learn more about lecturers, fees, and benefits of these courses here: http://rilemweek2021.uanl.mx/phd-courses/

NEW TCs

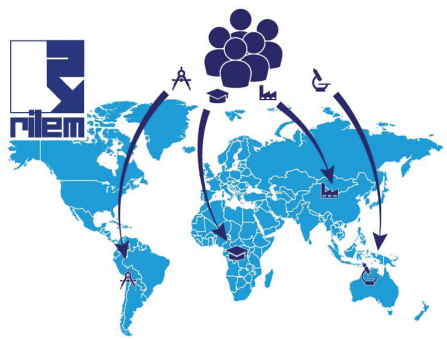

RILEM is proud to announce the establishment of 4 new Technical Committees (TCs) approved at the last RILEM Spring Convention in April:

- FEE-fume emissions evaluation for asphalt materials, Chaired by Johan BLOM
- PFC-performance requirements and testing of fresh printable cement-based materials, Chaired by Nicolas ROUSSEL
- ADC-assessment of additively manufactured concrete materials and structures, Chaired by Viktor MECHTCHERINE
- CNC-carbon-based nanomaterials for multifunctional cementitious matrices, Chaired by Florence SANCHEZ

More details about these TCs can be found here: bit.ly/2TAxUh4. If you are a RILEM member and you want to join these TCs, please send an email to assistant@rilem.org. Not a RILEM member yet? Please, consider to apply to become a RILEM member!

Report of the 4th RILEM Spring Convention

The report of the 4th RILEM Spring Convention and the 2021 RILEM Strategic Workshop is available online: www.rilem.net/news/445. The videos of the opening ceremony can be watched for free on our RILEM YouTube Channel: youtube.rilem.net.

STRENGTHENING OF BRIDGE-DECK OVERHANGS FOR SOUND WALL ADDITION USING NSM FRP COMPOSITES

ANNA PRIDMORE,
VISTASP M. KARBHARI*

Abstract

Increasing urban sprawl is resulting in buildings and inhabited areas being located closer to highways resulting in complaints regarding noise from traffic. Sound walls and noise barriers are often used to decrease noise. In the case of elevated bridges, the barriers have to be added to existing decks resulting in the need for substantial addition of overhang steel reinforcement to carry the additional load. In many cases related to older box-girder bridges, this either is not feasible structurally or requires substantial demolition of the existing structure with the consequent extensive disruption of traffic. The use of near surface mounted (NSM) fiber-reinforced composite (FRP) strips as additional reinforcement on the overhang region is shown to be an effective strategy enabling efficient and cost-effective rehabilitation of box-girder type bridge decks without extensive modification of the existing structure and much less disruption of traffic.

Keywords: Bridges, Fiber-reinforced composite, Near surface mounted, Noise barrier, Overhang, Strengthening, Sound walls.

1. INTRODUCTION

The increase in population and commerce in cities has resulted in increasing traffic. In the past, major roads carrying large amounts of traffic were away from residential areas as well as areas of business. However, urban sprawl and expansion through flyovers and elevated roadways has resulted in major highways and traffic routes carrying heavy traffic being situated in residential areas, next to schools, hospitals, and parks, causing significant disruption due to noise emanating from traffic. The noise is not only annoying but can result in other issues that affects the quality of life[1] and can also be the cause of issues that affect human wellness. Noise pollution from traffic increases as the volume of traffic increases and has become an aspect of significant concern globally resulting in it now being treated as an environmental issue of importance in planning. Increasingly, the level of noise and its effects are treated as important criteria in the placement of new roads and cities and have ordinances and policies associated with these.

However, there are many instances where roads already exist, and traffic volumes have increased substantially, or there are no reasonable options for placement in order to enable the effectiveness of commerce. In such cases, mechanisms to reduce the level and transmission of noise become extremely important. Ohiduzzaman *et al.*[2] have reviewed a range of techniques to reduce noise and hence these will not be repeated here. Among the more popular techniques is the placement of noise barriers or sound walls constructed along the roadway to mitigate noise from vehicles as well as from the interaction between tires and the road surfaces[3]. These are structural elements placed between the road/highway and the area that needs to be shielded from the noise with the goal of the barrier being to reduce the overall levels to between 7 dB and 10 dB at locations closest to the roadway[4] through both absorption of the noise by the barrier and reflecting it back onto the roadway itself. Sound waves can, however, carry over and around obstacles such as barriers and hence their viability can be constrained by distance[5]. Effective barriers are able to reduce the level of noise by as much as 50% with a barrier capable of effecting a 10 dB reduction reducing the sound level of a tractor-trailer to that of a car[6]. Aspects such as materials used in the barrier, its height, and details of placement all impact effectiveness[4,7]. A historical perspective of noise control on highways as well mechanisms for attenuation of its effect and various forms of barriers have been discussed by Ekici and Bougdah[8].

While noise attenuation mechanisms can be affected through changes in road surfacing and placement of walls/barriers/berms during the construction of new roads and highways, the modification of existing roadways continues to be a growing concern. In these cases the placement of sound/noise barriers can be complicated by issues such as space limitations and presence of K-rails, and in the case of elevated roadways, the lack of sufficient reinforcement in the existing overhang regions can cause further difficulties. As with a number of agencies, the California Department of Transportation has been retrofitting select roadways with sound barriers placing these on top of existing K-rails where necessary following their “memo to

*Corresponding author : Vistasp M. Karbhari, Email: vkarbhari@uta.edu

designers"[9]. Other similar guidelines are provided by Wassef *et al.*[10] and AASHTO[11]. Of special import is the rehabilitation of elevated roadways such as those on box-girder type bridges where the addition of sound walls on the overhang generally necessitates the addition of steel reinforcement to strengthen the overhang region primarily due to the substantial increase in dead-load on a narrow concentrated region at the extreme of the overhang in excess of the original design loads. The most common solution is to remove the entire edge region and rebuild it with additional reinforcement to accommodate the additional vertical and moment loading which results in an expensive and time-consuming process that also requires lane closures[12].

This paper investigates the use of near surface mounted (NSM) fiber-reinforced polymer (FRP) reinforcement as a means of rapidly and cost-effectively strengthening the existing overhang regions of box-girder type sections using the NSM FRP to provide the additional reinforcement without having to remove existing structural concrete or having to substantially delay traffic due to closures that might have been necessitated by conventional construction. Details related to the use of externally bonded FRP for strengthening of beams and slabs have been reported extensively in the literature and specifications were provided through a Transportation Research Board project[13, 14], and hence will not be repeated herein. Rather the focus is on experimental testing to show viability of use for rapid rehabilitation without necessitating extensive additional construction and lane closures, and to validate results of the design. In that vein, the assessment of load capacity, strain development, and failure modes are the primary focus of the research so as to assess the suitability of the technique for rapid and effective strengthening using near surface mounted FRP strips as an alternative to the extensive removal of existing concrete for the placement of additional steel reinforcement as would be done conventionally.

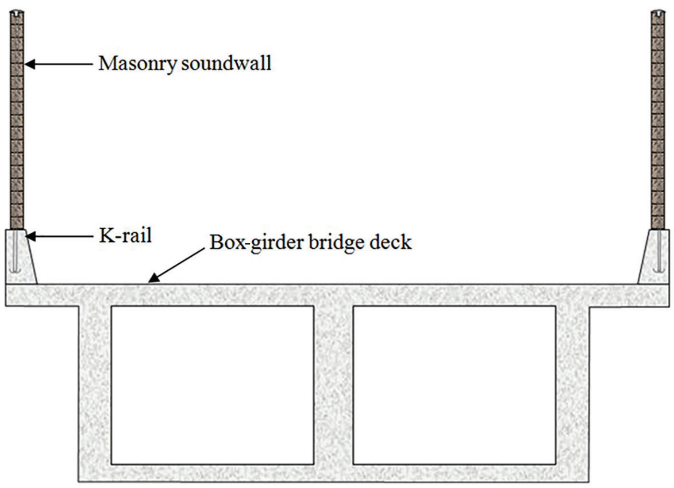

Figure 1(a): Schematic of sound wall placed onto the overhang of a box-girder bridge deck

2. SPECIMENS AND TEST CONFIGURATION

In order to replicate field conditions where the placement of sound walls would be difficult using conventional rehabilitation measures, the case of a sound wall as required by code in the case of placement on the overhang of an existing box-girder bridge section on top of the K-rail was considered[9]. This is shown schematically in Figure 1.

The overall test specimen was configured to be a reinforced concrete two-cell box-girder [as shown in sectional view in Figure 2(a)] with a center-to-center span of 1830 mm between each of the girders and a length of 3660 mm. The specimen deck is 178 mm thick and the distance from the stem wall to the edge of the overhang is 483 mm. The bottom slab was 152 mm thick and the widths of the outer and center girders were 254 mm and 305 mm, respectively. All steel reinforcements were implemented as per AASHTO-LRFD specifications[15]. The deck steel reinforcement consisted of a top and bottom layer of

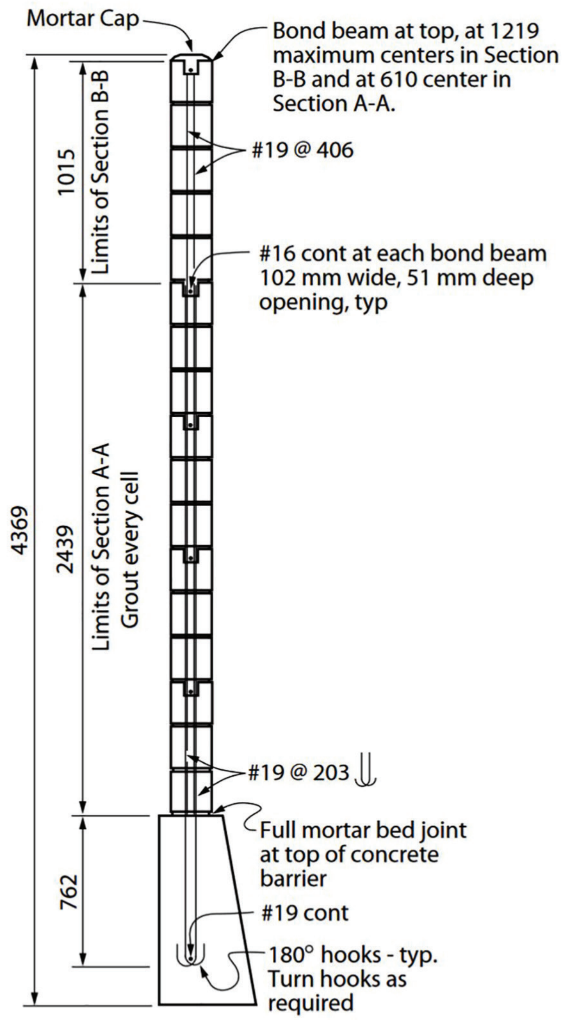

Figure 1(b): Details for the sound wall following Caltrans[9] (All dimensions are in mm. Note that #16 and #19 bars have nominal diameters of 15.875 mm and 19.05 mm, respectively)

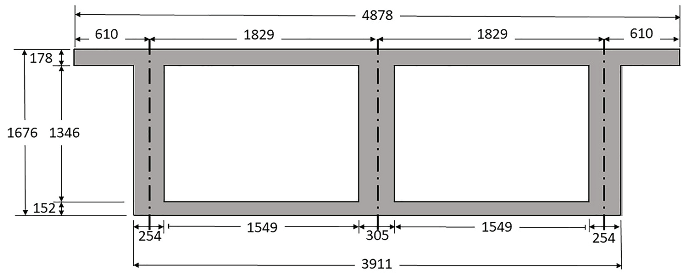

Figure 2(a): Cross-section of box-girder (all dimensions in mm)

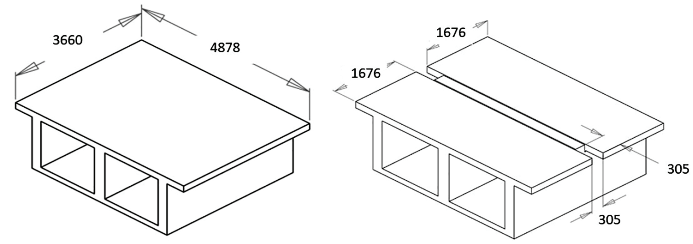

Figure 2(b): Schematic of deck specimen on left without cuts and on right with the central cut separating the specimen for two tests

15.9 mm diameter (#5) rebar with the transverse rebar spaced at 203 mm on center and variable spacing for the longitudinal rebar in order to accommodate the location of the girder stems. The remaining steel reinforcement consisted primarily of 15.9 mm diameter (#5) rebar for the bottom slab and the stem reinforcement, with two 22.2 mm diameter (#7) rebar at the bottom of each girder web and 9.5 mm diameter (#3) rebar used for shrinkage and temperature reinforcement in the longitudinal direction of the girder webs. Grade 60 steel was used for all the steel reinforcing bars. The specimen was constructed in two separate concrete pours with the initial pour for the bottom slab and the lower portion of the stems and the second pour for the deck slab and the upper portion of the stems using cement concrete with a nominal design compressive strength of f_c'= 34.5 MPa at 28 days and an average aggregate size of 12.7 mm. In order to enable two representative tests, i.e. the as-built and the rehabilitated tests, two 203 mm deep cuts located 305 mm (12 in) apart from each other were created that ran longitudinally along the entire width of the specimen as shown schematically in Figure 2(b). The two edge segments of the deck, bounded by the longitudinal cuts, were also removed so to allow for multiple independent loading on the edge slabs 1676 mm long. For purposes of comparison, two tests were conducted on adjacent sections of the test specimen, first in the as-built condition and then on the adjacent section, separated by the cuts, after placement of the NSM FRP strips to rehabilitate the specimen to meet the added demand from the sound wall.

The shear capacity of the existing overhang slab can be computed according to ACI 318[16] using both the general and the more detailed calculations. The general calculation given by Equation (1)

$$V_c = 2\sqrt{f_c'}b_w d \quad (1)$$

where

f_c' = concrete compressive strength (psi),

b_w = width of the concrete slab (in), and

d = distance from the extreme compression fiber to the centroid of the tension reinforcement (in).

results in a predicted capacity of 236 kN, which translates to an applied force of 118 kN per hydraulic jack, whereas the more detailed approach given by Equation (2)

$$V_c = \left(1.9\sqrt{f_c'} + 2500\rho_w \frac{V_u d}{M_u}\right) b_w d \quad (2)$$

where

ρ_w = steel reinforcement ratio of the slab in the direction perpendicular to traffic,

V_u = factored shear in the slab at the edge of the outer vertical stem, and

M_u = factored moment in the slab at the edge of the outer vertical stem.

results in the slightly more conservative result of 233 kN, for the slab, which translates to an applied force of 116 kN per hydraulic jack. The moment capacity of the slab was calculated as 97.0 kN-m using ACI 318[16] as

$$M_n = A_s f_y \left(d - \frac{a}{2}\right) \quad (3)$$

where

A_s = area of steel reinforcement in the direction perpendicular to traffic flow,

f_y = yield stress of the slab steel,

d = distance from the compression fiber to the centroid of the tension reinforcement, and

a = depth of the equivalent rectangular compression stress block.

A level of 117.2 kN-m is determined from a moment-curvature response calculation using RESPONSE[17], indicating that flexural failure would govern. Following Caltrans guidelines[9], the combined dead weight of a typical sound wall and traffic barrier used for bridges in California were determined to be 13.5 kN/m and 8.1 kN/m, respectively, for a combined weight per unit length of 21.6 kN/m. The resulting total load applied to the specimen from the sound wall and traffic barrier can be determined as the product of the weight per unit length (21.6 kN/m) and the length of the test specimen (1676 mm) to be 36.2 kN, of which only the traffic barrier can be sustained by the original design. The loads due to the addition of the sound wall would traditionally be addressed through removal of concrete and addition of new steel in the overhang region followed by recasting of concrete in the area of repair.

Using criteria from Caltrans guidelines [9], the additional load with a moment demand of 10.91 kN-m using the recommended factor of three for new methods translates to an additional demand of 32.7 kN-m which would need to be provided by the rehabilitation strategy. As reported in the next section, the experimentally determined moment capacity of the as-built reinforced concrete deck slab overhang prior to rehabilitation was found to be 110 kN-m. Therefore, the new moment capacity after strengthening should be at least 142.7 kN-m, which corresponds to a minimum required moment capacity increase of 29.7% over the capacity of the as-built specimen.

For the purposes of the current investigation, Sika Carbodur S512 strips were selected as the FRP reinforcement to be used in near surface mounted form for purpose of rehabilitation. The strips have a width of 50 mm, thickness of 1.2 mm, a tensile modulus of 165 GPa, and mean and design tensile strengths of 3100 MPa and 2800 MPa, respectively [18]. The quantity of additional reinforcement can be estimated through determination of the additional moment capacity required. The increased moment capacity due to FRP-strengthening can be taken to be the sum of the contribution from the tension steel (compression steel is ignored for this calculation) and the contribution from the FRP reinforcement as

$$M_{n\_strengthened} = A_s f_y \left(d - \frac{a}{2}\right) + \psi_f \; A_f f_{fe} \left(d_f - \frac{a}{2}\right) \qquad (4)$$

where

- A_s = total area of tension steel in slab overhang test specimen,
- f_y = experimentally determined yield strength of steel reinforcement,
- d = distance from extreme compression fiber to tension reinforcement,
- a = depth of concrete compression block, assuming rectangular stress distribution,
- Ψ_f = additional reduction factor from ACI 440 [19],
- d_f = distance from the compression fiber to the centroid of the FRP,
- f_{fe} = $E_f \cdot \varepsilon_{fe}$ effective stress in the FRP assuming elastic behavior,
- E_f = experimentally determined modulus of elasticity of FRP, and
- ε_{fe} = effective strain in FRP reinforcement.

A rearrangement of Equation (4) provides an expression for the area of FRP reinforcement required in order to achieve a specified moment capacity.

$$A_{f\_required} = \frac{M_{n\_strengthened} - A_s f_y \left(d - \frac{a}{2}\right)}{\psi_f \; f_{fe} \left(d_f - \frac{a}{2}\right)} \qquad (5)$$

Note that the area of FRP required is the total area needed for the specimen overhang and thus must be distributed along the width of the slab overhang.

Based on ACI 440 [19], as above, and manufacturer recommendations that center spacing of strips should be limited to no more than the lesser of 0.2 times the span length (*L*) or five times the slab thickness (*h*), the rehabilitation design consisted of 9 strips spaced at 203 mm centers with the strips extended past the point of inflection to achieve the necessary development length of 300 mm. Rectangular grooves were cut in the deck as shown in Figure 3(a) with a dimensional tolerance of 70-76 mm in width and 6-13 mm in depth of total length of 2.74 m [(Figure 3(b)]. The grooves were maintained at a concrete surface profile (CSP) of 3 as defined by the ICRI surface profile guidelines. A high-modulus and high strength structural epoxy paste, Sikadur 30, was used to bond the strips to the concrete. The tensile strength and elastic modulus of the cured adhesive were measured through tests to be 25.29 MPa and 6.93 GPa, respectively, with standard deviations of 2.54 MPa and 0.48 GPa, respectively. The installed strips with strain gauges attached to the surface are shown in Figure 3(c).

Vertical loads were applied to the edge region of the deck slab to simulate the load pattern from the addition of the sound wall using two hydraulic jacks spaced 1.83 apart and mounted below

Figure 3(a): Saw being used to cut grooves for placement of the FRP strips

Figure 3(b): Grooves prior to placement of adhesive and FRP strips

Figure 3(c): Specimen with strips installed in grooves with strain gauges

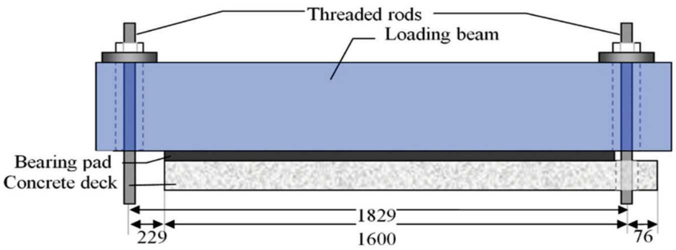

Figure 4(a): Schematic of loading beam at the edge of the deck overhang (all dimensions are in mm)

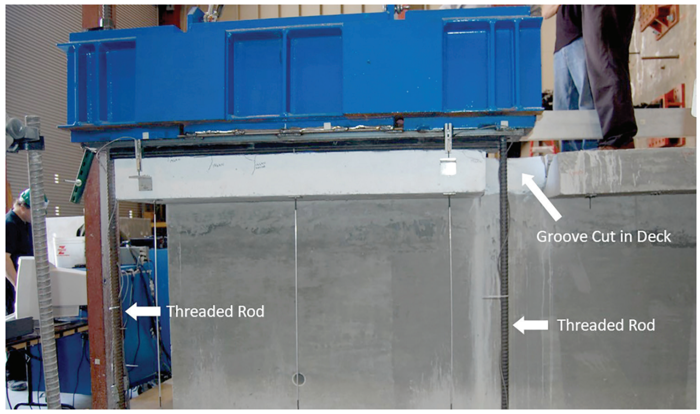

Figure 4(b): Side view of test specimen showing position of threaded rods in relation to the deck and specimen

Figure 4(c): Front view of test specimen showing the loading beam and linear potentiometers

Figure 4(d): Top view of test setup

the strong floor of the testing facility. The load was transferred through two 44.5 mm diameter threaded rods to a steel loading beam positioned 76 mm on-center back from the end of the overhang section of the deck. A 51 mm thick and 152 mm wide elastomeric bearing pad was placed between the steel beam and the deck slab in order to reduce stress concentrations and provide more even loading of the test specimen as shown schematically in Figure 4(a), as a side view in Figure 4(b) indicating placement of the threaded rods in relation to the deck and specimen, as a front view showing linear potentiometers in Figure 4(c), and with the overall test setup viewed from the top in Figure 4(d).

As seen in Figure 4(b), one of the threaded rods is set outside the deck specimen, whereas the second is inserted in the groove cut in the deck surface to separate the specimens. Instrumentation for purposes of measurement and monitoring consisted of linear potentiometers, load cells, and in the case of the FRP strips, strain gauges. 12 potentiometers were used to measure deflections of the slab as shown schematically in Figure 5(a). It is noted that the schematic represents the FRP-strengthened slab test section, but the configuration is a mirror image for the as-built test section. The deflection of the elastomeric bearing pad was measured using four linear potentiometers placed at each corner of the loading beam. Of

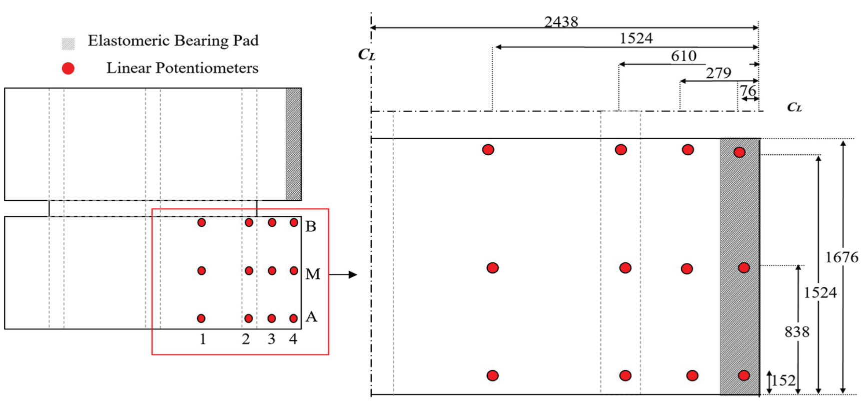

Figure 5(a): Schematic of positioning of linear potentiometers. The figure on the left is the plan view of the entire specimen and that on the right provides details on the deck section being tested. (all dimensions are in mm)

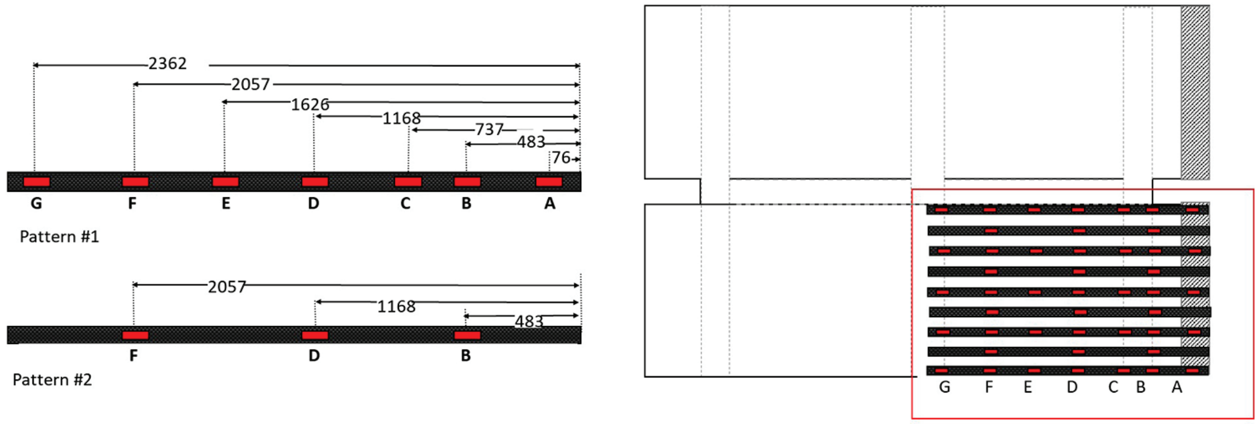

Figure 5(b): Strain gauge placement. Pattern and designation on the left and positioning on the deck at right (all dimensions are in mm)

Table 1: Loading protocol (steps 11-22 relate to the strengthened specimen only)

LOAD STEP	LOAD PER HYDRAULIC JACK (kN)	EQUIVALENT UNIFORMLY DISTRIBUTED LOAD (kN/m)	LOAD LEVEL DESCRIPTOR (WALL LOAD IS 21.6 kN/m AND LOAD LEVELS ARE INDICATED WHERE POSSIBLE AS APPROXIMATIONS OF MULTIPLES OF WALL LOADS AS DESCRIPTORS)
1	24	30	
2	36	45	~2 (Wall load)
3	48	60	
4	60	75	
5	72	90	~4 (Wall load)
6	84	105	
7	90	112.5	~5 (Wall load)
8	96	120	
9	102	126.3	Predicted moment capacity of as-built specimen
10	114	142.5	Ultimate capacity of as-built specimen
11	116	145	
12	130	162.5	
13	136	170	
14	142	177.5	~8 (Wall load)
15	148	185	
16	160	200	~9 (Wall load)
17	166	207.5	
18	172	215	
19	178	222.5	~10 (Wall load)
20	184	230	
21	190	237.5	
22	196	245	~11 (Wall load) Ultimate capacity of strengthened specimen

the 12 potentiometers, 9 were in contact with the top surface of the overhang [rows 1, 2, and 3 in Figure 5(a)] and 3 were in contact with the bottom surface of the overhang [row 4 in Figure 5(a)]. 47 strain gauges were applied to the top side of the FRP strips after they were bonded into the grooves cut in concrete. Two patterns were used as shown in Figure 5(b).

Load applied to the specimens was monotonically increased following the sequence shown in Table 1 with the load held briefly at each load level to enable observation of cracks and deterioration.

3. TEST RESULTS

An overall comparison of the load-deflection response of the two specimens is shown in Figures 6(a) and (b). The load reflects the level in each hydraulic jack and the deflection is as measured at center of the overhang. For purposes of comparison with theory, the vertical deflections of the deck slab overhang were predicted using a piecewise linear structural analysis that employs varying sectional properties throughout the system incorporating moment-curvature data from RESPONSE 2000 [17], with the moment profile for the deck slab being determined using RISA-2D [20]. The deck slab was modeled as a beam which was placed on three pinned supports located at the center of each vertical stem. The deck slab was sectioned into multiple pieces that maintain continuity throughout the member in order to allow different properties to be assigned to each piece. Moment values at different points along the deck slab were determined from the moment profile due to a downward vertical load applied to the end of the overhang region of the deck slab. The average moment acting within each section was determined and the moment of inertia value for each section was changed based on the input from moment-curvature data to determine the deflections of the deck slab overhang as loading was increased.

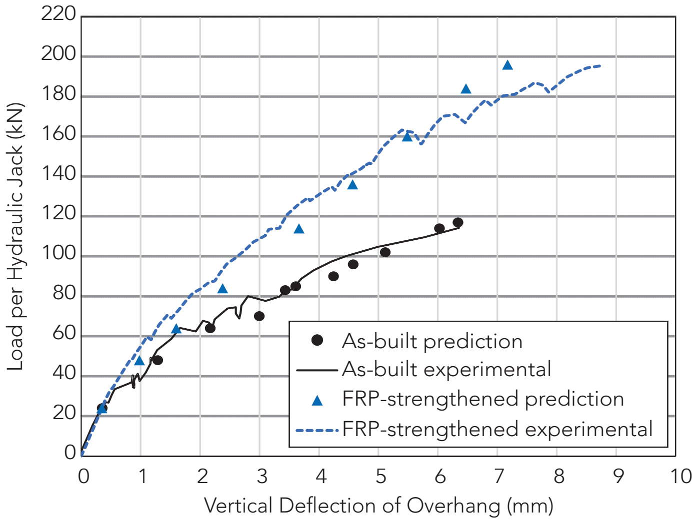

Figure 6(a): Comparison of load-deflection profiles

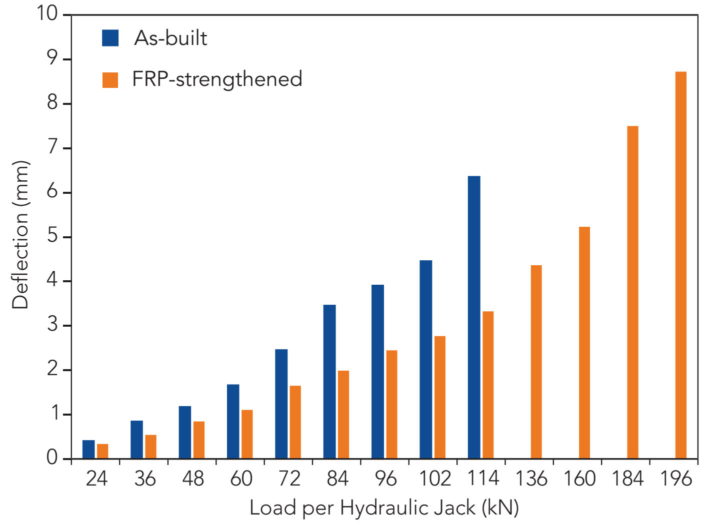

Figure 6(b): Comparison of deck overhang deflection at key load levels

For the unstrengthened specimen, the predicted moment capacity of 117.2 kN-m found via moment curvature analysis was within 6.5% of the actual moment applied, 110 kN-m, of the structure at the max loading of 114 kN per hydraulic jack. It is noted that the use of ACI 318 [16] results in a lower prediction of moment capacity of 97.0 kN-m. As seen in Figure 6(a), the predicted deflection values of the overhang compare well with the experimentally measured deflections through the loading range, with the predicted deflection of 6.03 mm at the ultimate load of 114 kN per jack being only 5.2% less than the experimentally measured value of 6.36 mm. In the case of the NSM FRP-strengthened specimen, predictions following ACI 440 and moment curvature analysis were 166 kN-m and 185 kN-m, which were within 12% and 2% of the experimental results, respectively. The predicted deflections for the overhang provide good correlation till a load of approximately 160 kN/jack. The over-prediction past this load is due to the assumption that full composite action is maintained for the section throughout the loading range, whereas experimentally, it was noted that there was a level of concrete cracking directly adjacent to the NSM FRP after this load level.

The ultimate capacity of the NSM FRP strip-rehabilitated slab was reached at an applied load of 196 kN, equivalent to a uniform distributed load of 245 kN/m. This ultimate capacity is 78% greater than that seen with the as-built specimen, which occurred at 114 kN per hydraulic jack, equivalent to a uniform distributed load of 142.5 kN/m. At the failure load level, the as-built specimen had a center deflection under the loading beam of 6.36 mm, whereas the FRP-rehabilitated specimen deflected approximately half that of the as-built specimen, 3.33 mm. The level of ultimate deflection of the unstrengthened specimen is reached by the NSM FRP-strengthened specimen at a load level of about 170 kN/jack which is about a 49% increase in equivalent capacity at that level. At ultimate capacity of the NSM FRP-rehabilitated specimen, the center deflection under the loaded beam was 8.73 mm, which indicates the rehabilitated specimen exhibited a 31.8% increase in deformation capacity over the as-built specimen with an increase in load of 72% per jack. In addition to increasing the overall load and deformation capacity of the system, the NSM FRP strips act to increase the stiffness and improve the stability of the system as can be seen from the increased stiffness and greater linear profile in Figure 6(a).

It is instructive to further compare the behavior of the individual specimens in terms of deflections and cracking. The ultimate capacity of the as-built specimen was reached at an applied load of 114 kN per hydraulic jack, equivalent to a uniform distributed load of 142.5 kN/m, which is 6.33x the nominal wall load. As the loading of the edge of the slab was increased, the top layer of transverse reinforcement above the outer edge of the stem yielded, followed by loss of aggregate interlock resulting in failure. Cracking was first observed on the top side of the overhang at the 84 kN load level per jack in the form of thin discontinuous cracks which approximately followed the two top longitudinal steel reinforcement bars adjacent to the edge of the stem wall, as shown in Figure 7(a), along with minor diagonal cracks along the exterior edge. Additional small cracks were observed with increasing load across the width of the specimen, till the load reached 114 kN per jack at which point a large diagonal crack opened and quickly propagated along the width of the overhang as seen in Figure 7(b). After the loading of the specimen was completed, loose concrete was removed in order to better observe the failure surfaces which are shown in Figures 7(c) and (d). Some yielding of the rebar in the areas of the crack was noted as well.

In comparison, the ultimate capacity of the NSM FRP-rehabilitated overhang was reached at an applied load of 196 kN per hydraulic jack, equivalent to a uniform distributed load of 245 kN/m. The first cracking observed in the as-built specimen occurred at the load level of 84 kN, whereas the first set cracking observed in the NSM FRP-rehabilitated specimen occurred at

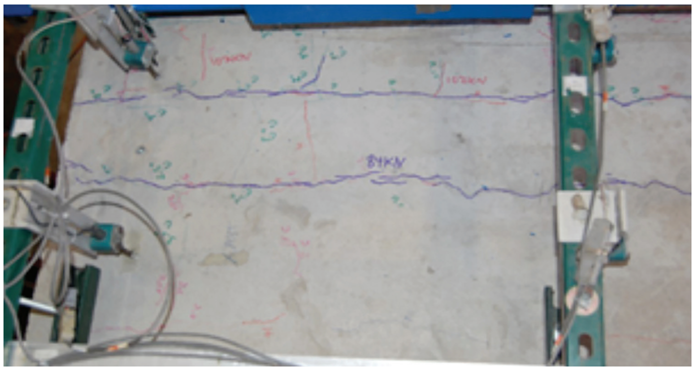

(a) Initial cracking along the longitudinal rebar

(c) Overhang edge prior to removal of loose concrete

(d) Overhang edge after removal of loose concrete

(b) Diagonal crack on edge going below concrete cover

Figure 7: Details of damage to overhang region

116 kN, which corresponds to a 38% greater load. A comparison of the deflection profiles along the center of the specimens at these loading levels, as shown in Figures 9(a) and (b), shows the clearly evident stiffening and strengthening effect of the NSM FRP strips.

At a level of 184 kN per jack, hair-line cracking was observed on the top of the overhang surface following the top longitudinal steel reinforcement bars. Minor diagonal cracks were noted along both the edges of the slab initiating from the top surface of the deck at this load level. At a load level of 196 kN per hydraulic jack, the ultimate tensile strength of the top concrete cover layer was exceeded and the bond between the FRP and the concrete was lost. This damage was quickly followed by the opening and propagation of a large diagonal crack along the strut formed, as shown in Figure 8(a), indicating attainment of ultimate capacity of the overhang for resisting vertical loads.

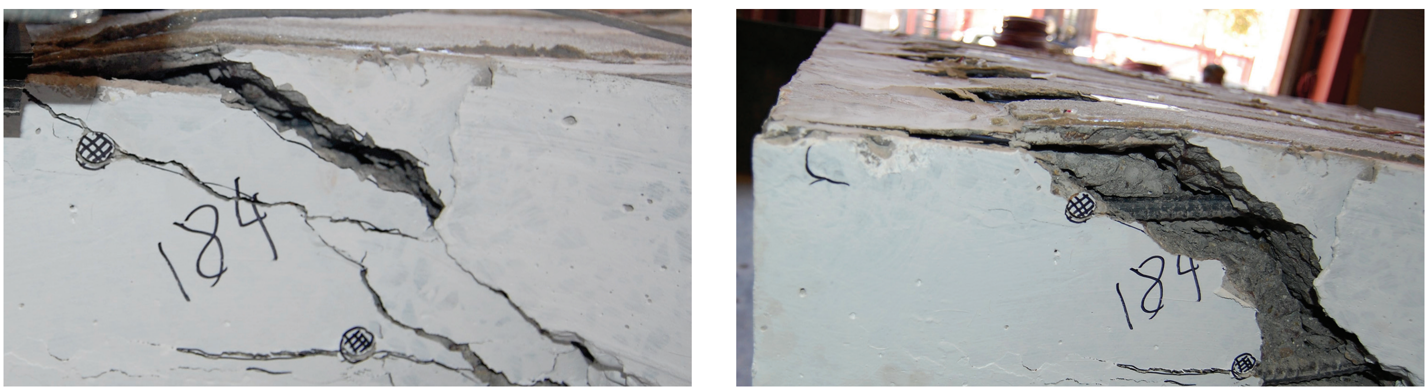

Figure 8: Damage at ultimate capacity showing concrete cracking and local debonding of the NSM FRP adhesive from the concrete in the right figure

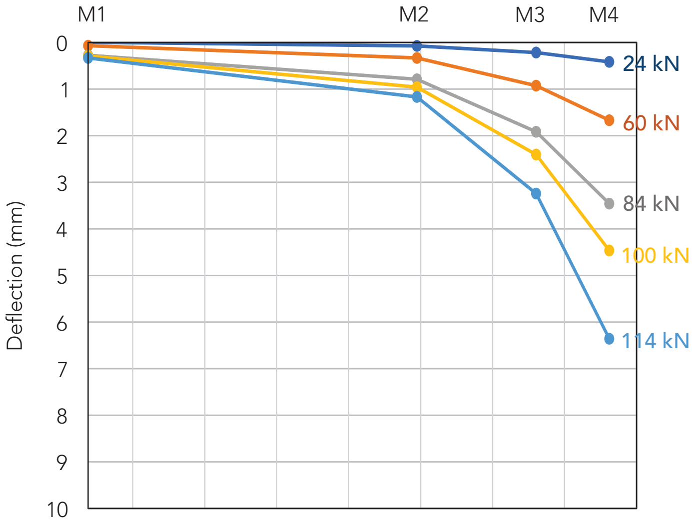

Figure 9(a): Deflection profile along center line of overhang [M-line in Figure 5(a)] in the unstrengthened state

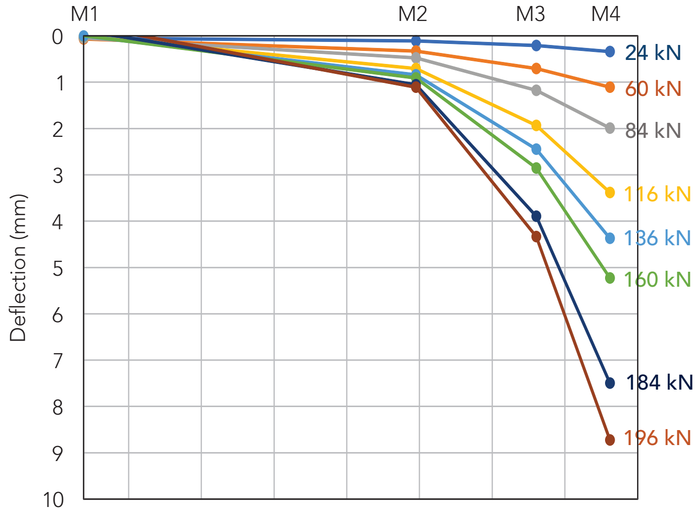

Figure 9(b): Deflection profile along center line of overhang [M-line in Figure 5(a)] in the NSM FRP-strengthened state

It is noteworthy that removal of loose concrete after testing showed that bond between the NSM FRP and concrete was largely maintained except in the area of diagonal cracking in the concrete [Figure 8(b)] in a manner similar to that of the as-built specimen but at a significantly higher load due to the strengthening action of the NSM FRP strips. The maximum strain value recorded in the CFRP strips at ultimate capacity was 3846 microstrain indicating that the FRP itself was not close to rupture.

It is of interest to compare deflection profiles as measured by the linear potentiometers between the as-built and strengthened specimens. Figures 9(a) and (b) compare profiles along the center line of the specimen denoted by line M in the layout in Figure 5(a), while Figures 10(a) and (b) compare profiles along line A in the layout in Figure 5(a) which is adjacent to an outer edge of the specimen.

It should be noted that position 2 [see Figure 5(a)] represents a location above the outer stem of the box-girder and therefore represents the end of the overhang. In all cases, it is seen that there is virtually no discernable deflection past this point. In both cases (center line and edge), the addition of the NSM FRP strips results in a decrease in deflection at comparable loads as measured by the two potentiometers closest to the overhang edge [points 3 and 4 in Figure 5(a)] with the deflections in the strengthened case as shown in Figure 10(b), as an example being between 68% and 78% of those in the unstrengthened case in Figure 10(a). The effectiveness of the NSM FRP strips is further highlighted by the fact that the deflection away from the edge is lower in the strengthened case even at the higher load levels.

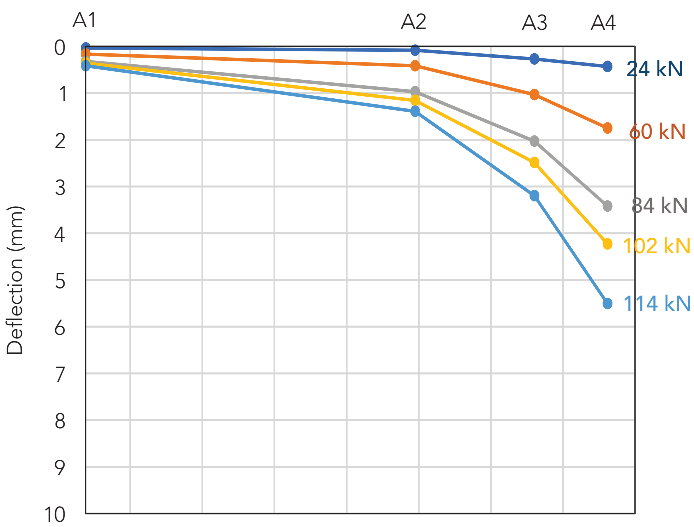

Figure 10(a): Deflection profile along a line of linear potentiometers adjacent to the edge of the unstrengthened test specimen

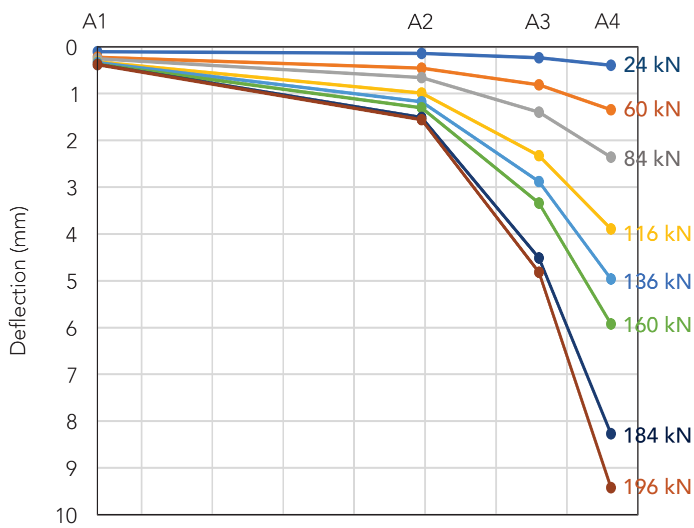

Figure 10(b): Deflection profile along a line of linear potentiometers adjacent to the edge of the test specimen in the NSM FRP-strengthened state

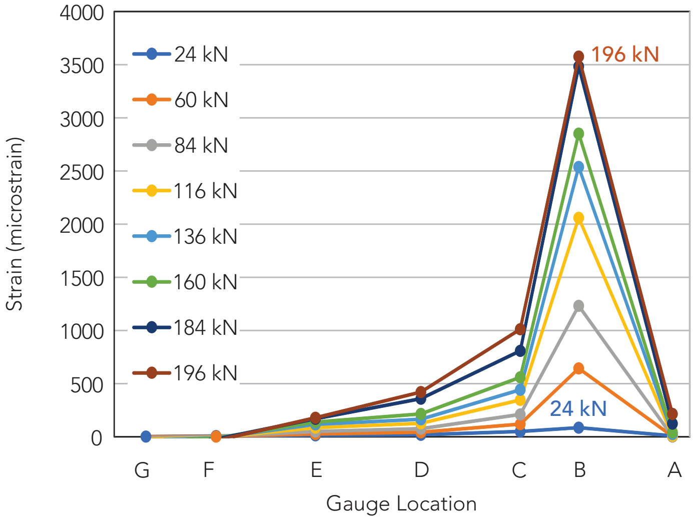

Figure 11: Strain profile along the central FRP strip. Location A is closest to the edge as shown in Figure 5(b)

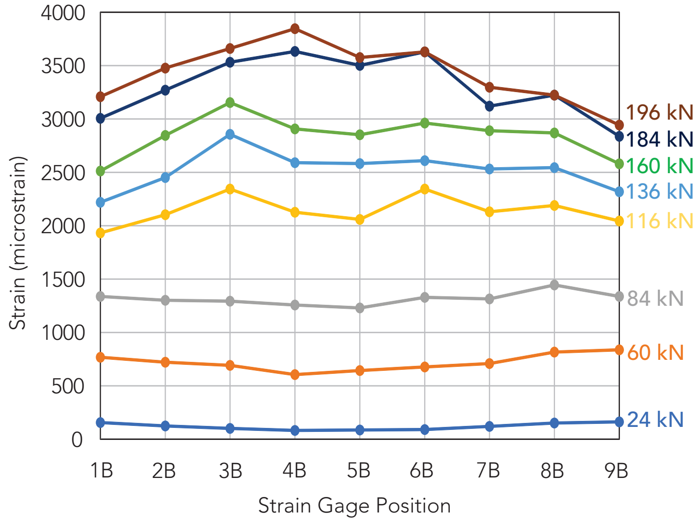

Figure 12: Strain along line B (483 mm from the edge of the overhang)

This can be further elucidated through the strain measurements from the NSM FRP strips. Figure 11 shows strain development along the central NSM FRP strip at the same load levels as in Figure 9(b). These strain profiles indicate that the maximum strain in the FRP strips occurs directly above the edge of the stem wall adjacent to the deck slab overhang, referenced as location "B" in the figure [details of location are shown in Figure 5(b)]. At ultimate capacity, the maximum strain measured across all strips was 3846 microstrain at a location along this line. The strains are noted to drop off sharply for distances further away from the end of the overhang, with the majority of the strain gages on the inner side of the stem wall (location "C") exhibiting less than a third of the strain values shown at location "B". The sharp drop in strain values at distances away from the stem wall and the minimal strains further away indicate that significantly shorter lengths of FRP strips could have been used to optimize material usage and improve constructability without affecting load transfer and overall system response.

Details for strain development along line B, the location where the maximum strains occur in the specimen, are shown in Figure 12, wherein it can be seen that the distribution of strains was even along the specimen until a load level of 116 kN per jack was reached. At this level, cracking was first observed in the specimen and higher loading levels resulted in less uniform strains along the specimen, as a result of local cracking and redistribution. The average strain along line B in the specimen at ultimate capacity was 3423 microstrain, whereas the minimum and maximum strains along line B were 2943 microstrain and 3846 microstrain, respectively. Using the strain data throughout the specimen and following the procedure described by Siem *et al.* [21], the shear stress between the concrete and the CFRP strips was determined to be 1.75 MPa in comparison to a listed shear strength of 24.8 MPa [22] again indicating the effectiveness of the NSM FRP and its ability to ensure a non-brittle failure.

4. SUMMARY AND CONCLUSIONS

The use of NSM FRP strips is seen to more than adequately strengthen the deck overhang to enable the addition of the sound barrier without premature failure. Failure was seen to be non-catastrophic within the concrete and at levels of moment capacity higher than required. The NSM FRP-rehabilitated specimen reached ultimate capacity under an applied load of 196 kN per hydraulic jack which is equivalent to an applied moment of 189.2 kN-m. This corresponds to a 72% increase in ultimate capacity over the as-built unstrengthened specimen, which failed under an applied load of 114 kN corresponding to an applied moment of 110.0 kN-m. In comparison with the unstrengthened specimen which showed significant drop in stiffness at the higher load levels after initial cracking, the NSM FRP-strengthened specimen showed better resilience and a progressive mode of failure based on separation of isolated individual strips within the concrete/adhesive. No fracture of the FRP strips themselves was seen.

The tests clearly show the viability of strengthening deck overhangs to allow for placement of additional weight on the edge such as would be required by sound/noise walls placed at the very edge of the overhang region due to space considerations. The ability to conduct rapid strengthening through the use of NSM FRP strips bonded to the concrete as an alternative to substantial removal of concrete and placement of additional reinforcing steel which would not require significant traffic disruption and time intensive construction is a major advantage. Since the FRP strips are prefabricated in long lengths which can easily be cut to size on site and then bonded into easily cut grooves with adhesives already used in the construction industry, the risk of the newer technique is extremely low since no special equipment or methods are needed. Rapid cure of the adhesive also results in faster opening of the rehabilitated structure to traffic. The test program validated both the concept and the design methodology and demonstrated that the failure levels are significantly higher than the capacities needed, and that final failure is staged rather than catastrophic.

ACKNOWLEDGEMENTS

Partial funding for the research was provided by the California Department of Transportation with Dr. Charles Sikorsky serving as the program manager.

REFERENCES

[1] Federal Highway Administration (FHWA), "*Highway traffic noise*: *Analysis and abatement guidance*", Report No. FHWA-HEP-10-025; US DOT: Washington, DC, USA, 2011.

[2] Ohiduzzaman, M., Sirin, O., Kassem, E., and Rochat, J. L. "State-of-the-art review on sustainable design and construction of quieter pavements–Part 1: traffic noise measurement and abatement techniques", *Sustainability,* 2016, *8*, Article # 742., 28 pp.

[3] Halim, H., Yusob, M. F. M., Abdullah, R., Nor, M. J. M., Rahman, N. A., Sukor, N. S. A., and Haron, Z. "Noise barrier as an option to reduce road traffic noise from highways in Klang valley, Malaysia", *AIP Conference Proceedings,* 2018, 2030, p. 020276.

[4] Bowlby, W., Pratt, G., Williamson, R., Knauer, H., and Kaliski, K. "*Noise barrier acceptance criteria*: *Analysis*", FHWA Publication No. FHWA-HEP-16-017; Federal Highway Administration, US Department of Transportation: Washington, DC, USA, 2016.

[5] Manuel, J. *"Clamoring for quiet*: *New ways to mitigate noise"*, Environmental Health Perspectives, 2005, 113(1), A46-A49.

[6] Brown, V. "*Survey of traffic noise reduction products, materials and technologies*", Final Report to Arizona DOT, 2008, 88 pp.

[7] Fleming, G. G., Volpe, J. A., Armstrong, R. E., Stusnick, E., Polack, K. D., and Lindeman, W. "*Transportation-related noise in the United States*", Transportation Research Board, 2000, A3B05, 9 pp.

[8] Ekici, I. and Bougdah, H. *"A review of research on environmental noise barriers", Building Acoustics*, 2003, 10, pp. 289 - 323.

[9] California Department of Transportation, "*Memo to designers*: 22-1. *Soundwall design criteria*", 2004, Sacramento, CA.

[10] Wassef, W. G., Kulicki, J. M., Withiam, J. L., Voytko, E. P., and Mertz, D. M. "*Application of AASHTO LRFD specifications to design of sound barriers*", Report for NCHRP Project 20-07, Task 270, National Cooperative Highway Research Program, 2010.

[11] AASHTO, "*Design of sound barriers, section* 15, *AASHTO LRFD bridge design specifications*", 8th Edition, 2017.

[12] California Department of Transportation, "*Response of reinforced concrete bridge deck overhang strengthened with near surface mounted CFRP*", Research Notes, The Earthquake Engineering Group, March 2009, 2 pp.

[13] Mirmiran, A., Shahawy, M., Nanni, A., and Karbhari, V. M., "*Bonded repair and retrofit of concrete structures using FRP composites*: *Recommended construction specifications and process control manual*", NCHRP 514, Transportation Research Board of the National Academies, 2004.

[14] Mirmiran, A., Shahawy, M., Nanni, A., Karbhari, V. M., Yalim, B., and Kalayci, A. S. "*Recommended construction specifications and process control manual for repair and retrofit of concrete structures using bonded FRP composites*", NCHRP 609, Transportation Research Board of the National Academies, 2008.

[15] American Association of State Highway and Transportation Officials, "*AASHTO LRFD bridge construction specifications*", 2nd ed. 2004, Washington, D.C.: American Association of State Highway and Transportation Officials.

[16] ACI Committee 318, "*Building code requirements for structural concrete and commentary*", American Concrete Institute, Farmington Hills, MI, USA.

[17] University of Toronto, RESPONSE 2000, "Moment-Curvature Program", http://www.ecf.utoronto.ca/~bentz/r2k.htm

[18] Sika Corporation, SIKA CarboDur S Data Sheet. https://usa.sika.com/content/dam/dms/us01/0/sika_carbodur_s.pdf

[19] ACI Committee 440, "*Guide for the design and construction of externally bonded FRP systems for strengthening concrete structures*", American Concrete Institute, MI, USA.

[20] Bates, B. R., RISA-2D, Risa Technologies.

[21] Seim, W., Vasquez, A., Karbhari, V. M., and Seible, F., "*Poststrengthening of concrete slabs*: *Full-scale testing and design recommendations*", *Journal of Structural Engineering*, 2003, 129(6), pp. 743-752.

[22] Sika Corporation, Sikadur 30 Product Data Sheet, https://www.sika-distributor.com/pdf/sikadur30/pds-cpd-Sikadur30-us.pdf

ANNA PRIDMORE is the Vice President for Strategic Market Development at Structural Technologies. She received her Ph.D. Degree in Structural Engineering from the University of California, San Diego, USA. She chairs and serves on numerous committees for AWWA, ASME, and ASTM related to the use of FRP for the upgrade of pipelines and other civil structures. Among other aspects, she specializes in asset management program support for nuclear power plants and municipal water/wastewater agencies.
Email: apridmore@structuraltec.com

VISTASP M. KARBHARI is a Professor in the Departments of Civil Engineering, and Mechanical & Aerospace Engineering at the University of Texas at Arlington, USA. His research interests include: the processing and mechanics of composite materials, infrastructure renewal and multi-threat mitigation, structural health monitoring, and deterioration science of polymers and composites. He is a fellow of the American Society of Civil Engineers, the Structural Engineering Institute, ASM International, the International Society for the Structural Health Monitoring of Intelligent Infrastructure, and the National Academy of Inventors, and is an elected member of the European Academy of Science and Arts.
Email: vkarbhari@uta.edu

Cite this article: Pridmore, A., Karbhari, V. M. (2021). "Strengthening of bridge-deck overhangs for sound wall addition using NSM FRP composites", *The Indian Concrete Journal*, Vol. 95, No. 6, pp. 8-19.

SINTERED FLY ASH LIGHTWEIGHT AGGREGATE - ITS PROPERTIES AND PERFORMANCE IN STRUCTURAL CONCRETE

P. N. OJHA,
BRIJESH SINGH*,
ASHOK KUMAR BEHERA

Abstract

The paper presents study conducted on sintered fly ash coarse aggregate produced indigenously. The sintered fly ash coarse aggregate [Low Density Aggregate (LDA) / Lightweight Aggregate (LWA)] is lower in density in comparison to normal weight aggregate. In the current study, class F fly ash has been used. The two fractions of sintered fly ash coarse aggregates (8-16 mm and 4-8 mm) were evaluated. Experimental programme evaluated the micro-structural, physical and chemical properties of sintered fly ash coarse aggregates for its suitability in making concrete for masonry units, hollow and solid lightweight concrete blocks, and structural lightweight concrete (SLC) for non-wearing surfaces. The paper also presents the experimental study on suitability of sintered fly ash lightweight aggregate in structural concrete. Concrete with sintered fly ash aggregate has been made at two water-cement ratios (0.55 and 0.45). The various mechanical properties such as compressive strength, flexural strength, split tensile strength, drying shrinkage, modulus of elasticity, and Poisson's ratio have been determined. The durability properties has also been investigated conducting rapid chloride ion penetration test (RCPT), electrical resistivity, chloride migration test, water permeability, and sorptivity (absorption) index. The mechanical and durability properties of LWAC have been compared with corresponding test results of normal weight aggregate concrete (NWAC) at same water-cement ratio of 0.55 and 0.45. The finding of the study has been useful for formulation of a new Indian Standard for production of structural lightweight concrete (SLC) using sintered fly ash lightweight coarse aggregate.

Keywords: Durability, Lightweight aggregate concrete (LWAC), Mechanical property, Normal weight aggregate concrete (NWAC), Structural lightweight concrete (SLC).

1. INTRODUCTION

1.1 General

Earlier lightweight aggregates (LWAs) were of natural origin, mostly volcanic origin like pumice and scoria by mechanical treatment [1]. As large quantities of the fly ash remain unutilized in most countries of the world, the manufacture of good quality lightweight fly ash aggregates seems to be an appropriate step to utilize a large quantity of fly ash and also yield significant environmental benefits. The Indian coal is of low grade having high ash content of the order of 30-45% producing large quantity of fly ash at coal/lignite-based thermal power stations in the country. The fly ash generation during 2018-19 is 217.04 million tonne due to combustion of 667.43 million tonne of coal/lignite, and fly ash utilization is around 168.40 million tonne which suggests an effective usage of 77.59%. Fly ash used in the study was taken from silo of super thermal power plant. Class F contains CaO of less than 8-10% and mostly contributes in pozzolanic reaction during hydration process. The official figures published by the Central Electricity Authority (CEA) in the annual

Table 1: Fly ash consumption in India as per Central Electricity Authority (CEA)

YEAR / DESCRIPTION	2014-15	2015-16	2016-17	2017-18	2018-19
Number of thermal power stations	145.00	151.00	155.00	167.00	195.00
Coal consumed (million tons)	549.72	536.64	536.40	624.88	667.43
Fly ash generation (million tons)	184.14	176.74	169.25	196.44	217.04
Fly ash utilization (million tons)	102.54	107.77	107.10	131.87	168.40
% Utilization	55.69	60.97	63.28	67.13	77.59

*Corresponding author : Brijesh Singh, Email: brijeshsehwagiitr96@gmail.com

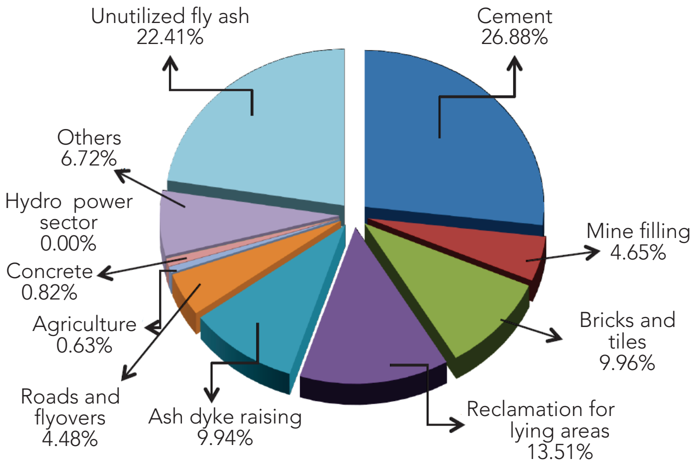

Figure 1: Major modes of fly ash utilization during the year 2018-19 (CEA annual report 2018-2019)

report of 2018-19 regarding fly ash consumption in India is given in Table 1. Some figures outlining the actual sector wise usage has been mentioned in Figure 1.

1.2 Production Process of Sintered Fly Ash Aggregate

Past studies [2-3] have already been conducted on the manufacturing processes of artificial lightweight aggregates from fly ash. Agglomeration techniques and hardening methods have been well researched. A division is made according to the method of hardening: sintering, autoclaving, or cold bonding. It is concluded that the bond between the fly ash particles in general diminishes; this effect, however, can be compensated by improving the degree of compaction of aggregates. The production process of sintered fly ash aggregate can be divided into four stages given below (Figure 2).

Raw material handling: The detail of raw mix used for production of sintered fly ash aggregate is 1-1.5% bentonite, 7-8% coal, and remaining class F fly ash. About 20-30% water is also mixed as binding agent during the production process. Fly ash, bottom ash, and grinded coal with binder are fed to continuous mixers. Fluidizing and blending in silos are required

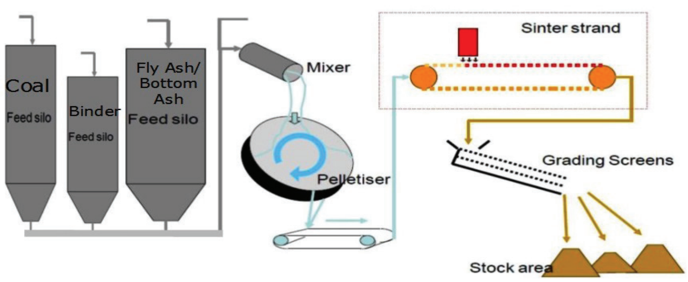

Figure 2: Schematic flow diagram for production of sintered fly ash aggregate

for homogeneous mixing. The dosage of binding agent is more important for making fly ash balls and the optimum range was found to be around 20% to 25% by the total weight of binders. Initially, some percentage of water is added in the binder as binding agent, and then poured in a disc; remaining water is sprayed during the rotating period because while rotating without water in the disc, the fly ash powder tends to form lumps and does not increase the distribution of particle size. The pellets were formed approximately in a duration of 20 min.

Pelletization: Some of the parameters, which need to be considered for the efficiency of production of pellet, include speed of revolution of pelletizer disc, moisture content, angle of pelletizer disc, and duration of pelletization. In this process, the wet mix is fed to pelletizers. Pelletizers make green pellets of various sizes. The disc pelletizer size is 570 mm diameter and side depth of the disc of 250 mm. It is fixed in a flexible frame with adjusting the angle of the disc as 35° to 55°, and to control for the rotate disc in vertical manner, speed should be varied as 35 to 55 rpm. The pellets were formed by agglomeration. The size of pellets is regulated with tilt and speed of the pelletizers. The green pellets were carried over conveyors for feeding to sinter strand.

Sintering: The sinter strand has three sections; a) firing section, b) sintering or soaking section, and c) cooling section. Green pellets were spread over the moving sintering strand. The pellets travel to firing zone with temperature range of 1100 to 1300 degree centigrade. The sintering happens in intermediary stage of sinter strand, and on the later part, they cool naturally. The burning of the carbon in the pellets and loss of moisture create a cellular structure bonded together by the fusion of fine ash particles.

Finish product handling: The cooled down pellets were passed through breaker to detach fused aggregates. The aggregates were then collected in different storage silos as per size, ready for onward dispatch to finish product yard. The particles formed were rounded in shape and range in size from 2 mm to 16 mm down to fines. These sintered aggregates were subsequently screened as per required sizes and were ready for use as per the requirement.

1.3 Properties of Sintered Fly Ash Aggregate

Research has already been done in past to evaluate engineering properties such as crushing strength, specific gravity, water absorption, particle size distribution, surface characteristics, and shear strength properties for the fly ash aggregates produced from fly ash and cement mixing by pelletization method. The experimental study showed that these aggregates were good alternative for wide range of civil engineering applications [4-8]. Internationally, ACI 213R-03 [9] and ASTM C 330 [10] are widely used as two standards for the use of lightweight aggregate (LWA) in

SLC. As per ACI 211.2-91 [11], the weight method can be used for proportioning the concrete with lightweight coarse aggregate and normal weight fine aggregate, whereas volumetric method can be used for concrete with all lightweight as well as combination of lightweight and normal weight aggregates. Grading of aggregate plays an important role because, if all the particles of an aggregate were of uniform size, the compacted mass will contain more voids and it will affect the strength of the concrete. In general, the aggregate should be well graded so that it can produce better bond. The size distribution of LWA shall confirm to Table 1 of ASTM C 330. As per ACI 213R-03, the practical range of relative densities of lightweight aggregate varies from almost ⅓ to ⅔ that of normal weight aggregate. As per ASTM C 330 and ASTM C 331 [12], the maximum dry loose bulk density of the lightweight coarse aggregate is 880 Kg/m^3. LWA generally absorb from 5 to 25% by mass of dry aggregate, depending on the aggregate pore system. Neville [13] indicated that water absorption of good quality lightweight aggregate for use in structural concrete usually should not be more than 15%. Sintered fly ash lightweight aggregates have shown water absorption in the range of 13-14% according to Swamy and Lambert [14] and Teychene [15]. The rate of absorption in lightweight aggregates is a factor that has a bearing on mix proportioning, handling, and control of concrete, and depends on the aggregate pore characteristics. The maximum loss on ignition of lightweight aggregate is 5% as per ASTM C 330 and ASTM C 331.

1.4 Properties of Structural Lightweight Concrete (SLC)

The lightweight concrete have been proving more advantages than normal weight in terms of structural load-bearing, as acoustic, thermal insulation, and less cost for transportation and building as the dead load from superstructure was decreased [16-17]. As per ASTM C 330, the conformity of concrete to SLC is evaluated on the basis of combined property of density, compressive strength, and split tensile strength. From the same batch of concrete, one or more of the compressive strength and split tensile strength requirements need to be satisfied without exceeding the corresponding maximum density values which is given in Table 2.

As per ACI 318 [18] code, flexural strength, $f_{cr} = \lambda\, 0.55 \sqrt{f_{ck}}\ (\mathrm{N/mm^2})$ where λ is the modification factor for lightweight concrete and equals 1.0 for normal weight concrete, 0.85 for sand-lightweight concrete, and 0.75 for all lightweight concrete. It indicates that in case of concrete made with normal weight sand and lightweight coarse aggregate, flexural strength value is 15% less than the concrete made with normal weight aggregate. In case of concrete made with all lightweight aggregates, the flexural strength value is 25% less than the concrete made with normal weight aggregate. Faust *et al.* [19] observed that ascending branch of stress-strain curve is comparatively linear in case of lightweight aggregate concrete in comparison with normal weight aggregate. They have also observed lower elastic modulus and less ductility in the post-cracking failure region. As per ACI 213R-03, generally, the modulus of elasticity for lightweight concrete varies between ½ to ¾ that of normal weight concrete of the same strength. As per ACI 213R-03, Poisson's ratio determined by static method for lightweight and normal weight concrete varies between 0.15 and 0.25 and averaged 0.2. As per ASTM C 330, the drying shrinkage of concrete specimens shall not exceed 0.07%. In India, IS: 9142 [20] refers to Specification for Artificial Lightweight Aggregates for Concrete Masonry Units and IS: 2185 (Part-II) refers to production of hollow and solid lightweight concrete blocks. In view of the above, an attempt has been made in the present work to develop a concrete with partial replacement of aggregates by sintered fly ash aggregates. The investigation covers various mechanical and durability properties of lightweight aggregate concrete (LWAC). The mechanical and durability properties of LWAC were compared with corresponding test results of normal weight aggregate concrete (NWAC) at same water-cement ratio of 0.55 and 0.45.

Table 2: Density, compressive strength, and split tensile strength of structural lightweight concrete (SLC)

SL. NO.	AVERAGE AIR DRY 28-DAY DENSITY, MAX (kg/m^3)	AVERAGE 28-DAY SPLIT TENSILE STRENGTH, MIN (MPa)	AVERAGE 28-DAY COMPRESSIVE STRENGTH, MIN (MPa)
	All lightweight aggregate		
1	1760	2.2	28
2	1680	2.1	21
3	1600	2.0	17
	Sand/lightweight aggregate		
4	1840	2.3	28
5	1760	2.1	21
6	1680	2.1	17

2. EXPERIMENTAL PROGRAM

The experimental program consists of two parts wherein the first part deals with the evaluation and characterisation of sintered fly ash aggregate and second part deals with the experimental investigation on suitability of sintered fly ash lightweight aggregate for application in structural concrete. Under the section of evaluation and characterisation of sintered fly ash aggregate, petrographic examination of aggregate and evaluation of physical and chemical properties of sintered fly ash aggregate have been carried out. Under the section of experimental investigation on suitability of sintered fly ash lightweight aggregate for application in structural concrete, concrete using sintered fly ash aggregate has been made at two water-cement ratios (0.55 and 0.45). The specimens of different sizes and types as per relevant Indian codes / International codes / test methods / specifications were used in the investigation to determine the engineering properties of structural lightweight concrete. The mechanical properties such as compressive strength, flexural strength, split tensile strength, drying shrinkage, modulus of elasticity, and Poisson's ratio have been determined. The durability properties studied include rapid chloride ion penetration test (RCPT), electrical resistivity, chloride migration test, and water permeability and sorptivity (absorption) index. The results of mechanical and durability properties of concerte made with sintered fly ash lightweight aggregates were also compared with normal lightweight aggregate concrete.

3. EVALUATION AND CHARACTERISATION OF SINTERED FLY ASH AGGREGATE

The study consists of petrographic examination as per IS: 2386 Part VIII for sintered fly ash aggregate of both fractions (8-16 mm and 4-8 mm) to check its suitability as an aggregate from the mineralogy point of view. After this, the physical and chemical properties of both the fractions of sintered fly ash aggregate were carried out as per the requirements of IS: 383-2016 [21].

3.1 Micro Structural Investigation on Properties of Sintered Fly Ash Aggregate

Petrographic analysis on both fractions of LDA (8-16 mm and 4-8 mm) were conducted under polarising type optical microscope. The minerals present were quartz, orthoclase-feldspar, glass, semi-glass, and opaque minerals (Figure 3). Grain size of quartz varies from 2 μm to 206 μm with an average of 102 μm. Majority of glass grains were in the size range of 70 μm to 100 μm. Grain size of glass varies from 2 μm to 161 μm with an average of 93 μm. Majority of glass grains were in size range of 60 μm to 90 μm.

The pelletizing action provides a rounded, spherical, and semi-spherical shape to the finished aggregate. The external grey

Figure 3: External appearance of sintered fly ash aggregate or LDA (30x)

colour and internal black core were related to carbon content and oxidation state of the iron present. The morphological, microstructural, and mineralogical characters of nodules give a clear picture of their pozzolonic characters which may enhance bond strength between cement paste and aggregate. The studies were also conducted in stereoscopic microscope for the in-situ nodules for the sintered fly ash aggregate for both fractions (8-16 mm and 4-8 mm). For fraction (4-8) mm, these LDA nodules were of various shapes and sizes with different morphological characters. Two types of nodules commonly present in this aggregate were as follows:

- Aggregate has rounded to semi-rounded nodules with corroded surface having numerous micro-cracks and voids. Outer surface of the nodule is light cream to grey in colour. Assemblage of grains of various shapes and sizes were clearly visible on the surface of the nodules. Majority of these grains were undigested material used for nodulization. Voids of various shapes and sizes were clearly marked on the surface of these types of nodules (Figure 4).

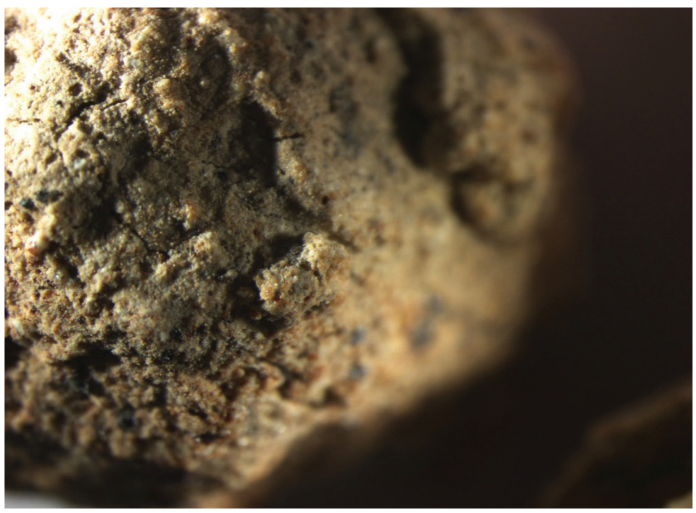

Figure 4: LDA size (4-8) mm (Plate 1): Sintered fly ash aggregate. Nodule with corroded surface and open voids grains in agglomerated form (1.5x)

Figure 5: LDA size (4-8) mm (Plate 2): Sintered fly ash aggregate. Nodule with smooth surface and cluster of sintered material (1.5x)

- Aggregates have rounded to semi-rounded nodules with very smooth surface were tightly packed with sintered grains of the material used. Dark brown color glass grains of various shapes and sizes were developed on the surface and inner portion of nodule. Outer margins of glass clusters were tightly cemented which developed cohesive margins between the glass clusters and matrix (Figure 5).
- For fraction (8-16) mm, these LDA nodules were of various shapes and sizes with different morphological characters. Two types of nodules commonly present in this aggregate were as follows:
  (1) Numerous continuous micro cracks of various thicknesses were present on the surface of nodule. Outer surfaces were well cemented on the sintered matrix. Very fine voids of shallow depth were present on the surface of the nodules (Figure 6).
  (2) In this nodule, rounded to semi-rounded clusters of molten glassy phase were cemented in matrix. Numerous pores and few discontinuous cracks of shallow depth were uniformly developed on the surface of the module. Surfaces of these nodules were very smooth in nature (Figure 7).

3.2 Physical and Chemical Properties of Sintered Fly Ash Aggregate

The representative samples of lightweight aggregate (LWA) (two fractions 8-16 mm and 4-8 mm) were collected and used for physical and chemical testing. The physical and chemical test results as obtained were presented in Table 3, Table 4, and Table 5.

Table 3: Results of sieve analysis

SIEVE SIZE (mm)	PERCENTAGE PASSING	
	FRACTION-I (8-16 mm)	FRACTION-II (4-8 mm)
40	100	100
20	100	100
10	21	100
4.75	00	09

Table 4: Test results of physical & chemical properties of sintered fly ash lightweight aggregate

TEST CARRIED OUT	FOR FRACTION 4-8 mm	FOR FRACTION 8-16 mm
Specific gravity	1.59	1.58
Water absorption, %	12.4	13.10
Abrasion, crushing, and impact value, %	-	32, 44, & 32
Loose bulk density, kg/m^3	810	845
Deleterious material (except coal & lignite), %	Nil	Nil
Loss on Ignition (LOI), %	-	3.55
Silica (SiO_2) and iron oxide (Fe_2O_3), %	-	59.13 & 3.57
Aluminium oxide (Al_2O_3), %	-	28.76
Calcium oxide (CaO) and sulphate (SO_3), %	-	1.58 & 0.10
Magnesium oxide (MgO) and chlorides, %	-	0.60 & 0.008
Alkalies: Na_2O and K_2O, %	-	0.25 & 0.40

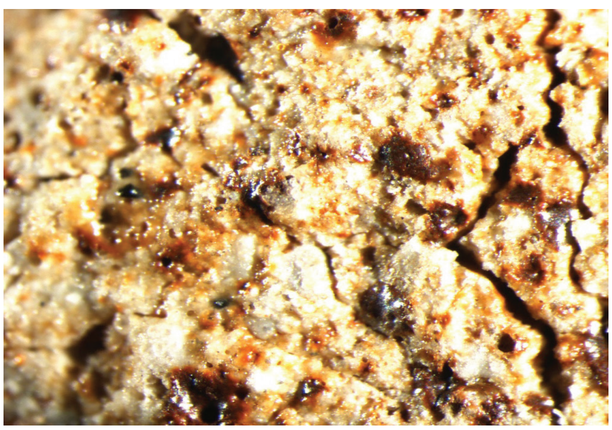

Figure 6: LDA size (8-16) mm (Plate 1): Sintered fly ash aggregate. Nodule with smooth surface and cluster of sintered material (2.5x)

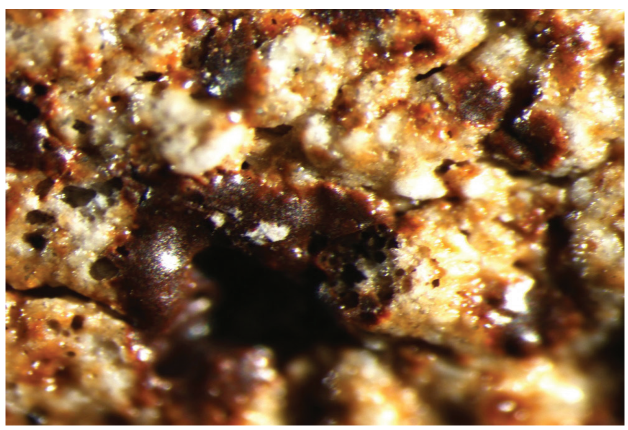

Figure 7: LDA size (8-16) mm (Plate 2): Sintered fly ash aggregate. Nodule with smooth surface and few micro cracks (2.5x)

Table 5: Accelerated mortar bar test (as per ASTM C 1260)

SAMPLE TYPE	1N NaOH 80°C	REMARKS
	14 DAY EXPANSION%	
Low density aggregate LDA-I	0. 02	Innocuous
Low density aggregate LDA-II	0. 01	Innocuous

One of important aspects of sintered fly ash low density aggregate is water absorption. The water absorption of sintered fly ash low density aggregate was determined by measuring the dry mass (m_{dry}) and the wet mass after immersion in water as per IS: 2386 Part-III for different time intervals discussed here (this is the saturated-surface-dry mass, m_{sat}). The water absorption of both the fractions of LDA at different time interval, i.e. 5 minute, 10 minute, 15 minute, 30 minute, 45 minute, 60 minute, 1:15 hours (75 minute), 1:30 hours (90 minute), 1:45 hours (105 minute), 2:00 hours (120 minute), 3:00 hours (180 minute), 4:00 hours (240 minute), 5:00 hours (300 minute), 6:00 hours (360 minute), and 6:30 hours (390 minute) was determined to analyse the rate of water absorption. The development of water absorption over time for selected fractions of the sintered fly ash aggregate is presented in Figure 8. The water absorption of the tested sintered fly ash stabilizes relatively quickly due to its more open pore structure and smaller differences between shell and interior of the particles in comparison with some expanded clays or shales.

The abrasion value of the LDA fraction (16 mm – 8 mm) is 32% which is not satisfactory as per IS: 383 [21] for the coarse aggregate to be used in concrete for wearing surfaces. However, the abrasion value is satisfactory for the coarse aggregate to be used in other concrete. The crushing value of the LDA fraction (16 mm – 8 mm) is 44% which is not satisfactory as per IS: 383 for the coarse aggregate to be used in concrete for wearing surfaces. However, the crushing value is satisfactory for the coarse aggregate to be used in other concrete. The impact value of the LDA fraction (16 mm – 8 mm) is 32% which is not satisfactory as per IS: 383 for the coarse aggregate to be used in concrete for wearing surfaces. However, the crushing value is satisfactory for the coarse aggregate to be used in other concrete. The test results of deleterious material for both fractions of LDA were satisfactory as per IS: 383. The sieve analysis result of LDA fraction-I (16 mm - 8 mm) and fraction II (8 mm – 4 mm) conforms to the grading requirements for lightweight aggregate for structural concrete with coarse aggregate of nominal size designation 19.00 mm – 4.75 mm and 9.5 mm – 2.36 mm as per Table 1 of ASTM C 330. Dry Loose bulk density of LDA fraction-I and fraction-II were 845 Kg/m^3 and 810 Kg/m^3, respectively, and conforms to the ASTM C 330, ASTM C 331, and IS: 2185 (Part-II), as per which the maximum dry loose bulk density of the lightweight coarse aggregate is 880 Kg/m^3. Water absorption of LDA fraction-I and fraction-II were 13.10% and 12.40%, respectively, which were in agreement with the existing literature [5] for lightweight aggregates used for structural concrete. As per existing literature [5], lightweight aggregates generally absorb from 5 to 25% by mass of dry aggregate. Neville [13] indicated that water absorption of good quality lightweight aggregate for use in structural concrete usually should not be more than 15%. The initial rate of water absorption of both the fractions of LDA is quite high. In first hour, LDA fraction-I and fraction-II water absorption were 9.09% and 9.01%, respectively, i.e. the LDA absorbs almost 70% of total water absorption in the first hour. Loss on Ignition (LOI) of LDA fraction (16 mm - 8 mm) is 3.55% which conforms to the ASTM

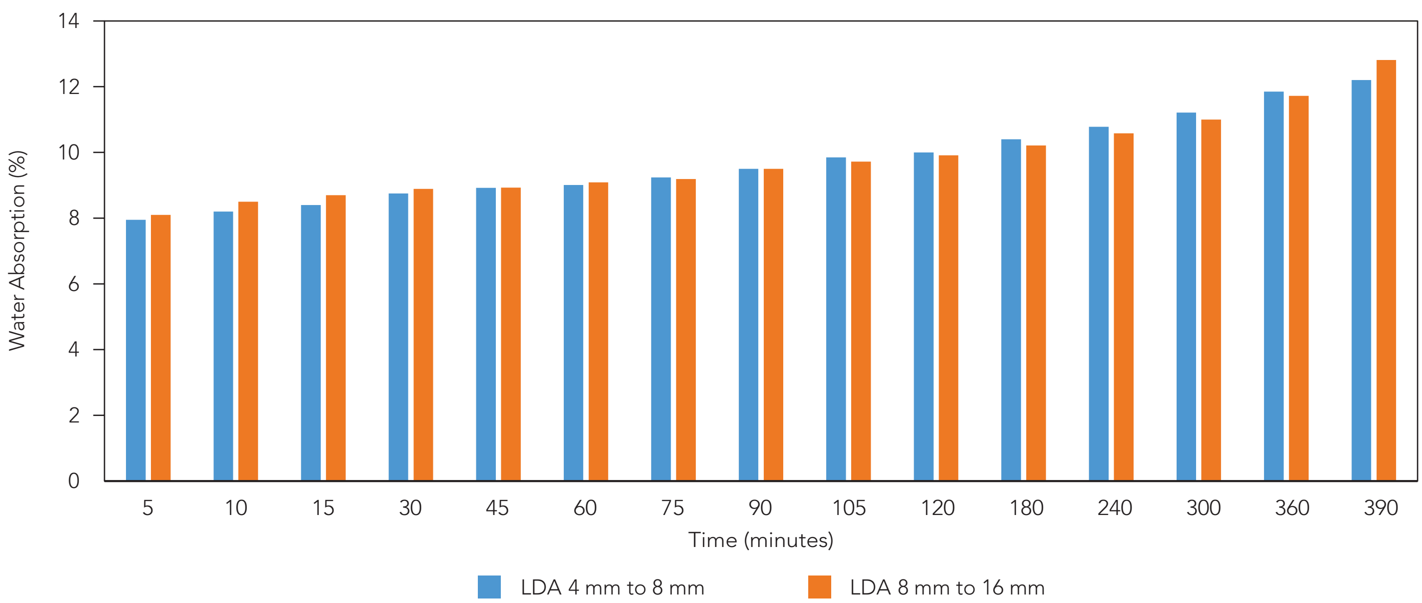

Figure 8: Water absorption at different interval for fraction 4-8 mm LDA and 8-16 mm LDA

C 330 and ASTM C 331 requirement of maximum loss on ignition of 5%. The LOI value also conforms to the IS: 9142 requirement of maximum loss on ignition of 4%. Accelerated mortar bar test as per ASTM C 1260 indicates that the expansion at 14 days on LDA is 0.02% which is less than 0.1%. Therefore, the LDA sample can be classified as innocuous as per ASTM C 1260.

4. EXPERIMENTAL INVESTIGATION ON SUITABILITY OF SINTERED FLY ASH LIGHTWEIGHT AGGREGATE IN STRUCTURAL CONCRETE

The experimental investigation consists of the evaluation of concrete making materials and concrete mix proportioning, followed by casting and testing of concrete samples. Natural river sand conforming to zone-II of IS: 383, one brand of OPC-43 Grade conforming to IS: 8112 [22], and Naphthalene-based super plasticizer conforming to IS: 9103 [23] were used in this study. The mix proportioning was done by absolute volume method.

Table 6: Mix proportions of LWAC

MIX CONSTITUENTS	AT W/C-0.55, MIX PROPORTIONS (Kg/cum)	AT W/C-0.45, MIX PROPORTIONS (Kg/cum)
Cement (OPC-43 grade)	300	333
Water	165	150
Normal weight fine aggregate	657	662
Lightweight coarse aggregate Fraction-I 8 mm - 16 mm (65%) Fraction-II 4 mm - 8 mm (35%)	 502 270	 505 272
Chemical admixture	2.40 litre @ 0.80% by weight of cement	1.67 litre @ 0.50% by weight of cement

In this method, the volume of fresh concrete produced by any combination of materials was considered equal to the sum of the absolute volumes of cementitious materials, aggregate, net water, and entrained air. The slump of the fresh concrete was kept in the range of 50-75 mm. The concrete mixtures were prepared in pan type concrete mixer. The mix proportions details of LWAC are presented in Table 6.

4.1 Tests Conducted on Concrete Samples

Different sizes and types of specimens as per relevant Indian codes/ International codes/ test methods/ specifications were used in the investigation to determine the engineering properties of hardened concrete. The details of tests conducted on concrete samples were presented in Table 7.

4.2 Tests Results and Discussion

4.2.1 *Mechanical properties of lightweight aggregate concrete*

The results of various mechanical properties such as compressive strength, flexural strength, split tensile strength, drying shrinkage, modulus of elasticity, and Poisson's ratio are presented in Table 8. The compressive strength of LWAC at 28 days for w/c-0.55 and 0.45 were 34.64 N/mm^2 and 44.19 N/mm^2, respectively, which is in the same range as that of NWAC. The flexural strength of LWAC at 28 days for w/c-0.55 and 0.45 were 3.79 N/mm^2 and 4.25 N/mm^2, respectively. As per IS: 456-2000 and past studies [31-34], the estimated values of flexural strength were 4.12 N/mm^2 and 4.65 N/mm^2 corresponding to the actual compressive strength of 34.64 N/mm^2 and 44.19 N/mm^2 of normal weight aggregate concrete, respectively. The main factors influencing the compressive strength in this study were found to be the volume of lightweight aggregates, maximum lightweight aggregate size, water-to-

Table 7: Detailed test program with standards and specimens dimension

SL. NO.	TYPE OF TEST	TESTING AGE (DAYS)	STANDARDS/CODES/PROCEDURE	SPECIMEN TYPE & SIZE (mm)
1	Compressive strength	1, 3, 7, 28	IS:516 [24]	Cube, 150 × 150 × 150
2	Flexural strength	28	IS:516	Beam, 150 × 150 × 700
3	Split tensile strength	28	IS:5816 [25]	Cylinder, Dia = 150 and Ht = 300
4	Drying shrinkage	28	IS:1199 [26]	Prism Bar, 75 × 75 × 300
5	Modulus of elasticity	28	IS:516	Cylinder, Dia = 150 and Ht = 300
6	Poisson's ratio	28	IS:516	Cylinder, Dia = 150 and Ht = 300
7	Rapid chloride ion penetration	28	ASTM C 1202 [27]	Cylinder, Dia = 100 and Ht = 200
8	Electrical resistivity	28	Four Point Wenner Probe Resistivity Meter	Slab, 300 × 300 × 100
9	Chloride migration	28	NT Built 492 [28]	Cylinder, Dia = 100 and Ht = 200
10	Water permeability	28	DIN:1048 (Part 5) [29]	Cylinder, Dia = 150 and Ht = 150
11	Sorptivity (absorption) index	28	ASTM C 1585 [30]	Cylinder, Dia = 100 and Ht = 200

Table 8: Test results of mechanical properties of LWAC

TEST CONDUCTED	AGE OF TESTING	MIX ID	
		LWAC (W/C - 0.55)	LWAC (W/C - 0.45)
Compressive strength (MPa)	1 day & 3 day	8.96 & 21.37	13.16 & 29.99
	7 day & 28 day	27.78 & 34.64	34.73 & 44.19
Flexural strength (MPa)	28 day	3.79	4.25
Split tensile strength (MPa)	28 day	3.13	3.50
Drying shrinkage (%)	28 day	0.022	0.018
Modulus of elasticity (MPa)	28 day	20694.00	22352.33
Poisson's ratio	28 day	0.190	0.203

binder ratio, etc. For lightweight concrete, strength decreases substantially with increasing volume fraction of aggregates and aggregate size. The actual flexural strength of LWAC is lowered by 8% and 8.6%, respectively, which is in agreement with the existing literature [7,15] for LWAC. It may be noted that ACI 318 estimates 15% lower value of flexural strength of SLC than that of normal weight aggregate concrete for the same compressive strength.

The moduli of elasticity (MOE) of LWAC at 28 days for w/c-0.55 and 0.45 were 20694 N/mm^2 and 22352.33 N/mm^2, respectively. As per IS: 456-2000, the estimated values of MOE were 29427.88 N/mm^2 and 33237.78 N/mm^2 corresponding to the actual compressive strength of 34.64 N/mm^2 and 44.19 N/mm^2 of normal weight aggregate concrete, respectively. The actual MOE of LWAC is lowered by 29% and 32.75%, respectively, which is in agreement with the literature [7,15] for SLC. It may be noted that as per ACI 213R-03, the MOE value of SLC can be lowered by 25% to 50% than that of normal weight aggregate concrete for the same compressive strength. The Poisson's ratios of LWAC at 28 days for w/c-0.55 and 0.45 were 0.19 and 0.203, respectively, which is in agreement with the existing literature [7,15] for SLC. The drying shrinkage of LWAC at 28 days for w/c-0.55 and 0.45 was 0.022% and 0.018%, respectively, which is less than the maximum limit of 0.07% specified in ASTM C 330.

4.2.2 *Durability properties of lightweight aggregate concrete*

The durability properties such as rapid chloride ion penetration (RCPT), electrical resistivity, chloride migration, water permeability, and sorptivity (absorption) Index have been investigated. The testing has been done as per relevant standards and results are given in Table 9.

The rapid chloride penetrability test (RCPT) of LWAC at 28 days for w/c-0.55 and 0.45 were 5832.70 Coulombs (high) and 3829 Coulombs (moderate), respectively. Corresponding RCPT values in case of normal weight concrete aggregate at same water-cement ratio were 2447 Coulombs (moderate) and 2298 Coulombs (moderate), respectively. This test was conducted on saturated sample of LWA concrete which may have higher pore water inside aggregate due to higher porosity in comparison with normal weight aggregate. This could have been the reason of higher RCPT values. In view of higher RCPT values in case of lightweight aggregates, it is advantageous to be used in dry climatic conditions and also in structures where the concrete remains dry. Necessary precautions with respect to water-to-binder ratio and type of cement shall be considered for structures in wet conditions. The electrical resistivity values of LWAC at 28 days for w/c-0.55 and 0.45 were 4.61 KΩ-cm

Table 9: Test results of durability properties of LWAC

TEST CONDUCTED	AGE OF TESTING	MIX ID			
		LWAC AT W/C - 0.55	*NWAC AT W/C - 0.55	LWAC AT W/C - 0.45	*NWAC AT W/C - 0.45
RCPT at 28 days (Coulombs)	28 day	5832.7 (High)	2447 (Moderate)	3829 (Moderate)	2298 (Moderate)
Electrical resistivity at 28 days (KΩ-cm)	28 day	4.61	9.60	5.39	11.00
Chloride migration test at 28 days (m^2/s)	28 day	26.42×10^{-12}	22.37×10^{-12}	21.14×10^{-12}	12.85×10^{-12}
Water permeability test at 28 days (mm)	28 day	14.67	23.00	12.33	33.00
Sorptivity (absorption) (mm/sec$^{1/2}$)	28 day	Initial-0.0141, Sec.-0.0047	Initial-0.0057, Sec.-0.0047	Initial-0.0179, Sec.-0.0031	Initial-0.0039, Sec.-0.0024

* Mix using normal weight aggregate concrete (NWAC) is taken from NCB data bank.

and 5.38 K'Ω-cm, respectively. Corresponding electrical resistivity values in case of normal weight concrete aggregate at same water-cement ratio were 9.6 K'Ω-cm and 11.00 K'Ω-cm, respectively. This test was conducted on saturated sample of LWA concrete which may have higher pore water inside aggregate due to higher porosity in comparison with normal weight aggregate. This could have been the reason of lower resistivity values of LWAC. The chloride migration test results of LWAC at 28 days for w/c-0.55 and 0.45 were 26.42 × 10^{-12} m^2/s and 21.14 × 10^{-12} m^2/s, respectively. Corresponding test results vales in case of normal weight concrete aggregate at same water-cement ratio were 22.37 × 10^{-12} m^2/s and 12.85 × 10^{-12} m^2/s, respectively. This indicates higher migration of chlorides in LWAC than normal weight concrete.

The water permeability values of LWAC at 28 days for w/c-0.55 and 0.45 were 14.67 mm and 12.33 mm, respectively. Corresponding water permeability values in case of normal weight concrete aggregate at same water-cement ratio were 23.00 mm and 33.00 mm, respectively. This result indicates that LWAC has better resistance against water penetration in comparison with normal weight aggregate concrete. It seems that the lower penetration value is because of better aggregate-paste bond in interfacial zone in case of LWAC. The Initial and secondary sorptivity (absorption) values of LWAC at 28 days for w/c-0.55 were 0.0141 mm/$sec^{1/2}$ and 0.0047 mm/$sec^{1/2}$. Corresponding Initial and secondary absorption values in case of normal weight concrete aggregate at same water-cement ratio were 0.0057 mm/$sec^{1/2}$ and 0.0047 mm/$sec^{1/2}$, respectively. Similarly, initial and secondary sorptivity (absorption) values of LWAC at 28 days for w/c-0.45 were 0.0179 mm/$sec^{1/2}$ and 0.0031 mm/$sec^{1/2}$ respectively. Corresponding initial and secondary absorption values in case of normal weight concrete aggregate at same water-cement ratio were 0.0039 mm/$sec^{1/2}$ and 0.0024 mm/$sec^{1/2}$, respectively. It seems that higher absorption values were due to the cellular structure of LWA in upper layer of concrete specimen. However, lower water permeability indicates that porosity in the LWA is discontinuous and aggregate-paste bond is stronger in LWAC.

5. CONCLUSIONS

Based on the test results of the performed investigations and literature studied, it can be concluded that:

1. Micro-structural, physical, and chemical properties of sintered fly ash lightweight aggregates of fraction-I (16 mm - 8 mm) and fraction-II (8 mm - 4 mm) conforms to the criteria of IS: 9142, ASTM C 331, and IS: 2185 (Part-II), and it can be used in concrete masonry units for production of hollow / solid lightweight concrete blocks. However, results of abrasion, crushing, and impact values indicate that lightweight aggregate shall not be used for concrete to be used in wearing surfaces.
2. The results on mechanical and durability properties of LWAC indicate that concrete made with lightweight coarse aggregate can be used as structural concrete. However, various structural design codal provisions need to be established for structural lightweight concrete since parameters such as flexural strength and modulus of elasticity values were lower than that of normal weight concrete for same compressive strength.
3. Codal provision such as minimum cement content, maximum water-cement ratio, concrete cover to the reinforcement, etc. shall be made further stringent than that of normal weight aggregate concrete to ensure similar level of durability in the same exposure conditions.
4. The findings of the study have resulted in formulation of Bureau of Indian standard IS: 9142 (Part-2)-2018 on sintered fly ash lightweight coarse aggregate in structural applications.

REFERENCES

1. Chandra, S. and Berntsson, L. (2003). "For lightweight aggregate concrete (science, technology and applications)", *Noyes Publications.*
2. Ramamurthy, K. and Harikrishnan, K. I. (2006). "Influence of binders on properties of sintered fly ash aggregate", *Cement Concrete Comp.,* Vol. 28, pp. 33-38.
3. Domagala, L. (2020). "Durability of structural lightweight concrete with sintered fly ash aggregate", Materials, Vol.13, No. 20, pp. 4565.
4. Atluri, S., Srikanth, K., and Desai, V. B. (2017). "Brief study on concrete modified with artificial cold bonded pelletized lightweight fly ash aggregates", *IOSR Journal of Engineering,* Vol. 7, pp. 35-41.
5. Zhang, M. H. and Gjorv, O. E. (2010). "Characteristics of lightweight aggregates for high-strength concrete", *ACI Materials Journal,* Vol. 88, No. 2, pp.150-157.
6. Senapati, M. R. (2011). "Fly ash from thermal power plants waste management and overview", *Current Science,* Vol. 100, No. 20, pp. 1791-1794.
7. Lo, T. Y., Tang, W. C., and Cui, H. Z. (2007). "The effects of aggregate properties on lightweight concrete", *Building and Environment.* Vol. 42, No. 8, pp. 3025-3029.
8. Chalermphan, N. and Arnon, C. (2018). "Phase characterizations, physical properties and strength of environment-friendly cold-bonded fly ash lightweight aggregates", *Journal of Cleaner Production,* Vol. 171, pp. 1094-1100.

9. ACI 213R (2003). "Guide for structural lightweight-aggregate concrete", American Concrete Institute (ACI), USA.

10. ASTM C 330 (2000). "Standard specification for lightweight-aggregates for structural concrete", *ASTM Standard,* USA.

11. ACI 211.2 (1991). "Standard practice for selecting proportions for structural lightweight concrete", American Concrete Institute (ACI), USA.

12. ASTM C 331 (2005). "Standard specification for lightweight aggregates for concrete masonry units", *ASTM Standard,* USA.

13. Neville, A. M. (1995). "Properties of concrete-fourth & final edition", Pearson Prentice Hall, United Kingdom.

14. Swamy, R. N. and Lambert, G. H. (1981). "The microstructure of lytag aggregates", Intj. Comp. Lightweight Aggregate, Vol. 3, No. 4, pp. 273-282.

15. Teychene, D. C. (1968). "Lightweight aggregates-their properties and uses in concrete in the UK", *Proc.*1st *Int. Congress on Lightweight Concrete,* Vol. 1, pp. 23-37.

16. Razak, R., Abdullah, M. M. A., Bakri, Al., Hussin, K., Ismail, K. N., Hardjito, D., and Yahya, Z. (2015). "Optimization of NaOH molarity, LUSI mud/alkaline activator, and Na_2SiO_3/NaOH ratio to produce lightweight aggregate-based geopolymer". *Int. J. Mol. Sci.,* Vol. 16, pp. 11629-11647.

17. Bijen, J. M. J. M. (1986). "Manufacturing process of artificial lightweight aggregates from fly ash", *The Int. J. Cement and Lightweight Concrete,* Vol. 8, No. 3, pp. 191-199.

18. ACI 318 (2008). "Building code requirements for structural concrete", *American Concrete Institute,* Detroit, USA.

19. Faust, T. *et al*. (1998). "High strength lightweight-aggregate concrete", *Institute of Structural Engineering & Building Material,* 2nd *Int. Ph.D. Sysmpo. in Civil Engineering,* Budapest, Hungary.

20. IS: 9142 (1997). "Specification for artificial lightweight aggregate for concrete masonry units", *BIS,* New Delhi, India.

21. IS: 383 (2016). "Specification for coarse and fine aggregate from natural sources of aggregates", *BIS,* New Delhi, India.

22. IS: 8112 (2013). "43 Grade ordinary portland cement-specification", *BIS,* New Delhi, India.

23. IS: 9103 (1999). "Concrete admixtures-specification", *BIS,* New Delhi, India.

24. IS: 516 (2018). "Methods of tests for strength of concrete", *BIS,* New Delhi, India.

25. IS: 5816 (1999). "Method of test for split tensile strength of concrete", *BIS,* New Delhi, India.

26. IS: 1199 (1959). "Method of sampling & analysis of concrete", *BIS,* New Delhi, India.

27. ASTM C 1202 (2019). "Standard test method for electrical indication of concrete's ability to resist chloride ion penetration", *ASTM Standard,* USA.

28. NT Build 492 (1999). "Nordtest method for determination of the chloride migration co-efficient in concrete, mortar or cement-based repair material from non-steady-state migration experiments", *Nordtest Method,* Finland.

29. DIN 1048-5 (1991) "Testing of hardened concrete", *German Institute for Standardization,* Germany.

30. ASTM C 1585 (2004). "Standard test method for measurement of rate of absorption of water by hydraulic-cement properties", *ASTM Standard,* USA.

31. IS: 456 (2000). "Plain & reinforced concrete – code of practice", *BIS,* New Delhi, India.

32. Arora, V. V., Singh, B., and Jain, S. (2017). "Effect of indigenous aggregate type on mechanical properties of high strength concrete", *Indian Concrete Journal,* Vol. 91, No. 1, pp. 34-44.

33. Arora V. V., Singh, B., and Jain, S. (2016). "Experimental studies on short term mechanical properties of high strength concrete", *Indian Concrete Journal,* Vol. 90, No.10, pp. 65-75.

34. Singh, B., Arora, V. V., and Patel, V. (2018). "Study on stress strain characteristics of high strength concrete", *The Indian Concrete Journal,* Vol. 92, No. 6, pp 37-43.

P. N. OJHA is a Joint Director and Head of Centre for Construction Development and Research in National Council for Cement and Building Materials, Ballabgarh, Haryana, India. He has more than 29 years of experience in the field of cement and concrete technology – new product development, high performance concrete, ultra high-performance concrete, durability of concrete, structural design & condition assessment of existing concrete structure, reinforcement corrosion mitigation, laboratory proficiency testing, and development of reference material. He has published more than 45 research papers in various international and national conferences and journals. He is a member of various Beauru of Indian Standard (BIS) committees and member of ISO panel of BIS on cement and concrete. Email: cdrncbb@gmail.com

BRIJESH SINGH holds a B.E. Degree in Civil Engineering and M.Tech. Degree in Structural Dynamics from Indian Institute of Technology (IIT) Roorkee, India. He is a Group Manager in Centre for Construction Development and Research in National Council for Cement and Building Materials, Ballabgarh, Haryana, India. He has overall experience of twelve years in the field of condition assessment, quality assurance and audit of concrete structures and research, and development in the field of cement and building materials. His major research interests are: durability of concrete, high strength, and high performance concrete. He has published more than 65 research papers in various international and national conferences and journals. He is a member of various BIS committees on earthquake engineering, concrete reinforcement, national building code, and plain and reinforced concrete as well as prestressed concrete. Email: cdrncbb@gmail.com

ASHOK KUMAR BEHERA holds a B.Tech. Degree in Mechanical Engineering and PGDM. He is Vice President, Head Corporate Affairs and legal, Head Business Development, Indian Metals, and Ferro Alloys Ltd, Bhubaneswar, India. He is a member of BIS committee. He has 33 years of experience in thermal power plant, plant projects, environmental improvement projects, waste management, new product, and business development. He has published more than 5 research papers in national and regional seminars and journals. He is considered a pioneer in sintered fly ash aggregate process and application in concrete. Email: ashokbehera@imfa.in

Cite this article: Ojha, P. N., Singh, B., Behera, A. K. (2021). "Sintered fly ash lightweight aggregate - its properties and performance in structural concrete", *The Indian Concrete Journal*, Vol. 95, No. 6, pp. 20-30.

NOVEL TEXTILE-REINFORCED CONCRETE-COLD FORM STEEL CAVITY WALL PANEL SYSTEM FOR FAST TRACK CONSTRUCTION

V. RAMESH KUMAR,
SMITHA GOPINATH*

Abstract

Resilient infrastructure creation in a fast track manner is the need of the day. In this context, textile-reinforced concrete (TRC) is a highly promising construction material when integrated with cold form steel. This paper presents the development of a novel cavity wall panel system consisting of two prefabricated composite of TRC panels and profiled cold form steel sheet connected together using a spacer system. The novelty is hinged upon the spacer being used in this construction of cavity wall panel system facilitating an easy and efficient construction. Preliminary investigations were carried out on proposed wall panel system under axial compressive loading. Experimental results were examined with respect to response characteristics and failure modes for load-bearing wall panel applications.

Keywords: Axial compression, Cavity wall panel, Cold-form steel, Spacer system, Textile-reinforced concrete.

1. INTRODUCTION

Conventional cavity wall system generally consists of outer skins separated by a hollow space or cavity. The needs and functions of a good wall is to provide strength, stability, weather exclusion, thermal insulation, sound insulation, durability, fire resistance, and appearance. For the aforementioned requirements, the cavity wall tends to cater almost all the requirements with proper adoption of skin material, connection methodology, and insulation material. The most commonly used cavity wall construction is by using masonry with brick or concrete block as outer layers [1, 2]. Masonry being an absorbent material tends to draw rain water or even humidity into the wall from outside as well as inside the house. One of the main challenges with masonry cavity wall is that they act as a passage of moisture. Hence, materials with less moisture permeability and water absorption can be instrumental to bridge this gap. Yet another aspect is that the construction practices followed for conventional cavity walls are more time consuming. Faster construction methods are the need of the day, and the use of prefabricated building components can be instrumental for creating a resilient infrastructure.

Use of non-conventional materials is gaining popularity for construction of prefabricated wall panels [3-6]. However, the information about prefabricated cavity wall panel systems in this context is limited in literature. A recent advancement in the prefabrication construction is by use of textile-reinforced concrete (TRC). It is a non-corrosive material consisting of fine grained cementitious binder and non-metallic textiles as reinforcement. Due to fine grained nature, the porosity and water absorption of TRC is considerably less. Though TRC has been implemented as non-load-bearing wall panels [7, 8], its application as load-bearing wall panel is not explored much. The present paper proposes a first-of-its kind cavity wall panel system consisting of TRC and cold formed steel, and the cavity is created using a spacer system. The spacer system developed in this paper is a novel technique, which helps towards easy assembly and installation of the cavity wall panel system at site.

2. EXPERIMENTAL INVESTIGATIONS

Preliminary experimental investigations were carried out to determine the axial load-carrying capacity of textile-reinforced concrete-cold form steel cavity wall panel system. Pre-fabricated TRC was used as a skin material and a profile steel sheet with embossments were used as core material. Each TRC skin is of dimension of 800 × 1500 × 25 mm.The profile steel sheet used was of size 800 × 1500 × 1.2 mm. The connection between TRC and profile sheet was provided with self-tapping screws. A spacer connection using z-section was developed for connecting two sets of TRC-cold form steel, so that higher load-carrying ability can be achieved for the overall system. The overall load-bearing wall panel system is of size 1500 × 800 × 250 mm.

*Corresponding author : Smitha Gopinath, Email: smithag@serc.res.in

2.1 Material Properties

TRC is composed of a thin layer of fine grained cementitious matrix as a binder and an alkali-resistant glass textile as reinforcement. The binder consist of Portland cement (578 kg/m^3), fly ash (206 kg/m^3), silica fume (41 kg/m^3), quartz sand (589 kg/m^3), quartz powder (354 kg/m^3), water (330 kg/m^3), and polycarboxylate-based superplasticizer. The maximum aggregate size used is limited to 0.6 mm to allow for more penetration of binder to glass textile. Superplasticizer was also added to obtain an improved flowing capability for the binder. The cube compressive strength of the binder is 44.5 MPa (±4.2%) and the cylindrical compressive strength is 34 MPa (±3.2%).

In TRC used structures, the textiles are alkali-resistant and thus will not be affected due to corrosion. As a result, in which the excess protective cover is not required, ultimately being able to produce thin structures. The most advantageous property of this material is the control over the orientation of the textiles, which can be arranged easily in the direction of stresses. Alkali-resistant glass textile was used as reinforcement in TRC panel. In the glass textile, all filaments were coated with poly acrylic to prevent the alkali silica reaction in cementitious binder. The textile is having a mesh size of 25 × 25 mm and weight of 225 g/m^2. Maximum tensile stress of the textile is 1420 MPa. The stress-strain response obtained from uniaxial tensile characterization of the textile is shown in Figure 1.

TRC coupons of size 500 × 60 × 10 mm were tested under uniaxial tension to determine the tensile response. Three layers of textile reinforcement were used in the specimens. The stress-strain response of the textile obtained from uniaxial tensile characterization of TRC is shown in Figure 1.The tensile stress experienced by the textile in TRC is 910 MPa. Details about the experimental investigation can be seen in [9].

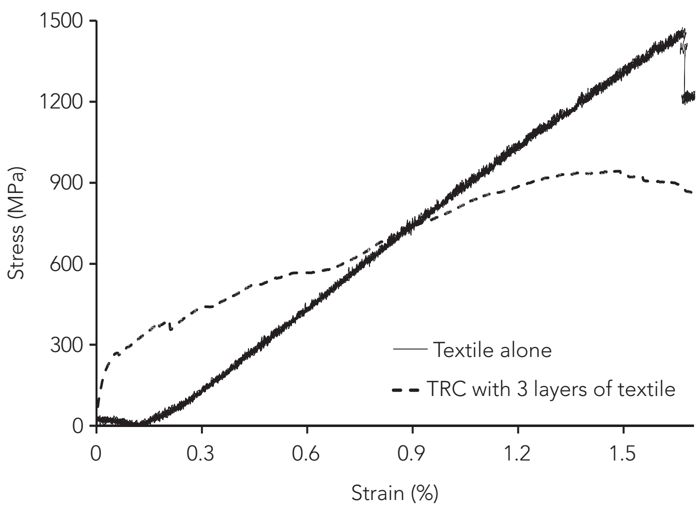

Figure 1: Tensile characteristics of textile

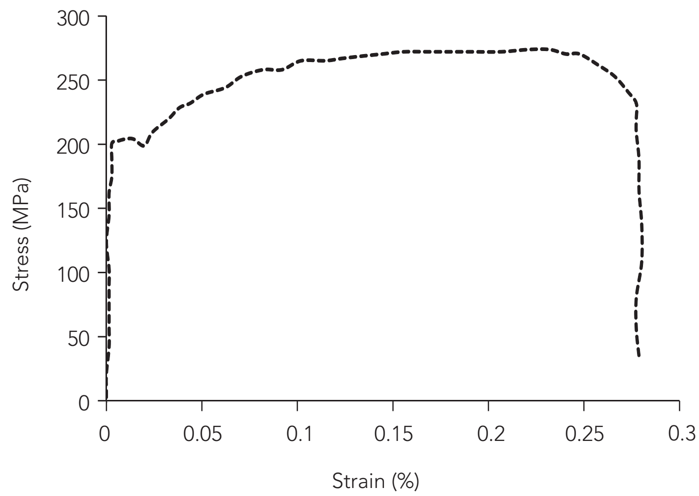

Figure 2: Stress-strain response for steel used in profile steel

Profile steel sheet used is cold form sheet of grade Fe 250. Based on the uniaxial characterization on dumbelled shape steel specimen, the stress-strain behavior of cold form steel obtained from the experiment is shown in Figure 2. It is observed that, up to the stress of 202.59 N/mm^2, a linear behavior is seen and after that behavior changes to plastic. The material used for spacer system as z-section is same as the cold-formed sheet profiled steel of grade Fe 250. Dumbelled shape steel specimen is used to carry out the uniaxial tension test. The stress-strain behavior of cold-formed steel obtained from the experiment is shown in Figure 2.

2.2 Prefabrication of Textile-Reinforced Concrete-Cold Form Steel Cavity Wall Panel System

For casting of TRC skin, first, the polythene sheet was laid with wooden planks provided on four sides of it. Then, the layer of 10 mm thick cementitious binder was applied on sheet. After that, 3 layers of textile were laid. Subsequently, the final layer of TRC was cast till the desired thickness of 25 mm achieved. The TRC skins were cured with water by converting with wet gunny bags. After curing, in order to make the TRC composite wall panel, two skins of TRC were attached with profile steel sheet by using self-tapping screws. Screws were of 4 mm diameter, having 13 threads. Length of screw used was 40 mm. Diameter of screw head was 12 mm. Screw strength was around 400 MPa. Total 4 rows of screws were provided to attach top TRC with steel core. Two rows of screws were provided to attach bottom TRC with steel core. In each row, 8 screws were provided with center-to-center dimension of 150 mm and end distance of 75 mm. Screws were drilled with their heads at the bottom.

The textile-reinforced concrete skins were attached to cold formed profile sheet using self-tapping screws to form textile-reinforced cold formed profile sheet composite wall panels. Two

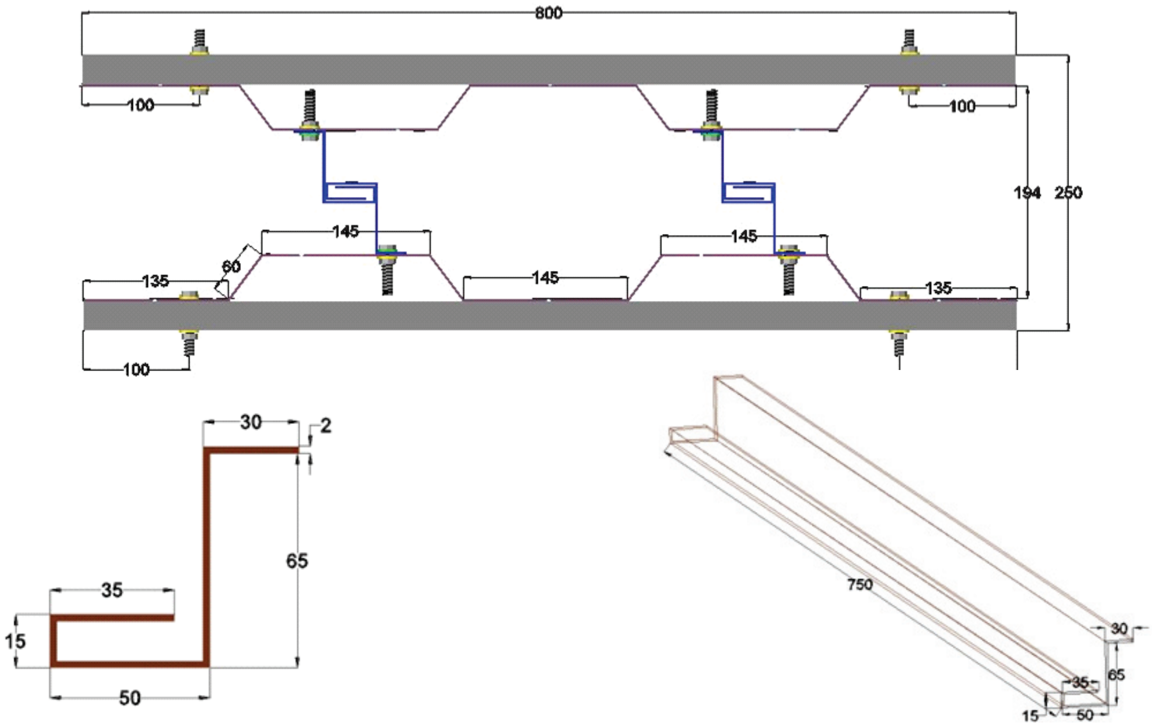

Figure 3: Geometrical details of various components of TRC-Cold form steel cavity wall panel

such panels are interlinked together using cold formed steel z-shaped spacer system as shown in Figure 3. Various stages involved in the prefabrication of TRC-cold form steel cavity wall panel system are shown in Figure 4.

Two specimens were tested under axial compressive loading. The specimens were loaded using 100 ton Enerpac jack. The loading rate was controlled by adjusting the oil pump pressure. The specimen was tested under axial load condition. The

Figure 4: Various stages involved in the fabrication of TRC-cold form steel cavity wall panel system

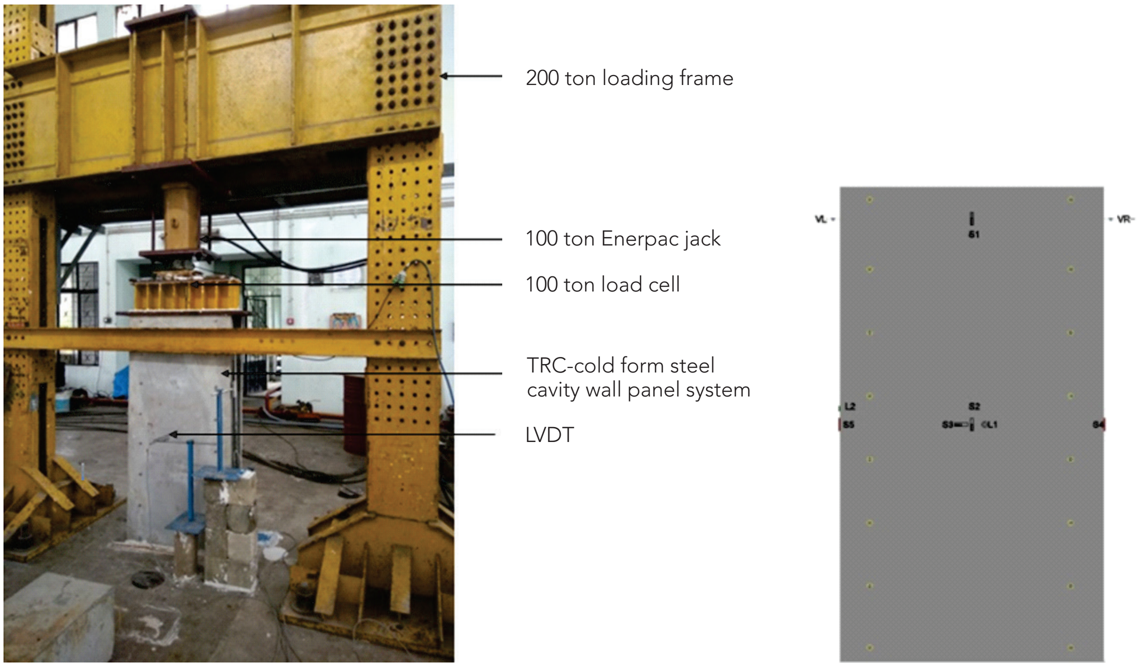

(a) Test setup

(b) Location of instrumentation

Figure 5: Test setup and instrumentation details

support condition provided is hinge-hinge condition. The system was loaded through a 100 ton load cell to capture the load being applied to the setup. The overall test setup is shown in Figure 5(a). LVDTs and strain gauges were used to capture displacement and strain at various locations in the cavity wall panel system. Locations of the instrumentation are shown in Figure 5(b). Two strain gauges (S2 and S3) were fixed in the middle of the panel; one parallel to the loading direction (S2) and the other perpendicular to the loading direction (S3) in order to capture the nature of bending of the panel. Strain gauge (S1) was placed near loading side of the panel to check for the uniformity of the loading and to monitor the amount of Saint-Venant effect being developed at the support. Two strain gauges, S4 and S5, were fixed to the profile sheet in order to monitor its behavior. One LVDT was provided at the mid-level of the panel to monitor the out of plane deflection of the panel. Two LVDTs (VR and VL) were provided at the loading side of the panel in order to check for any torsion being generated.

3. RESULTS AND OBSERVATIONS

The stress-strain characteristics were captured for one of the specimens. The response obtained is shown in Figure 6. The strain gauge (S1) was located near the loading area of the specimen. After reaching the 100 kN load, local crushing of the panels occurred near the loading zone which is depicted in Figure 6. Among the two specimens tested, in one of the specimen, the test was stopped before reaching the ultimate load. The second specimen was tested up to ultimate load, and load vs. deflection behavior is shown in Figure 7. From the

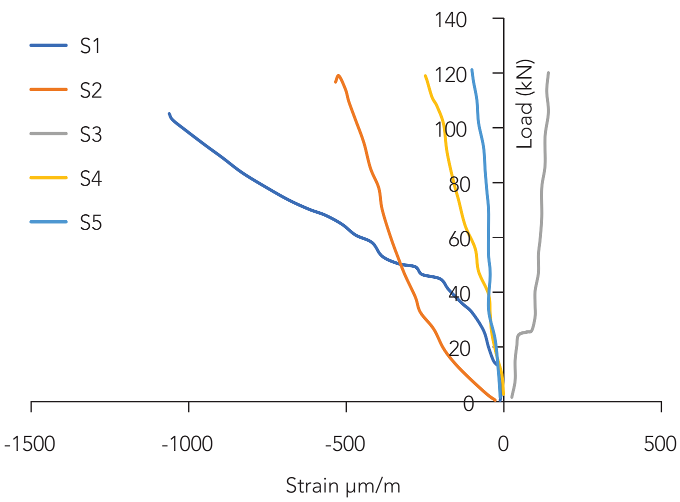

Figure 6: Stress-strain characteristics

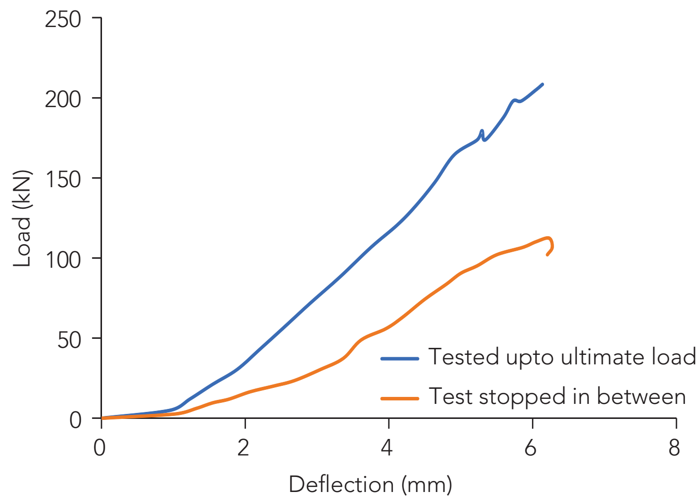

Figure 7: Load-deflection behavior

Figure 8: Failure pattern

results obtained, it can be seen that the system exhibited elastic behavior till 50 kN. Beyond 50 kN, the systems' load-carrying capacity is influenced by the strain hardening of the steel as it is shown from the sudden change in the stiffness of the load-deflection curve beyond 50 kN. From the experimental study, it was found that the buckling of the individual component of the panel was suppressed and the panel failed by cross-section yielding. From this, it can be seen that the spacer system prevented the buckling of the individual components and enabled the section to attain the full load-carrying capacity due to the increased inertia. From the strain data (S2 & S3) given in Figure 6, it can be seen that each component of the panel underwent two-way bending. Along the axial load direction, the bending occurred about the supports but in the direction perpendicular to the loading direction, and the spacer system acted as support creating two-bending action as shown in the strain profile. Hence, it can be observed that the spacer system, apart from preventing the individual buckling of the panel component, also acted as a support to create two-bending thereby improving the load-carrying capacity of the panel and also converting the panel into a stiffened system.

From the failure pattern, shown in Figure 8, it can be seen that the failure occurred by local crushing of the TRC near the support at the yield local. Due to this crushing, the concrete was not able to provide the adequate stiffness to the steel plate resulting in local bending of the plate. Hence, it can be concluded that the spacer system, apart from imparting inertial strength and stiffness to the panel, also prevents the isolated buckling of the connected structural components and converts the one-way bending system into two-bending system which has better strength and stiffness characteristics compared to a one-way system.

The identification of parameters that influence the performance of the "spacer" with respect to the overall performance of wall panel and their extend of influence can be appropriately assessed and optimised to exploit the full potential of the proposed system. The proposed panels can be used in various applications such as: infill, industrial buildings, multi storied buildings, and external facades. The system can offer advantages such as: easy erection on site, less skill intensive, less labour intensive, fast track construction, In built space for services, better thermal /acoustic insulation, spacer system facilitates for adjustable wall thickness, and more strength-to-weight ratio as compared to conventional masonry walls. A conceptual image for arrangement of TRC-cold form steel cavity wall panel system towards achieving faster construction is shown in Figure 9.

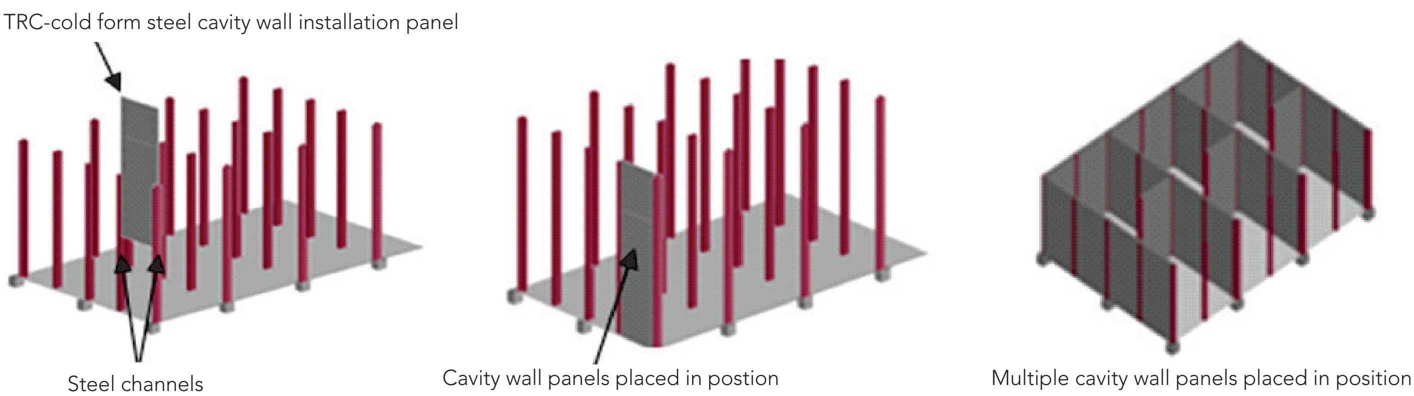

Figure 9: Conceptual fast track installations of TRC-coldform steel cavity wall panel system

4. CONCLUSIONS

In many applications, the use of TRC is limited to non-load-bearing applications till date. However, the present study is the demonstration of possible potential of TRC by integration with cold form steel sheet for load-bearing applications. When the panels were tested under axial compression, the final failure of the panel system was by buckling of the cold form steel sheet, before compressive failure of the TRC. The spacer system conceived in the study facilitates fast track construction method and is instrumental for addressing functionality requirements in a building system. Simple connection between TRC skin with cold form steel using self-tapping screws and subsequent integration of spacer system is novel and has the potential in various applications for creating resilient infrastructure. The experimental studies conducted under axial compression can further be expanded for optimizing the system performance.

ACKNOWLEDGEMENTS

Authors thank the help provided by Syed Ibrahim, Technician, CSIR-SERC for conducting the experiments.

REFERENCES

[1] Hens, H., Janssens, A., Depraetere, W., Carmeliet, J., and Lecompte, J. (2007). "Brick cavity walls: A performance analysis based on measurements and simulations", *Journal of Building Physics*, Vol. 31, pp. 95-124.

[2] Aftab, A., Maslehuddin, M., and Alhems, L. M. (2014). "In situ measurement of thermal transmittance and thermal resistanceof hollow reinforced precast concrete walls", *Energy and Buildings*, Vol. 84, pp. 132-141.

[3] Rice, M. C., Fleischer, C. A., and Zupan, M. (2006). "Study on the collapse of pin-reinforced foam sandwich panel cores", *Journal of Experimental Mechanics*, Vol. 46, pp. 197-204.

[4] Mohamad, N., Omar, W., and Abdullah, R. (2012). "Structural behavior of precast lightweight foamed concrete sandwich panel as a load-bearing wall", *International Journal of Sustainable Development*, Vol. 5, No. 3, pp. 49-58.

[5] Shams, A., Stark, A., Hoogen, F., Hegger, J., and Schneider, H. (2015). "Innovative sandwich structures made of high-performance concrete and foamed polyurethane", *Composite Structures*, Vol. 121, pp. 271-279.

[6] Paul, S., Cherian, P., Menon, D., and Prasad, A. M. (2016). "Use of glass fiber reinforced gypsum panels with reinforced concrete infills for construction of walls and slabs", *The Indian Concrete Journal*, Vol. 90, No. 12, pp. 19-32.

[7] Chira, A., Kumar, A., Vlach, T., Laiblova, L., and Hajek, P. (2015). "Textile-reinforced concrete facade panels with rigid foam core prisms", *Journal of Sandwich Structures and Materials*, DOI: 10.1177/1099636215613488.

[8] Hegger, J., Horstmann, M., and Scholzen, A. (2008). "Sandwich panels with thin-walled textile-reinforced concrete facings", *ACI SP*-251, pp. 109-124.

[9] Gopinath, S., Gettu, R., and Iyer, N. R. (2018). "Influence of prestressing the textile on the tensile behavior of textile-reinforced concrete", *Materials and Structures*, Vol. 51, No. 3, pp.1-12.

V. RAMESH KUMAR is a Senior Scientist in CSIR-Structural Engineering Research Centre, Chennai, India. He holds a Bachelor's Degree in Civil Engineering and Master's Degree in Structural Engineering from Indian Institute of Technology (IIT) Madras, India. Presently, he is pursuing his doctorate with research work on topic "Steel beam-column buckling interaction" at AcSIR. His main research interests include steel-concrete composites and performance evaluation of structures. Email:

SMITHA GOPINATH is a Principal Scientist in CSIR-Structural Engineering Research Centre, Chennai, India. She holds a Bachelor's Degree in Civil Engineering from Govt. Engineering College Thrissur, Kerala, Master's Degree in Structural Engineering from PSG College of Technology, Coimbatore, and Doctoral Degree from Indian Institute of Technology (IIT) Madras, India. Her interests are primarily in textile-reinforced concrete, repair and retrofitting, and computational modeling of structures. She is the recipient of ICI-Young Scientist Award-2016 and Institution of Engineer's Young Engineer Award-2012. Email: smithag@serc.res.in

Cite this article: V. Ramesh Kumar, Gopinath, S. (2021). "Novel textile-reinforced concrete-cold form steel cavity wall panel system for fast track construction", *The Indian Concrete Journal*, Vol. 95, No. 6, pp. 31-36.

FRACTURE STUDIES ON FIBER-REINFORCED RUBCRETE

ANAND RAJ*,
PRAVEEN NAGARAJAN,
A. P. SHASHIKALA

Abstract

This paper presents the details of studies carried out to investigate the fracture energy of fiber-reinforced rubcrete with an aim to assess the improvement in ductility. A three-point bend beam test was carried out using 18 mixes with compressive strength of 20 N/mm^2 as per RILEM TC-50 FMC. Experiments were carried out on four rubcrete mixes (with 5, 10, and 15% replacement of fine aggregates with crumb rubber), three polypropylene fiber-reinforced concrete mixes (with 0.1, 0.2, and 0.3% of polypropylene fibers occupying the total volume of concrete), and four steel fiber mixes (with 0.25, 0.5, 0.75, and 1% of steel fibers occupying the total volume of concrete). The fiber-reinforced rubcrete mixes included rubcrete mixes with 15% of fine aggregate replacement with crumb rubber. Fracture energy obtained using the work of fracture method provides an insight into the ductility and toughness of concrete. The results of the study indicated that for rubcrete beams, the fracture energy was increased by 14% for rubcrete with 15% crumb rubber. The fracture energy of steel fiber-reinforced concrete beam with 1% steel fiber content was 56% higher than the fracture energy of ordinary concrete. The fracture energy of steel fiber-reinforced rubcrete beam with 1% steel fiber content and 15% crumb rubber content was 92% more than the fracture energy of the ordinary concrete beam. For polypropylene fiber-reinforced concrete beam with 0.3% polypropylene fiber content, the fracture energy was improved by 27%. In the polypropylene fiber-reinforced rubcrete beam with 15% crumb rubber content and 0.3% polypropylene fibers, the enhancement in fracture energy was 57%. Significant improvement in ductility was achieved using steel fiber-reinforced rubcrete mix with 1% steel fibers and 15% crumb rubber when compared to concrete.

Keywords: Fiber-reinforced rubcrete, Fracture energy, Polypropylene fibers, Rubcrete, Steel fibers.

1. INTRODUCTION

The vast outreach of concrete as a construction material has been phenomenal [1,2]. Being the most prominent material used in the construction industry, concrete has been extensively researched [3]. One of the main drawbacks of using concrete is its brittle nature [4,5]. The use of reinforced concrete in structures has been able to impart some amount of ductility to structural elements. But, still, the demand for improved ductility is rising owing to the urge of the designers to push the structures to their limiting strength. So, efforts have been undertaken to further improve the ductility of concrete [6,7,8]. One of the means to enhance the ductility of concrete is by using tyre crumb rubber as a replacement of fine aggregates in concrete [9,10]. The concrete in which the mineral aggregates are replaced with rubber particles is generally termed as Rubcrete [11]. Along with the improvement in ductility, enhanced energy absorption characteristics and toughness make rubcrete an attractive substituent to ordinary concrete. But, the compressive strength and tensile strength of rubcrete are lower than that of ordinary concrete when worn-out tyre rubber was used to replace aggregates [12]. The reduction in compressive strength and tensile strength could be compensated to some extent if the graded rubber particles used were pre-treated [13]. Improvements in energy absorption characteristics and toughness of concrete can be achieved by the addition of fibers. An increase in strength can be noticed by the addition of steel fibers in concrete [14]. Hence, when steel fibers are added into rubcrete, the resulting fiber-reinforced rubcrete possesses improved strength when compared to ordinary rubcrete. Presence of internal voids in rubcrete leads to a quicker generation of microcracks in rubcrete in comparison with ordinary concrete [15]. A remedy to this problem can be achieved by using polypropylene fibers in rubcrete. Polypropylene fibers suppress the generation of microcracks in concrete to an extent [16]. Cifuentes [17] have reported that the fracture energy of concrete increases with the addition of polypropylene fibers. Using fiber-reinforced rubcrete can result in saving precious natural aggregates. Utilising worn-out crumb rubber provides a solution for problems associated with their disposal. Thus, using fiber-reinforced rubcrete sustains the natural resources for the use of future generations.

But, before utilizing the materials in actual structures, a thorough understanding of the material behavior is essential. Fracture energy is an ideal tool for analysing the ductility of concrete [18,19]. Fracture energy is defined as the energy that has to be spent to generate a unit area of crack [20]. The work of fracture method proposed by Hillerborg [21] is considered as an effective method to determine the fracture energy of concrete [22-25]. Fracture energy is an effective tool to quantify the toughness of a quasi-brittle material like concrete [26]. The characteristic fracture length

*Corresponding author : Anand Raj, Email: anandrajce@gmail.com

of materials obtained by using the work of fracture method gives an indication of the ductility of the material [27,28]. Though fiber-reinforced rubcrete has the potential to be used in applications that require high energy absorption capacity and ductility, it is essential to prove its ability through scientific investigations. Hence, this paper highlights the fracture energy studies, as per RILEM TC-50 FMC, carried out on beams 60 × 100 × 500 mm [29] for steel and polypropylene fiber-reinforced rubcrete.

2. EXPERIMENTAL INVESTIGATIONS

Fracture energy (G_f) of conventional concrete, rubcrete, fiber-reinforced concrete, and fiber-reinforced rubcrete was found out using beams of dimension 60 × 100 × 500 mm. The effective span of the beam during loading was 400 mm.

2.1 Materials and Mix Proportions

Portland pozzolana cement adhering to IS 1489 (Part 1): 1991, manufactured sand, 12.5 mm size coarse aggregate, crumb rubber, and fibers were used in the study. The specific gravity of manufactured sand and coarse aggregates were 2.67 and 2.79, respectively. The crumb rubber of density 650 kg/m^3 was sieved to get the same particle size as that of the manufactured sand. The gradation curve for fine aggregates with crumb rubber is shown in Figure 1. Crimped steel fibers and polypropylene fibers have been used to enhance the energy absorption capacity of concrete. The properties of the fibers used in the study are shown in Table 1. Tables 2 and 3 show the details of the specimens and mix proportions for the mixes. The maximum percentage of replacement of fine aggregates with crumb rubber was limited to 15% since the preliminary study on the compressive strength of rubcrete with 20% crumb rubber indicated a reduction in strength of more than 30% of that of the conventional concrete.

Initially, the aggregates were mixed thoroughly. Then cement was added, and mixing was carried out to obtain a uniform mix. The crumb rubber particles were immersed in polyvinyl alcohol solution, having 2% of polyvinyl alcohol of the weight of water used to dip them. After 30 minutes of soaking in polyvinyl

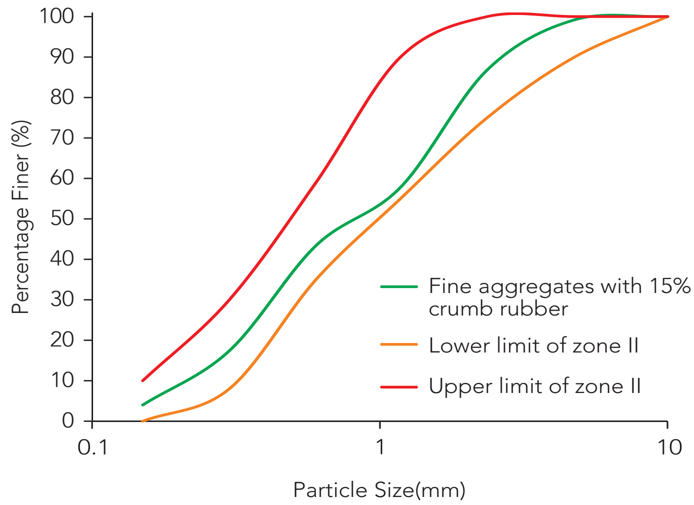

Figure1: Gradation curve for fine aggregates

alcohol solution, the crumb rubber particles were added to the fine aggregates and mixed thoroughly. Sufficient care was taken to obtain a uniform mixture during the addition of fibers.

Table 1: Properties of fibers used in the study

STEEL FIBERS	
Length	30 mm
Aspect ratio	60
Tensile strength	1100 N/mm^2
POLYPROPYLENE FIBERS	
Fiber length	12 mm
Tensile strength	551 N/mm^2
Diameter	0.02

2.2 Testing of Notched Beams

The fracture energy (G_f) was determined by conducting experimental investigations on notched beam specimens of dimension 60 × 100 × 500 mm. A notch depth of 30 mm was provided at the center of the beam bottom. The load-deflection curve of the notched beam subjected to a three-point bend beam test can be used to determine the fracture energy of concrete as per RILEM TC-50 FMC. Figures 2 and 3 present the details of testing of notched beams. Testing of the notched beam was carried out on a displacement-controlled universal testing machine at a strain rate of 0.2 mm per minute.

$$G_f = \frac{W_0 + mg\delta_0}{A_{lig}} \tag{1}$$

where G_f is the fracture energy in Nm/m^2, W_0 is the area under the load-deflection graph expressed in Nm, m is the sum of self-weight of the beam between the supports expressed in kg, δ_0 is the deformation of the beam at failure in meter, and A_{lig} is the projection of the fracture zone on a plane perpendicular to the beam axis expressed in m^2.

A typical load-deflection curve obtained from the testing of notched beams is shown in Figure 4. The area under the curve was estimated by using the trapezoidal rule. The maximum deflection at failure is directly measured using the dial gauge fixed at the bottom of the beam.

The characteristic fracture length of materials was calculated based on Equation 2.

$$L_c = \frac{E_c G_f}{f_t^2} \tag{2}$$

Table 2: Details of specimens

SPECIMEN ID	NUMBER OF SPECIMENS CAST	RUBBER CONTENT (%)	STEEL FIBER CONTENT (%)	POLYPROPYLENE FIBER CONTENT (%)	COMPRESSIVE STRENGTH (N/mm²)
R1	3	0	0	0	35
R2	3	5	0	0	34
R3	3	10	0	0	30
R4	3	15	0	0	26
S1	3	0	0.25	0	35
S2	3	0	0.5	0	36
S3	3	0	0.75	0	37
S4	3	0	1	0	37
SR1	3	15	0.25	0	33
SR2	3	15	0.5	0	35
SR3	3	15	0.75	0	36
SR4	3	15	1	0	35
P1	3	0	0	0.1	33
P2	3	0	0	0.2	34
P3	3	0	0	0.3	35
PR1	3	15	0	0.1	26
PR2	3	15	0	0.2	27
PR3	3	15	0	0.3	29

Note: R1, R2, R3, and R4 : Rubcrete with 0, 5, 10, and 15% replacement of fine aggregates with crumb rubber
S1, S2, S3, and S4 : Steel fiber-reinforced concrete with 0.25, 0.5, 0.75, and 1% steel fibers
SR1, SR2, SR3, and SR4 : Steel fiber-reinforced rubcrete (15% crumb rubber) with 0.25, 0.5, 0.75, and 1% steel fibers
P1, P2, and P3 : Ordinary concrete with 0.1, 0.2, and 0.3% with polypropylene fibers
PR1, PR2, and PR3 : Polypropylene fiber-reinforced rubcrete (15% crumb rubber) with 0.1, 0.2, and 0.3% polypropylene fibers

where L_c is the characteristic fracture length in mm, E_c and f_t are the modulus of elasticity and tensile strength of concrete, respectively, obtained as per IS: 456 (2000), and G_f is the fracture energy of concrete in Nmm/mm².

3. RESULTS AND DISCUSSIONS

Figure 5 presents the load-deflection curves for rubcrete specimens in which the fine aggregates were replaced with crumb rubber by 5, 10, and 15%. It can be observed that, as the percentage of crumb rubber replacing an equal volume of fine aggregates increases, the peak load decreases. The initial slope of the load-deflection curve decreased, and the deflection at the peak load had shifted when compared to the ordinary concrete beam. The decrease in the initial slope of the load-deflection

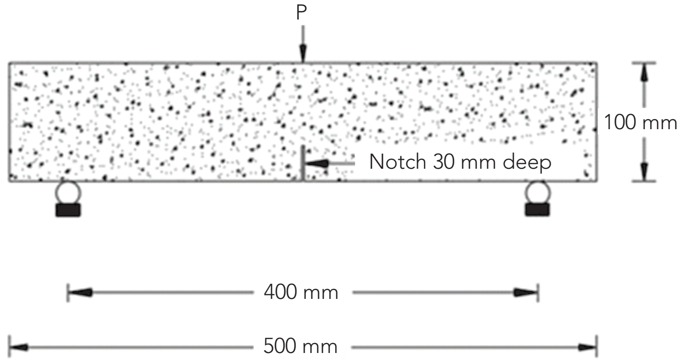

Figure 2: Schematic diagram of testing of beams

Figure 3: Testing of beams

Table 3: Mix proportions

MIX ID	CEMENT	COARSE AGGREGATES	WATER	RUBBER	STEEL FIBERS	POLYPROPYLENE FIBERS	FINE AGGREGATES
R1	1	3.788	0.45	0	0	0	1.908
R2	1	3.77	0.45	0.024	0	0	1.854
R3	1	3.77	0.45	0.047	0	0	1.757
R4	1	3.77	0.45	0.071	0	0	1.659
S1	1	3.788	0.45	0	0.056	0	1.908
S2	1	3.788	0.45	0	0.113	0	1.908
S3	1	3.788	0.45	0	0.169	0	1.908
S4	1	3.788	0.45	0	0.227	0	1.908
SR1	1	3.788	0.45	0.071	0.056	0	1.659
SR2	1	3.788	0.45	0.071	0.113	0	1.659
SR3	1	3.788	0.45	0.071	0.169	0	1.659
SR4	1	3.788	0.45	0.071	0.227	0	1.659
P1	1	3.719	0.45	0	0	0.0026	1.873
P2	1	3.719	0.45	0	0	0.0052	1.873
P3	1	3.719	0.45	0	0	0.0078	1.873
PR1	1	3.719	0.45	0.07	0	0.0026	1.629
PR2	1	3.719	0.45	0.07	0	0.0052	1.629
PR3	1	3.719	0.45	0.07	0	0.0078	1.629

Note: The proportions presented in Table 3 are in terms of weight fractions per kilogram of cement.

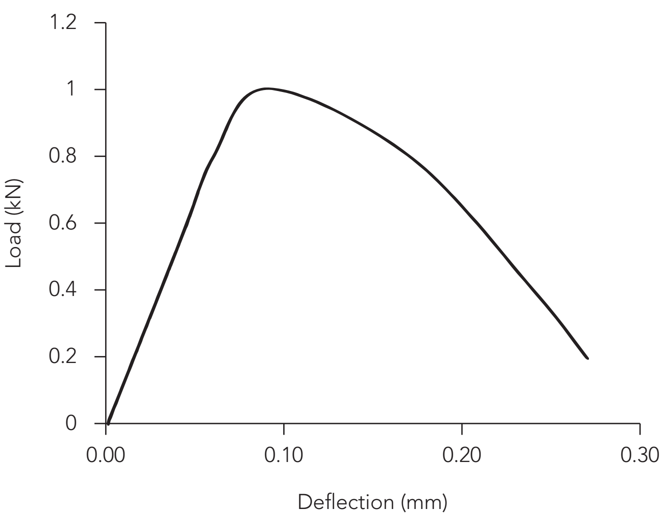

Figure 4: Sample load-deflection curve

curve can be related to the significant deflection of the beam at a particular load with an increase in the crumb rubber content. It can also be noticed from the load-deflection curve of the rubcrete beams that as the percentage of crumb rubber in the concrete increases, the hardening of the descending part of the post-peak section of the load-deflection curve showed an increase. As a result, the maximum deformation for the beam increased by 9%, with an increase in the crumb rubber content by 15%. The reduction in the peak loads with the increase in crumb rubber content may be due to the relatively quick breaking of the inter material bonds within the material matrix due to the presence of voids induced by the introduction of crumb rubber. Due to the aforementioned reasons, the fracture energy of rubcrete beams increased with an increase in crumb rubber content.

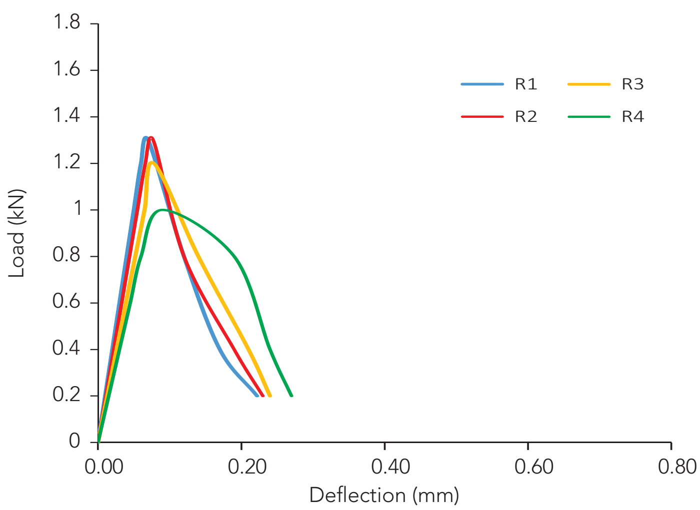

Figure 5: Load-deflection curves of rubcrete beams

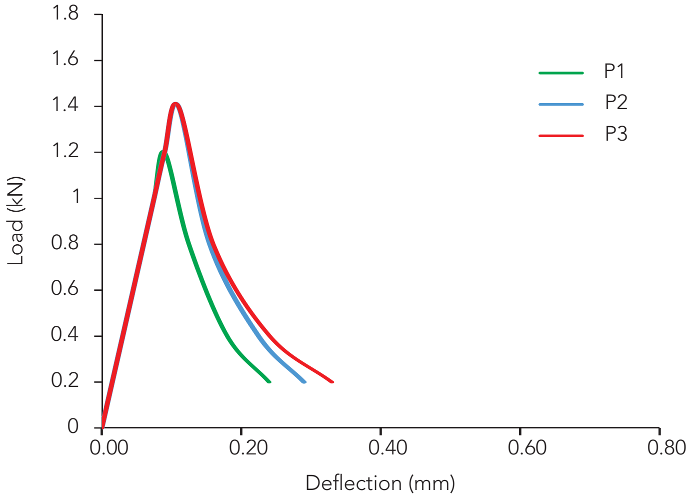

Figure 6: Load-deflection curves of polypropylene fiber-reinforced concrete beams

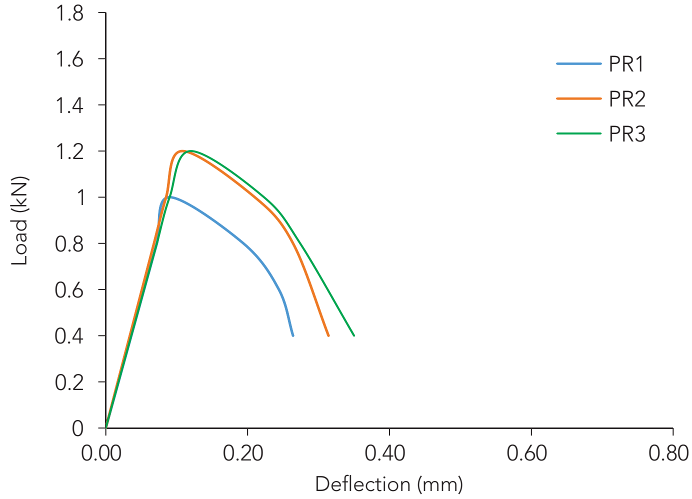

Figure 7: Load-deflection curves of polypropylene fiber-reinforced rubcrete beams

Figures 6 and 7 present the load-deflection curves of the polypropylene fiber-reinforced concrete and polypropylene fiber-reinforced rubcrete beams. From the load-deflection curve of the polypropylene fiber-reinforced concrete, it can be seen that the deflection corresponding to the peak load increased with an increase in fiber content. This is primarily because of the ability of the polypropylene fibers to hold the material constituents together until the generation of microcracks. Hence, higher energy had to be expended to break the bonds established by polypropylene fibers with other material constituents. Once the microcracks had widened, the polypropylene fibers did not have any significant effect on the behavior of concrete. For polypropylene fiber-reinforced rubcrete beams, apart from the action of polypropylene fibers, the effect of crumb rubber had resulted in a prolonged deflection at peak load. The descending part of the polypropylene fiber-reinforced concrete beams had a reduced softening trend in comparison with the descending curve of the ordinary concrete beam. The reduction in softening of the post-peak slope can be attributed to the action of the polypropylene fibers that were still able to provide some resistance to the generation of cracks. As a result, for the polypropylene fiber content of 0.2 and 0.3%, the fracture energy had shown an increase with an increase in fiber content. The maximum deflection at the failure of polypropylene fiber-reinforced rubcrete beams was 9% greater than that of polypropylene fiber-reinforced concrete beams. This combined action of polypropylene fibers and crumb rubber resulted in increased fracture energy for polypropylene fiber-reinforced rubcrete beams with an increase in polypropylene fiber content.

Figures 8 and 9 depict the load-deflection curve of steel fiber-reinforced concrete and steel fiber-reinforced rubcrete beams. It can be noticed that for steel fiber-reinforced concrete beams, the softening slope in the post-peak section of the load-deflection curve was reduced when the content of steel fibers was increased. In the case of steel fiber-reinforced

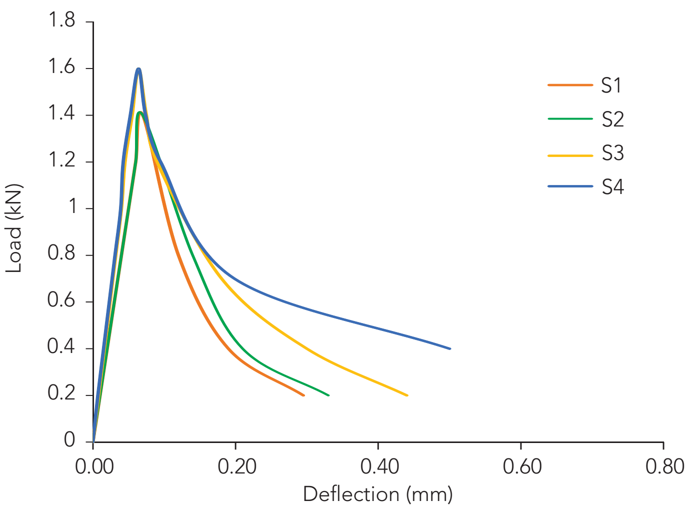

Figure 8: Load-deflection curves of steel fiber-reinforced concrete beams

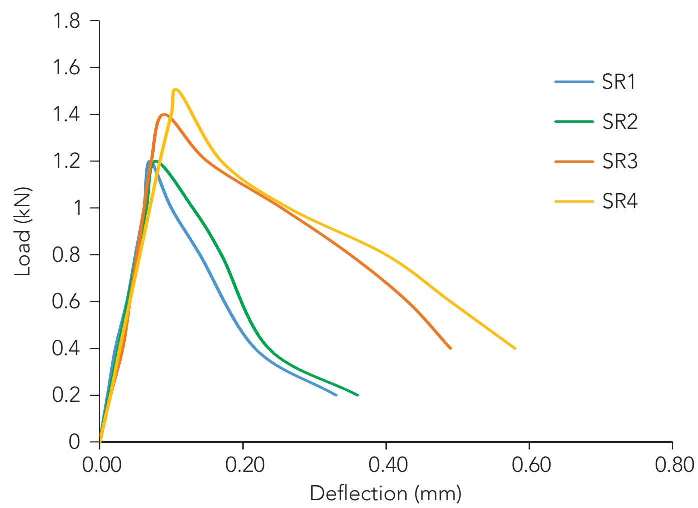

Figure 9: Load-deflection curves of steel fiber-reinforced rubcrete beams

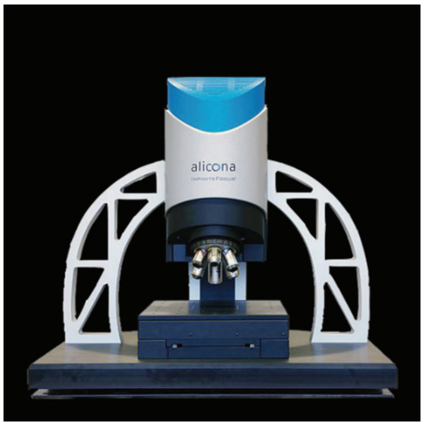

Figure 10: ALICONA instrument

rubcrete beams, the softening slope of the descending part of the curve was further reduced. The maximum deflection for steel fiber-reinforced rubcrete beams was increased by 15% for a steel fiber content of up to 0.5% when compared to that of steel fiber-reinforced concrete beams. The increase in the deflection of steel fiber-reinforced rubcrete beam having steel fiber content of 1% was 22% more than the maximum deflection of steel fiber-reinforced concrete beam having the same steel fiber content. It can be seen that the percentage increase in the maximum deflection is greater for steel fiber-reinforced rubcrete beams when compared to that of polypropylene fiber-reinforced rubcrete beams. This may be because of the ability of steel fibers to enforce macrocrack control, whereas the action of polypropylene fibers is insignificant after the peak load.

The profile of the fractured surface was obtained using the ALICONA instrument (Figure 10). The failure profile of concrete specimens subjected to the three-point bend beam test, plotted using the ALICONA instrument, is provided in Figure 11. It can be seen from the failure profile that the failure plane comprised of an even profile indicating a brittle nature of the failure. The failure profile of rubcrete specimens subjected to a three-point bend beam test can be seen in Figure 12. When compared to the profile of the failure plane of the concrete specimen, the profile of the rubcrete specimen has more consecutive troughs and peaks. The presence of these consecutive troughs and peaks indicates a less brittle failure when compared to that of the concrete specimen. As a result, the fracture energy obtained for rubcrete specimens was more than that of the concrete specimen.

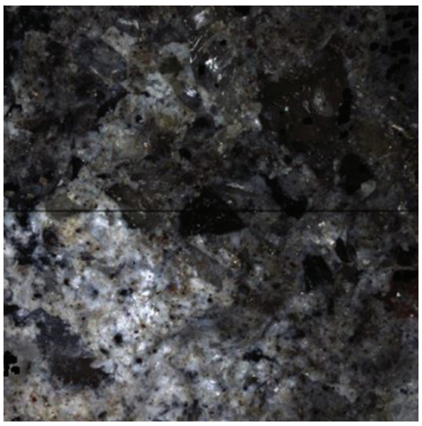

Fractured surface

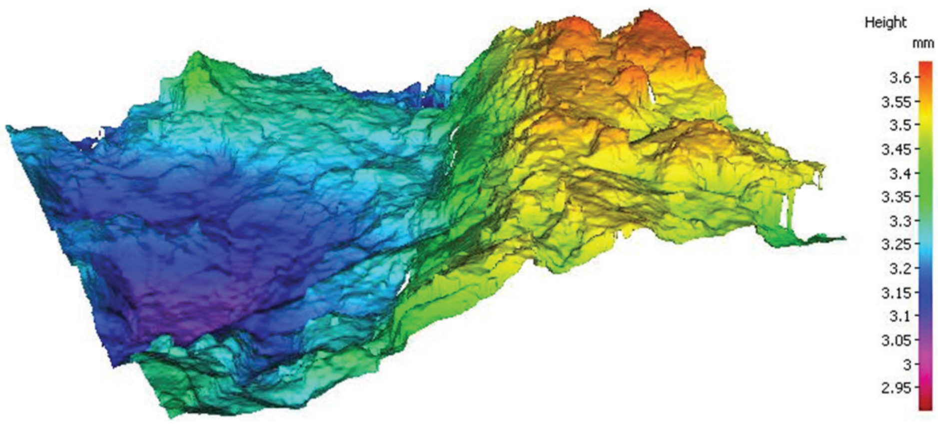

Profile of fractured surface

Figure 11: Failure profile of concrete specimen subjected to three-point bend beam test

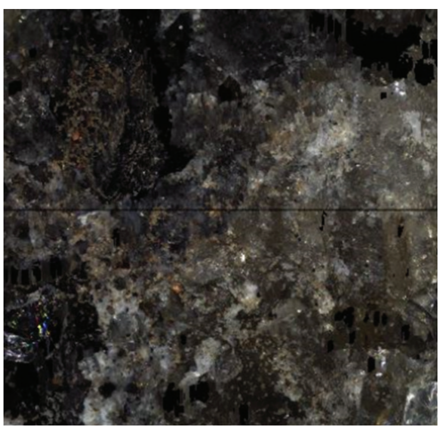

Fractured surface

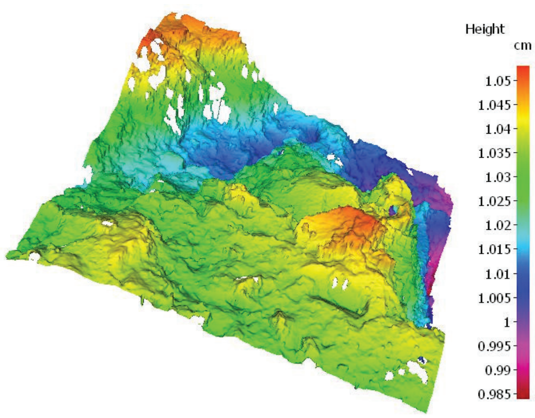

Profile of fractured surface

Figure 12: Failure profile of rubcrete specimen subjected to three-point bend beam test

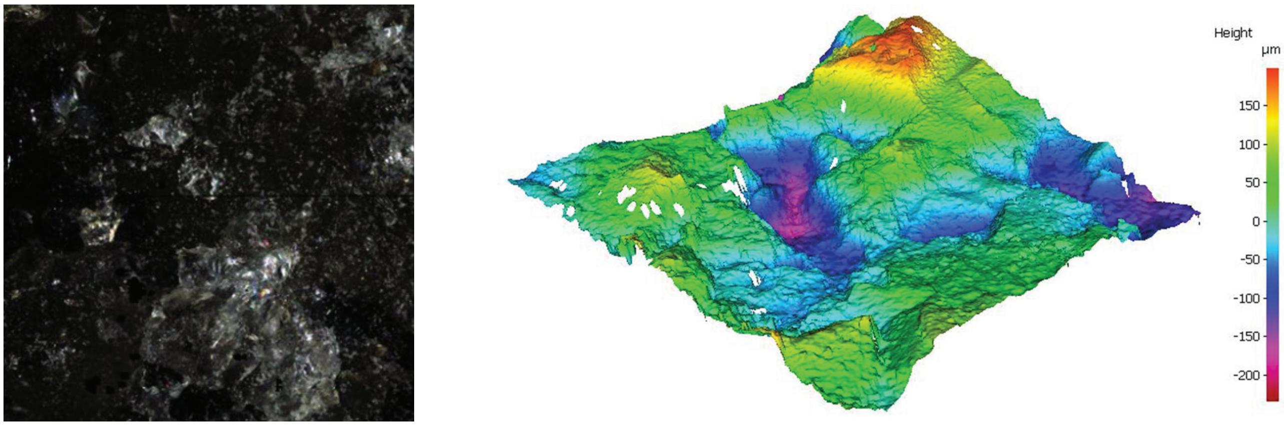

Fractured surface

Profile of fractured surface

Figure 13: Failure profile of polypropylene fiber-reinforced rubcrete specimen subjected to three-point bend beam test

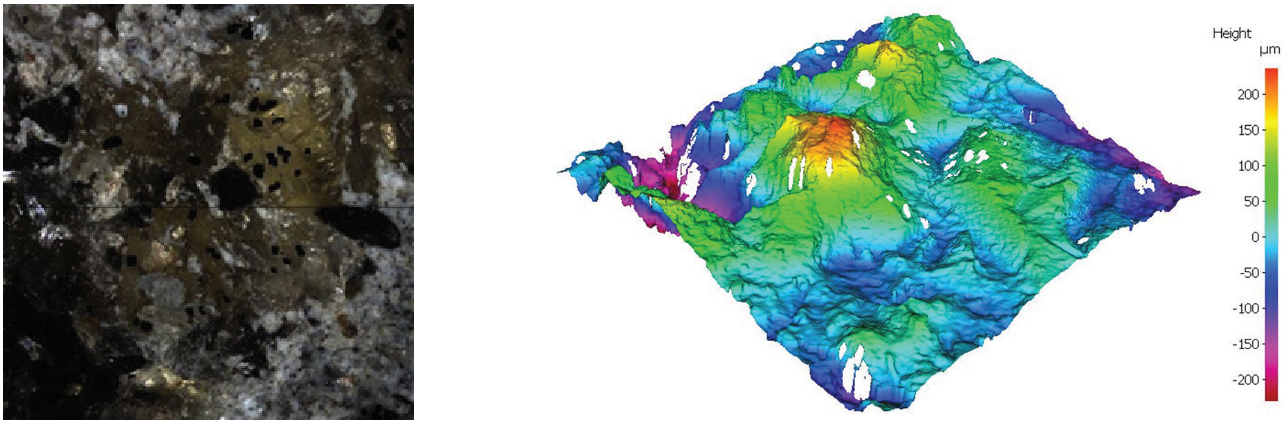

Fractured surface

Profile of fractured surface

Figure 14: Failure profile of steel fiber-reinforced rubcrete specimen subjected to three-point bend beam test

Figure 13 presents the failure profile of a portion of the polypropylene fiber-reinforced rubcrete specimen subjected to a three-point bend beam test. The profile of the failure plane of polypropylene fiber-reinforced rubcrete specimen comprised of more profound valleys and peaks when compared to that of the concrete and rubcrete specimen. This may indicate the resistance offered by the polypropylene fibers to the process of degeneration of bonds between the particles of the components of the material matrix. The failure profile of a portion of the steel fiber-reinforced rubcrete specimen, presented in Figure 14, indicates much more regular arrangement of peaks and valleys. This regular arrangement indicates the resistance offered by the bonds to failure and a predominantly ductile failure. The irregularities in the failure profiles of steel fiber-reinforced rubcrete and polypropylene fiber-reinforced rubcrete justify the increase in their fracture energies.

Table 4 shows the fracture energy absorbed by the beams. It can be noted that as the percentage of the volume of fine aggregates replaced by crumb rubber increases, the fracture energy of the specimen increases. The enhancement in the fracture energy of rubcrete beams were 4, 7, and 14% for crumb rubber content of 5, 10, and 15%, respectively. Improvement in fracture energy of steel fiber-reinforced concrete specimens were by 9, 22, 39, and 56% for the steel fiber content of 0.25, 0.5, 0.75, and 1%, respectively. For steel fiber-reinforced rubcrete beams with 15% replacement of fine aggregates by crumb rubber, improvement of 16, 31, 83, and 99% was observed in fracture energy for the steel fiber content of 0.25, 0.5, 0.75, and 1%, respectively. No significant improvement in fracture energy was noted for polypropylene fiber-reinforced concrete beams with 0.1% polypropylene fiber content in comparison with the fracture energy of ordinary concrete beams. Enhancement in fracture energy was 21 and 27% for polypropylene fiber-reinforced concrete beams with 0.2 and 0.3% polypropylene fiber content, respectively. For polypropylene fiber-reinforced rubcrete beams, the fracture energy was improved by 23, 51, and 26% for polypropylene fiber content of 0.1, 0.2, and 0.3%, respectively.

Table 4: Fracture energy absorbed by beams

SPECIMEN ID	TOTAL WORK DONE (Nm)	FRACTURE ZONE PROJECTION (m^2)	FRACTURE ENERGY (Nm/m^2)	% INCREASE
R1	0.196	0.0042	46.31	0.00
R2	0.2025	0.0042	48.21	4.10
R3	0.2098	0.0042	49.95	7.86
R4	0.222	0.0042	52.86	14.14
S1	0.212	0.0042	50.48	9.00
S2	0.239	0.0042	56.9	22.87
S3	0.2712	0.0042	64.5	39.28
S4	0.3027	0.0042	72.5	56.55
SR1	0.2405	0.0042	53.8	16.17
SR2	0.294	0.0042	60.9	31.51
SR3	0.305	0.0042	84.9	83.33
SR4	0.3887	0.0042	92.5	99.74
P1	0.1905	0.0042	45.3	-2.18
P2	0.236	0.0042	56.19	21.33
P3	0.2484	0.0042	59.14	27.70
PR1	0.2405	0.0042	57.26	23.65
PR2	0.294	0.0042	70	51.16
PR3	0.305	0.0042	72.6	56.77

Table 5 presents the characteristic fracture length obtained for the materials. It can be seen that 32% improvement was noticed in the characteristic fracture length of rubcrete with 15% crumb rubber when compared to that of concrete. The characteristic fracture length of steel fiber-reinforced concrete was improved by 52% when compared to that of concrete when the steel fiber content was 1%. An enhancement of 100% was obtained in the characteristic fracture length of steel fiber-reinforced rubcrete with 1% steel fiber content and 15% crumb rubber. The polypropylene fiber-reinforced rubcrete beams and polypropylene fiber-reinforced concrete beams showed an improvement of 72 and 28%, respectively, when their characteristic fracture length was compared with that of concrete. An increase in characteristic fracture length indicates improvement in ductility of the material. Hence, it can be noticed that significant improvement in ductility can be obtained when steel fiber-reinforced rubcrete beams having steel fiber content of 1% and crumb rubber content of 15% are used instead of concrete.

4. CONCLUSION

Three-point bend beam tests were conducted on 18 beams of dimension of 60 × 100 × 500 mm made of steel and polypropylene fiber-reinforced rubcrete mixes of grade M 20. The characteristic fracture length of the materials was

Table 5: Characteristic fracture length of materials

SPECIMEN ID	FRACTURE ENERGY (Nm/m^2)	MODULUS OF ELASTICITY (N/mm^2)	TENSILE STRENGTH OF MIXES (N/mm^2)	CHARACTERISTIC FRACTURE LENGTH (mm)	% INCREASE
R1	46.31	29580.4	4.14	79.9	0
R2	48.21	29154.76	4.08	84.4	6
R3	49.95	27386.13	3.83	93.1	17
R4	52.86	25495.1	3.57	105.8	32
S1	50.48	29580.4	4.14	87.1	9
S2	56.9	30000	4.20	96.8	21
S3	64.5	30413.81	4.26	108.2	35
S4	72.5	30413.81	4.26	121.6	52
SR1	53.8	28722.81	4.02	95.6	20
SR2	60.9	29580.4	4.14	105.0	32
SR3	84.9	30000	4.20	144.4	81
SR4	92.5	29580.4	4.14	159.5	100
P1	45.3	28722.81	4.02	80.5	1
P2	56.19	29154.76	4.08	98.3	23
P3	59.14	29580.4	4.14	102.0	28
PR1	57.26	25495.1	3.57	114.6	43
PR2	70	25980.76	3.64	137.5	72
PR3	72.6	26925.82	3.77	137.6	72

determined to assess the ductility of the beams. The major conclusions from the study are as follows.

- The fracture energy of rubcrete beams increased with an increase in the percentage replacement of fine aggregates with crumb rubber. In the case of rubcrete beams, the fracture energy was increased by 14% for rubcrete beams with 15% crumb rubber. The characteristic fracture length was increased by 32%.
- For polypropylene fiber-reinforced concrete beam with 0.3% polypropylene fiber content, the fracture energy was improved by 27%. In the polypropylene fiber-reinforced rubcrete beam with 15% crumb rubber content and 0.3% polypropylene fibers, the enhancement in fracture energy was 57%. Improvement in characteristic fracture length of 28 and 72%, respectively, was observed for polypropylene fiber-reinforced concrete and polypropylene fiber-reinforced rubcrete, respectively.
- The fracture energy and characteristic fracture length of steel fiber-reinforced concrete with 1% steel fiber content were enhanced by 56 and 52%, respectively, over that of ordinary concrete. The fracture energy and characteristic fracture length of steel fiber-reinforced rubcrete with 1% steel fiber content and 15% crumb rubber content was, respectively, 92 and 100% more than that of the ordinary concrete.
- A notable improvement in ductility can be obtained when steel fiber-reinforced rubcrete beams with a steel fiber content of 1% and crumb rubber content of 15% are used instead of concrete beams.

It can be concluded that the increased fracture energy of fiber-reinforced rubcrete makes it suitable for application in structures which require significant energy absorption. The use of fiber-reinforced rubcrete results in limiting the exploitation of fine aggregates. Thus, fiber-reinforced rubcrete helps to sustain the precious natural resource.

REFERENCES

[1] Kumar, P. and Kaushik, S. K. (2003). "Some trends in the use of concrete: Indian scenario", *The Indian Concrete Journal*, Vol. 77, pp. 1503-1508.

[2] Aïtcin, P. C. (2000). "Cements of yesterday and today", *Cement and Concrete Research*, Vol. 30, pp. 1349-1359.

[3] Monteiro, P. J. M., Miller, S. A., and Horvath, A. (2017). "Towards sustainable concrete", *Nature Materials*, Vol. 16, pp. 698-699.

[4] Kotsovos, M. D. (1984). "Concrete. A brittle fracturing material", *Matériaux et Constructions* , Vol. 17, pp. 107-115.

[5] Pietruszczak, S. and Xu, G. (1995). "Brittle response of concrete as a localization problem", *International Journal of Solids and Structures*, Vol. 32, pp. 1517-1533.

[6] Shah, S. P. and Rangan, B. V. (1970). "Effects of reinforcements on ductility of concrete", *Journal of the Structural Division*, Vol. 96, pp. 1167-1184 .

[7] Lok, T. S. and Pei, J. S. (1996). "Impact resistance and ductility of steel fiber-reinforced concrete panels", *Transactions*, Vol. 3, pp. 7-16.

[8] Balendran, R. V., Zhou, F. P., Nadeem, A., and Leung, A. Y. T. (2002). "Influence of steel fibers on strength and ductility of normal and lightweight high strength concrete", *Building and Environment*, Vol. 37, pp. 1361-1367.

[9] Son, K. S., Hajirasouliha, I., and Pilakoutas, K. (2011). "Strength and deformability of waste tyre rubber-filled reinforced concrete columns", *Construction and Building Materials,* Vol. 25, pp. 218-226.

[10] Kaloush, K. E., Way, G. B., and Zhu, H. (2005). "Properties of crumb rubber concrete", *Transportation Research Record*, pp. 8-14, doi:10.3141/1914-02.

[11] Youssf, O., Hassanli, R., Mills, J. E., and Abd Elrahman, M. (2018). "An experimental investigation of the mechanical performance and structural application of LECA-Rubcrete", *Construction and Building Materials*, Vol. 175, pp. 239-253.

[12] Siddique, R. and Naik, T. R. (2004). "Properties of concrete containing scrap-tire rubber-an overview", *Waste management*, Vol. 24, pp. 563-569.

[13] Ganesan, N., Raj, J. B., and Shashikala, A. P. (2013). "Flexural fatigue behavior of self compacting rubberized concrete", *Construction and Building Materials,* Vol. 44, pp. 7-14.

[14] Ding, Y. and Kusterle, W. (2000). "Compressive stress-strain relationship of steel fiber-reinforced concrete at early age", *Cement and Concrete Research*, Vol. 30, pp. 1573-1579.

[15] Bisht, K. and Ramana, P. V. (2017). "Evaluation of mechanical and durability properties of crumb rubber concrete", *Construction and Building Materials*, Vol. 155, pp. 811-817.

[16] Zhang, S. and Zhao, B. (2012). "Influence of polypropylene fiber on the mechanical performance and durability of concrete materials", *European Journal of Environmental and Civil Engineering*, Vol. 16, pp. 1269-1277.

[17] Cifuentes, H., García, F., Maeso, O., and Medina, F. (2013)."Influence of the properties of polypropylene fibers on the fracture behavior of low-, normal- and high-strength FRC", *Construction and Building Materials*, Vol. 45, pp. 130-137.

[18] Barros, J. A. O. and Senacruz, J. (2001). "Fracture energy of steel fiber-reinforced concrete", *Mechanics of Composite Materials and Structures*, Vol. 8, pp. 29-45.

[19] Kazmi, S., Junaid, M., Wu, Y., and Patnaikuni, I. (2018). "Effect of macro-synthetic fibers on the fracture energy and mechanical behavior of recycled aggregate concrete", *Construction and Building Materials*, Vol. 189, pp. 857-868.

[20] Peterson, P. E. (1980). "Fracture energy of concrete: Method of determination", *Cement and Concrete Research*, Vol. 10, pp. 79-89.

[21] Hillerborg, A. (1985). " The theoretical basis of a method to determine the fracture energy G_F of concrete", *Materials and Structures*, Vol. 18, pp. 291-296.

[22] Bazant, Z. P. (1996). "Analysis of Work-of-Fracture Method for measuring fracture energy of concrete", *Journal of Engineering Mechanics*, pp. 138-144.

[23] Ghasemi, M., Ghasemi, M. R., and Mousavi, S. R. (2018). "Investigating the effects of maximum aggregate size on self-compacting steel fiber reinforced concrete fracture parameters", *Construction and Building Materials*, Vol. 162, pp. 674-682.

[24] Raisi, E. M., Amiri, J. V., and Davoodi, M. R. (2018). "Influence of rice husk ash on the fracture characteristics and brittleness of self-compacting concrete", *Engineering Fracture Mechanics*, Vol.199, pp. 595-608.

[25] Ríos, J. D., Cifuentes, H., Leiva, C., and Seitl, S. (2019). "Analysis of the mechanical and fracture behavior of heated ultra-high-performance fiber-reinforced concrete by X-ray computed tomography", *Cement and Concrete Research*, Vol. 119, pp. 77-88.

[26] Wittmann, F. H., Mihashi, H., and Nomura, N. (1990). "Size effect on fracture energy of concrete", *Engineering Fracture Mechanics*, Vol. 35, pp. 107-115.

[27] Alyhya, W. S., Dhaheer, M. S. A., and Karihaloo, B. L. (2016). "Influence of mix composition and strength on the fracture properties of self-compacting concrete", *Construction and Building Materials*, Vol. 110, pp. 312-322.

[28] Noaman, A. T., Bakar, B. H. A., Akil, H., and Alani, A. H. (2017). "Fracture characteristics of plain and steel fiber-reinforced rubberized concrete", *Construction and Building Materials*, Vol. 152, pp. 414-423.

[29] 50-FMC Draft Recommendation (RILEM). (1985). "Determination of the fracture energy of mortar and concrete by means of three-point bend tests on notched beams", *Mat~riaux et Constructions*, Vol. 8, pp. 285-296.

ANAND RAJ holds a B.Tech. Degree in Civil Engineering and M.Tech. Degree in Computer Aided Structural Engineering from Mahatma Gandhi University Kottayam, Kerala, India. Currently, he is pursuing Ph.D. Degree in the Department of Civil Engineering, National Institute of Technology Calicut (NITC). His research interests are in the area of fiber-reinforced concrete, rubcrete, and impact studies on structures. Email: anandrajce@gmail.com

PRAVEEN NAGARAJAN is a Professor in Civil Engineering Department at National Institute of Technology Calicut (NITC), India. His current research interests are in the area of reinforced and prestressed concrete, bridge engineering, and structural reliability. Email: praveen@nitc.ac.in

A. P. SHASHIKALA is a Professor (HAG) in Civil Engineering Department at National Institute of Technology Calicut (NITC), India. Her current research interests are in the area of structural dynamics, multibody offshore structures, and floating structures. Email: apska@nitc.ac.in

Cite this article: Raj, A., Nagarajan, P., Shashikala, A. P. (2021). "Fracture studies on fiber-reinforced rubcrete", *The Indian Concrete Journal*, Vol. 95, No. 6, pp. 37-46.

PERFORMANCE OF POLYMER-MODIFIED FIBER-REINFORCED HIGH STRENGTH CONCRETE

PRAPHULLA K. DESHPANDE*,
KESHAV K. SANGLE,
YUWARAJ M. GHUGAL

Abstract

This paper presents the results of polymer-modified fiber-reinforced concrete (PMFRC). The various strengths considered in this investigation are compressive, flexural, and shear strengths. The regimes of dry air curing are 28 days and 90 days. The M-40 grade of concrete is used as a reference mix. The fiber content was varied from 1% to 10% by weight of cement at the interval of 1% with 5% constant dosage of SBR (Styrene Butadiene Rubber) polymer. Cubes, prisms, and push-off specimens were prepared and tested subsequently at the ages of 28 days and 90 days. The significant improvement in compressive, flexural, and shear strengths, as well as ductility and toughness is observed due to synergistic effect of polymer and fibers. The results of effect of number and pull-out length of fibers on failure plane are presented.

Keywords: Polymer, PMFRC, Deformations, Strengths, Toughness, Stress-strain, Number of fibers.

1. INTRODUCION

Concrete is widely used as a construction material in the world, and it is very difficult to find another material of construction as versatile as concrete. Though concrete is versatile material, it suffers from delayed hardening, low tensile strength, large drying shrinkage, and low chemical resistance. The use of high strength and high stiffness structural fibers in concrete resultes in composite materials with substantial improvement in the mechanical properties such as strengths, toughnesses, and durability of concrete structures due to crack arresting mechanism being developed in concrete matrix.

Addition of fibers in concrete reduces workability and increases the air content in the matrix, which results in reduction of various strengths. Due to balling effect of fibers, there is no effective dispersion of fibers in the concrete matrix. Also, the interface transition zone between fiber and cement substrate is associated with the large number of pores, giving rise to the weak bonding among cement hydrates, fibers, and aggregates.

Addition of polymer into the fiber-reinforced concrete (FRC) improves workability of fresh mix, reduces the air content and drying shrinkage, improves the impermeability, and improves the pore structure of the matrix and the bond strength between the cement hydrates, aggregates, and the fibers, and may thus offer the potential advantage of more uniform dispersion of the fibers in composites prepared by mixing, as well as facilitate the incorporation of greater fiber contents.

Comprehensive reviews on the use of polymer-based admixtures in cement mortar and concrete, and properties of polymer-modified concretes are given by Ohama [1,2], Kardon [3], and Beaudoin [4].

Li *et al.* [5] studied the properties of polymer-modified steel fiber-reinforced cement concretes such as compressive strength, flexural strength, and microstructure of the concrete. The flexural strength and pore size distribution were shown to be improved significantly at 5% of SBR latex. Kalwane *et al.* [6, 7] investigated the synergistic effect of steel fibers and polymer (SBR latex) on compressive, flexural, shear, bond strength, and corresponding toughnesses of polymer-modified fiber-reinforced concrete, and showed significant improvement in these properties as a synergistic effect of fibers and polymer. Lin *et al.* [8] and Issa *et al.* [9] studied the properties of concrete overlays for polymer and steel fiber. It was shown that the concrete composites produced had lower shrinkage and permeability properties with high bond strength and high cracking resistance.

Chen and Liu [10] studied the effect of curing conditions and polymer-cement ratio on the compressive and flexural strengths of polymer-modified concrete. It was shown that combined dry and wet curing enabled the development in both the strengths of cement matrix and SBR films together. Significant increase in compressive and flexural strength was observed at 7 days wet curing and 21 days dry curing and 1 day dry, 3 days wet, and 24 days dry curing, respectively. Wang *et al.* [11] studied the physical and chemical modification mechanism of polymer latex-modified cement, which were responsible for covering of surface of crystals, filling the cracks and pores, and formation

*Corresponding author : Praphulla K. Deshpande, Email: pkdeshpande_p17@st.vjti.ac.in

Table 1: Properties of fiber and polymer

SR. NO.	PROPERTIES OF STEEL FIBER		PROPERTIES OF POLYMER SBR LATEX	
	PROPERTIES	RESULTS	PROPERTIES	RESULTS
1	Thickness of fiber (t_f)	1 mm	Name	SBR latex
2	Length of fiber (l_f)	50 mm	Appearance	Milky white
3	Equivalent diameter (d_f)	1.66 mm	Particle size	0.22 µm
4	Aspect ratio ($\lambda = l_f / d_f$)	30	Total solids	44%
5	Modulus of elasticity	200 GPa	Water content	56%
6	Tensile strength	>1100 MPa	Specific gravity (at 20°C)	1.01
7	Deformation	6 undulation	pH	11
8	Number of fibers per kg	2850	Viscosity (at 20°C)	20 Cp

of 3D network structure with the hydration products, and both the mechanisms led to increase in flexural strength. Karadelis and Lin [12] studied the flexural strength, shear strength, bond strength, and fiber efficiency of steel fiber-reinforced roller compacted polymer-modified concrete. It was shown that the new material developed for structural material exhibited a significant improvement in strengths and cracking resistance.

Xu *et al.* [13], Xu *et al.* [14], Chakraborty *et al.* [15], Huang *et al.* [16], Ghugal [17], and Bijen [18] studied the properties of polymer-modified fiber-reinforced concrete with non-metallic fibers. The improvement in various properties was observed in this fiber polymer concrete system.

Meraj *et al.* [19] studied flexural behavior of latex-modified steel fiber-reinforced concrete. It was shown that the neglect of fiber and latex contribution may considerably underestimate the flexural strength. It was also shown that the ductility in latex-modified fiber-reinforced concrete was increased by 50.27%.

It is observed from the literature survey that the use of steel fibers and SBR latex polymer has been proved to be effective in improving the mechanical properties of concrete and durability of concrete composites. However, the studies on high strength fiber-reinforced concrete with high fiber volume fractions and SBR latex are limited. Hence, the objective of this study is to investigate the various strengths, ductility, and toughness with synergistic effect of polymer and steel fibers with high fiber volume fractions.

The novelty of the present investigation is that the concrete composite with high fiber volume fraction is developed successfully with the addition of SBR latex (polymer). The strength, deformation, and toughness characteristics of the present concrete composite system with high fiber volume fraction are examined critically and presented precisely in this investigation. To predict the flexural strength and shear strength, new expressions are presented in terms of compressive strength and fiber volume fraction using regression analysis. The observations on the fiber pull-out length with number of fibers across the failure planes are presented for the first time and related to the failure of the present composite material under flexure and shear along with the critical length of fiber.

2. EXPERIMENTAL PROGRAMME

Materials: Ordinary Portland cement with 53 grade confirming to IS:12269 [20] and fine and coarse aggregates confirming to IS:383 [21] were used. The fineness modulus of sand was 2.9 and those of 10 mm and 20 mm coarse aggregates were 6.87 and 7.25, respectively. Crimped steel fibers confirming to ASTM A-820 [22] and varying from 1% to 10% and Styrene Butadiene Rubber (SBR) Latex with constant dosage of 5% by weight of cement were used with material properties as shown in Table 1.

Concrete composite: The M-40 grade of concrete having mix proportion of 1: 2.52: 0.68: 1.02, i.e. cement: fine aggregate: coarse aggregate (20 mm: 10 mm) with w/c ratio of 0.38 was used throughout the experimental investigation. The concrete mix design was carried out according to IS:10262 [23]. Fibers were added in dry state of concrete mix and again ingredients were mixed thoroughly. The water modified by 5% polymer of weight of cement was added to the dry mix and the ingredients were mixed thoroughly to obtain the homogeneous, cohesive, and workable mix. The mixing time after addition of polymer-modified water was kept strictly constant. The water contained in the polymer was included in the total water content of the mix. A water-cement ratio of 0.38 used for normal concrete was kept constant for polymer-modified fiber-reinforced concrete (PMFRC) by considering water present in the polymer (SBR latex).

Specimens: Cubes of 150 mm size for compressive strength, beams of size of 150 × 150 × 700 mm for flexural strength, and push-off specimens of size of 150 × 150 × 450 mm for shear strength were cast incorporating 1% to 10% crimped steel fibers at the interval of 1% by weight of cement. For each test, three specimens were cast with and without fibers. Compaction of all

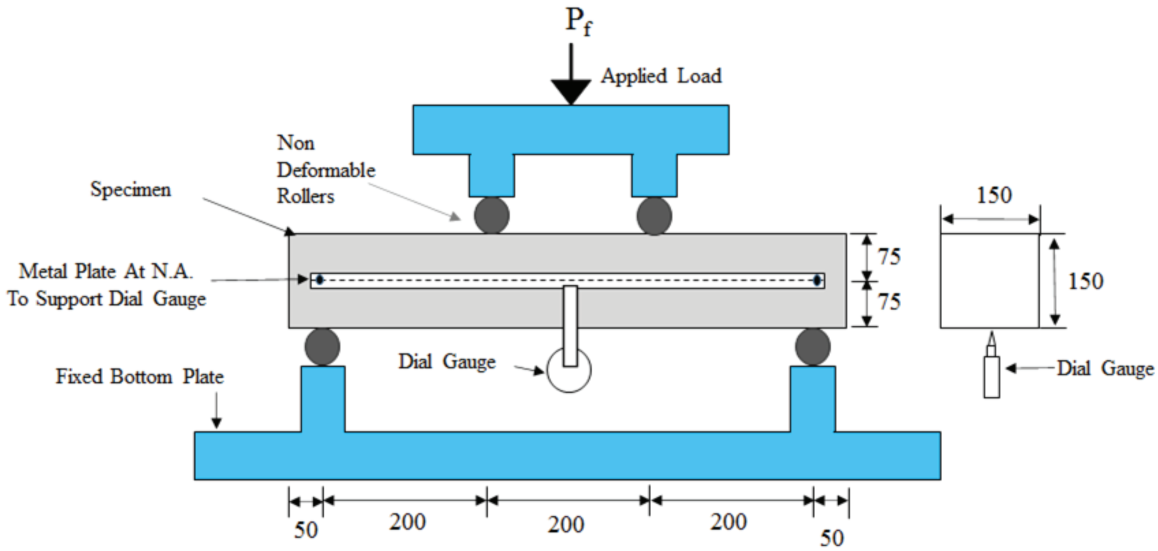

Figure 1: Four-point bending test setup (all dimensions are in mm)

the specimens was done using table vibrator to avoid balling of fibers. Specimens with polymer content, after demoulding, were moist cured for 3 days and air cured for remaining ages. Normal concrete specimens were water cured up to 28 days and 90 days, respectively. All the specimens were tested subsequently at the desired age of curing. Each value of the results presented in this paper is the average of three test samples.

2.1 Test Conducted

2.1.1 *Compressive strength test on cube*

The cube compression test was performed to find out compressive strength of normal concrete, polymer-modified concrete, and polymer-modified steel fiber-reinforced concrete using cube specimens confirming to IS: 516 [24]. The test was carried out using compression testing machine of capacity of 2000 kN. Loads and deformations were recorded to study the elastic behavior of PMSFRC under compression in elastic range and post-peak range. The compressive strength results are shown in Table 2.

2.1.2 *Flexural strength test on beam*

To find out flexural strength of concrete, prism specimens of size of 150 × 150 × 700 mm were used and tested according to IS: 516 [24]. The arrangement for loading of flexure test specimen is shown in Figure 1.

The flexural strength of the beam, expressed as the modulus of rupture (f_{cr}), is calculated by using the following formula as per strength of material theory.

$$f_{cr} = \frac{P_f L}{bd^2} \tag{1}$$

In this test, deflections have been recorded with reference to neutral axis of the beam to get the correct load-deflection behavior and to compute the correct flexural toughness using load-deflection graphs. The flexural strength results are shown in Table 2.

2.1.3 *Shear test on push-off type specimen*

To find out shear strength of concrete, push-off type specimen was designed according to information available in the literature [25, 26, 27, 28, 29] as shown in Figure 2(a). The specimen was designed to fail in shear only with a shear plane of size 150 × 150 mm. The vertical reinforcement was provided in all push-off specimens to eliminate any possible failure modes other than shear alone as shown in Figure 2(b). The shear strength of the concrete is determined by the formula:

$$\tau_s = \frac{P_s}{A_s} \cdot \tag{2}$$

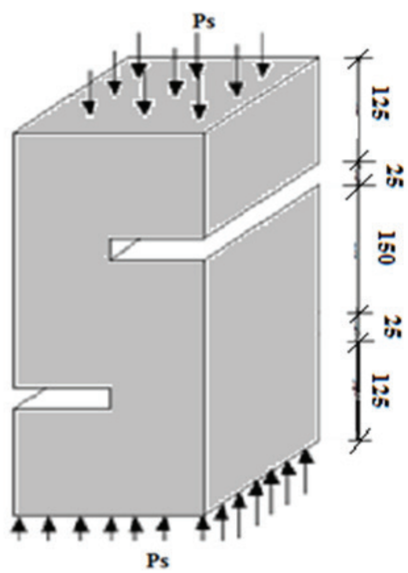

Figure 2(a): Push-off type specimen (all dimensions in mm)

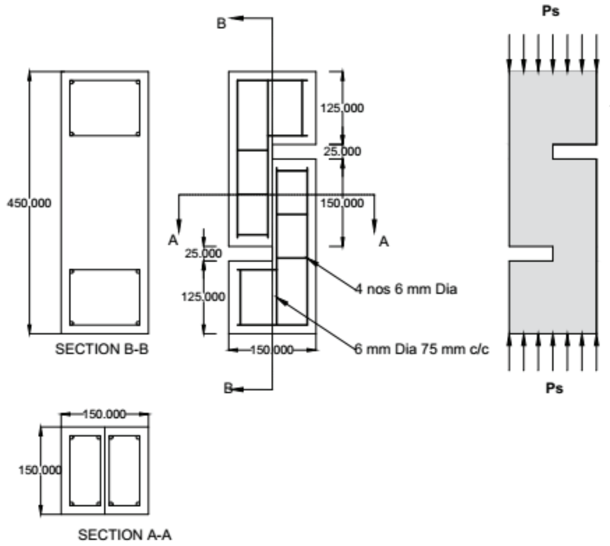

Figure 2(b): Reinforcement in push-off specimen for shear strength

In this test, shear deformations/vertical slip (shear strain) have been recorded to obtain the stress-strain behavior under single shear. The shear strength results are shown in Table 2.

3. RESULTS AND DISCUSSION

3.1 Compressive Strength

Compressive strength (f_{cu}) of normal concrete, PMC, and PMFRC results are shown in Table 2, and stress-strain behavior is shown in Figure 3. It is observed that the compressive strength of PMC slightly decreased as compared to normal concrete for 28 days; however, for 90 days, it increased marginally. At 28 days and 90 days, the maximum percentage increase of 10.84% and 21.35% in compressive strength, respectively, as compared to normal concrete, was observed at 2% of fiber content and then decreased continuously up to 10% of fiber content. However, the strengths of PMFRC with 8% and 10% fiber contents at 28 days and 90 days, respectively, are still higher than the target design strength of reference mix which satisfy the acceptance criteria. The compressive strength of PMFRC does not increase substantially over normal concrete. The decrease in compressive strength may be attributed to the increased air content due to increase in fiber content.

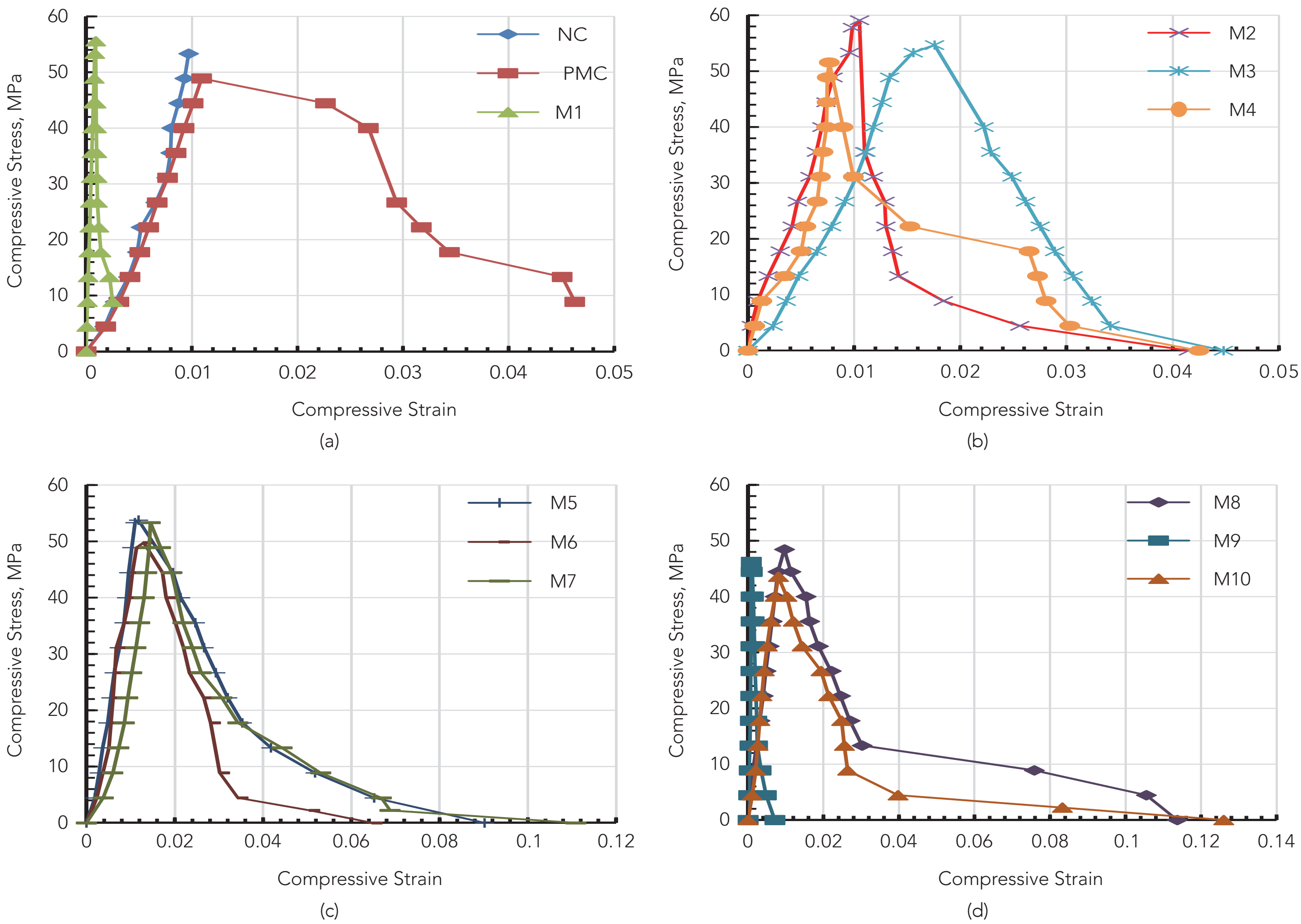

Figure 3: Variation of compressive stress with compressive strain at 28 days

The variation of compressive stress with compressive strain showed the well-defined elastic behavior up to first crack and strain softening in post-peak range as can be seen from Figures 3(a)-(d). In these curves, a substantial increase in the strain at the peak stress can be noted, and the slope of the descending portion is more steep with increased strain than that of PMC. This is indicative of substantially higher toughness, where toughness is a measure of ability to absorb energy during deformation, and it can be estimated from the area under the stress-strain curves. Normal concrete does not show any post-peak behavior.

3.2 Flexural Strength

The results of flexural strength (f_{cr}) of normal concrete, polymer-modified concrete (PMC), and polymer-modified fiber-reinforced concrete (PMFRC), and results of correlation constant, k_{cr}, between the flexural strength and compressive strength of concrete are presented in Table 2, whereas load-deflection behavior is shown in Figure 4.

It is observed that addition of steel fibers increased the flexural strength continuously up to 10% fiber content. For 28 days and 90 days, the maximum flexural strength was achieved at 10% fiber content, which was 5.97 MPa and 7.94 MPa, i.e. 27.29% and 30.59% increase over normal concrete, respectively. This increase may be attributed to the improved crack resistance mechanism, improved bond strength between the fiber and matrix with increased fiber content, and its uniform dispersion due to addition of polymer.

The variation of flexural load with deflection up to first crack showed increased flexural stiffness with decrease in deflection. Softening of deflection in post-peak range is observed as seen from Figures 4(a)-(d).

Normal concrete, polymer-modified concrete, and concrete with 1% of fiber content showed first crack and peak flexural strengths with marginal increase in flexural load between first crack and peak crack range [see Figure 4(a)], whereas in case of PMFRC specimens, substantial increase in flexural load is observed with increase in deflection due to strain hardening phenomenon as seen from Figures 4(b)-(d). In post-peak range,

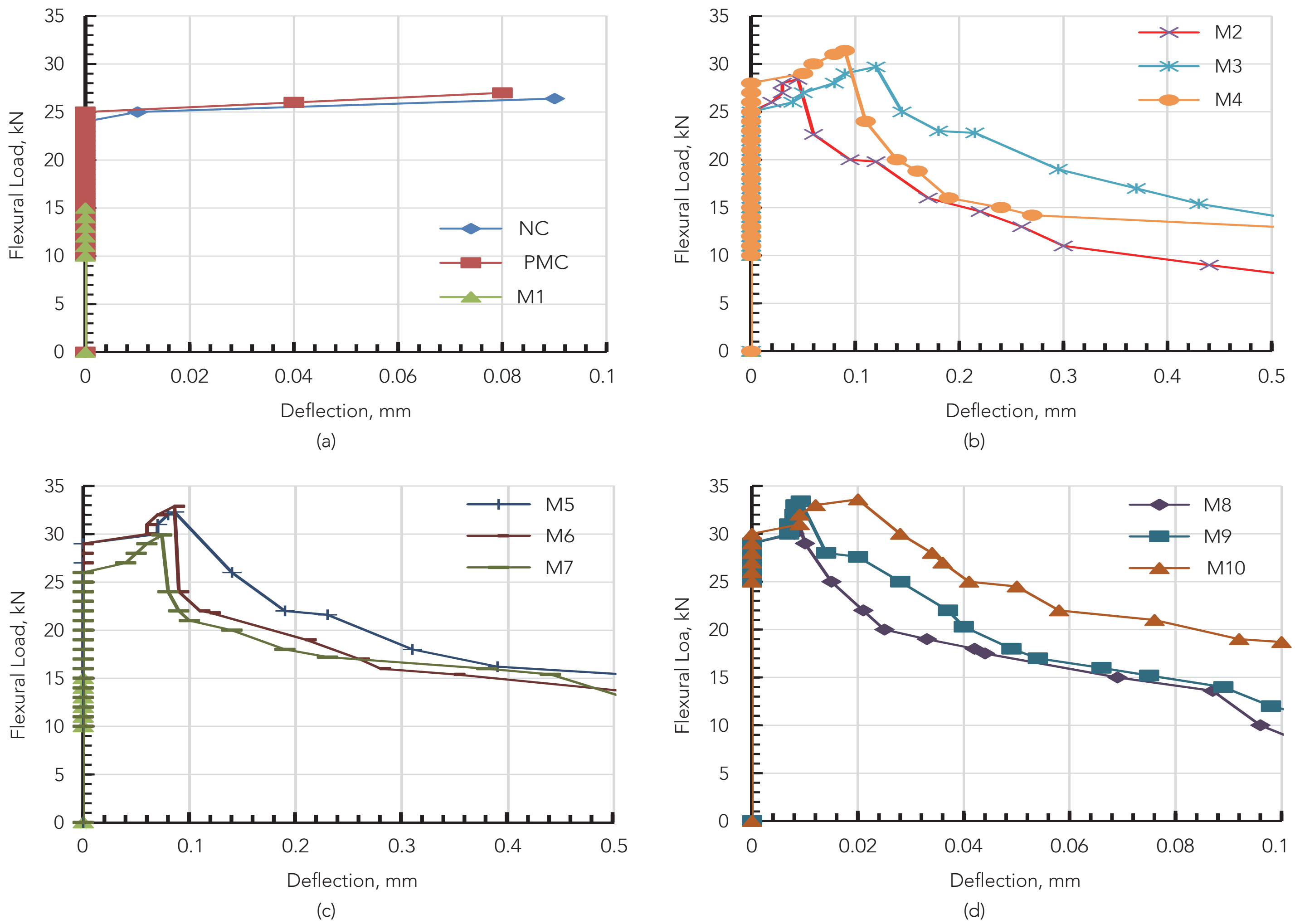

Figure 4:. Variation of flexural load with deflection at 28 days

softening of deflection is observed in all PMFRC specimens except M1 as seen from Figures 4(b)-(d).

The flexural strength of concrete is expressed in terms of compressive strength with the help of correlation constant (k_{cr}) at various fiber contents. The relation between correlation constant (k_{cr}) and fiber content (V_f%) is presented in Figure 5. The empirical relations for flexural strength in terms of fiber content and compressive strength are developed using regression analysis as follows.

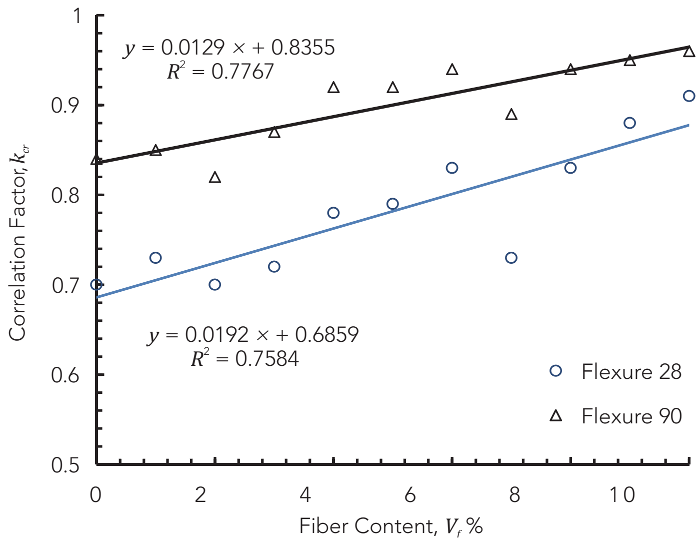

Figure 5: Variation of correlation factor with fiber content in flexure

$$f_{cr} = (0.6859 + 0.0192V_f)\sqrt{f_{cu}},\quad R^2 = 0.7584 \text{ for 28 days.} \qquad 3(a)$$

$$f_{cr} = (0.8355 + 0.0129V_f)\sqrt{f_{cu}},\quad R^2 = 0.7767 \text{ for 90 days.} \qquad 3(b)$$

The regression analysis shows linear relationship with square root of compressive strength as given by equations 3(a) and (b).

3.3 Shear Strength Using Push-off Specimen

The results of shear strength (τ_s) of normal concrete, PMC, and PMFRC, and results of correlation constant, k_s, between the shear strength and compressive strength of concrete are shown in Table 2, whereas stress-strain behavior is shown in Figure 6. It is observed that addition of steel fibers increased the shear strength continuously up to 4% and 6% fiber contents at 28 days and 90 days, respectively. The maximum percentage increase in shear strength of 20.81% and 32.73% over normal concrete was observed at 28 days and 90 days, respectively. This increase may be attributed to the improved fiber bridging mechanism across the shear plane, improved bond strength between the fiber and matrix with increased fiber content, and its uniform dispersion due to addition of polymer.

As excepted, shear failure in NC and PMC was sudden and catastrophic. The specimen lost its capacity to carry load instantly without a residual load-carrying capacity beyond the peak load, and this occurred within the range of 1 mm to 2.6 mm of shear strain [see Figure 6(a)]. The variation of shear stress with shear strain showed elastic behavior up to first crack. Normal concrete, polymer-modified concrete, and concrete with 1% fiber content do not show post-peak variation of shear strain.

Table 2: Compressive, flexural, and shear strengths of normal concrete (NC), polymer-modified concrete (PMC), and polymer-modified fiber-reinforced concrete (PMFRC), as well as correlation constant (k_{cr}) for flexure and k_s for shear

FIBER CONTENT V_f (%)	COMPRESSIVE STRENGTH f_{cu} (MPa)		FLEXURAL STRENGTH f_{cr} (MPa)		$k_{cr} = f_{cr} / \sqrt{f_{cu}}$		SHEAR STRENGTH τ_s (MPa)		$k_s = \tau_s / \sqrt{f_{cu}}$	
	28 DAYS	90 DAYS	28 DAYS	90 DAYS	28 DAYS	90 DAYS	28 DAYS	90 DAYS	28 DAYS	90 DAYS
0 (NC)	53.33	54.55	4.69	6.08	0.67	0.82	4.71	5.50	0.64	0.74
Mp (PMC)	48.89	55.01	4.80	6.27	0.70	0.84	5.11	5.82	0.73	0.78
1	55.55	62.77	5.42	7.02	0.73	0.85	5.24	6.03	0.70	0.73
2	59.11	66.20	5.05	6.54	0.70	0.82	5.33	6.13	0.69	0.75
3	54.66	62.04	5.28	6.87	0.72	0.87	5.56	6.26	0.75	0.81
4	53.77	58.76	5.58	7.29	0.78	0.92	5.69	6.43	0.78	0.82
5	53.33	62.10	5.74	7.49	0.79	0.92	5.56	6.61	0.76	0.86
6	51.55	57.73	5.85	7.71	0.83	0.94	5.02	7.30	0.69	0.93
7	49.77	61.59	5.31	6.88	0.73	0.89	4.49	6.08	0.64	0.77
8	48.44	55.22	5.70	7.45	0.83	0.94	4.22	5.95	0.61	0.80
9	46.22	52.69	5.93	7.89	0.88	0.95	4.09	5.86	0.60	0.80
10	43.55	50.30	5.97	7.94	0.91	0.96	5.63	6.02	0.57	0.84

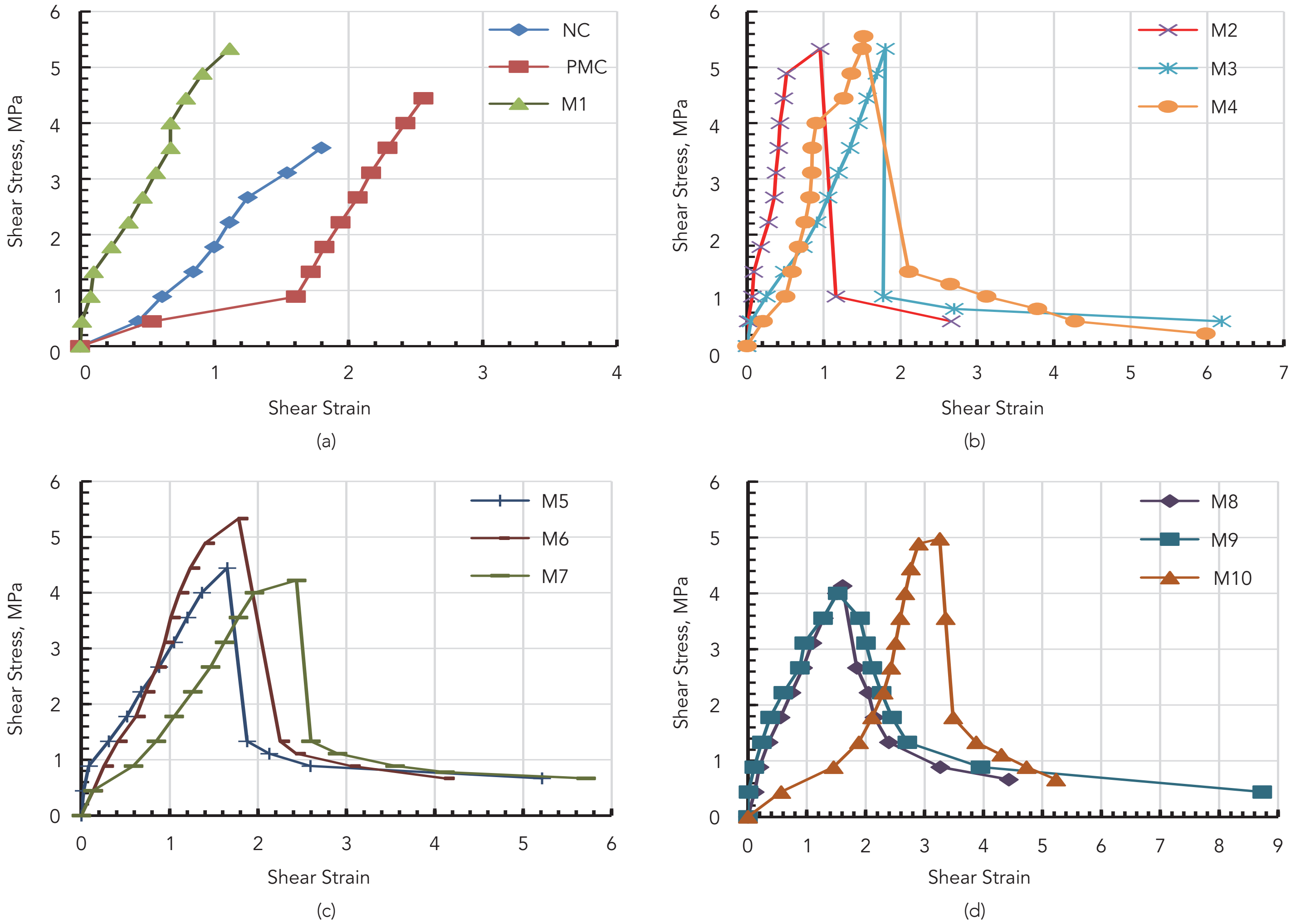

Figure 6: Variation of shear stress with shear strain (vertical slip, mm) at 28 days

The strain hardening within small range was observed in mixes M2, M4, M5, M6, M7, and M10 from first crack stress to peak stress. In post-peak range, softening of shear deformation is observed in all PMFRC specimens except M1 as seen from Figures 6(b)-(d). Sudden drop in shear stress from its peak value to a minimum shear stress of 1 MPa is observed due to loss of bond between fiber and matrix during fiber pull-out in all PMFRC specimens except M1 as seen from Figures 6(b)-(d).

The shear strength of concrete is expressed in terms of compressive strength with the help of correlation constant (k_s) at various fiber contents. The relation between correlation constant (k_s) and fiber content (V_f%) is presented in Figure 7. The empirical relations for shear strength in terms of fiber content and compressive strength are developed using regression analysis as follows.

$$\tau_s = (0.7 + 0.015V_f)\sqrt{f_{cu}}\,,\ R^2 = 0.4167 \text{ for 28 days } (0\% \le V_f \le 4\%) \tag{4(a)}$$

$$\tau_s = (0.9218 - 0.0368V_f)\sqrt{f_{cu}}\,,\ R^2 = 0.9527 \text{ for 28 days } (4\% < V_f \le 10\%) \tag{4(b)}$$

$$\tau_s = (0.7279 + 0.0279V_f)\sqrt{f_{cu}}\,,\ R^2 = 0.7792 \text{ for 90 days } (0\% \le V_f \le 6\%) \tag{4(c)}$$

$$\tau_s = (0.624 + 0.021V_f)\sqrt{f_{cu}}\,,\ R^2 = 0.8909 \text{ for 90 days } (7\% \le V_f \le 10\%) \tag{4(d)}$$

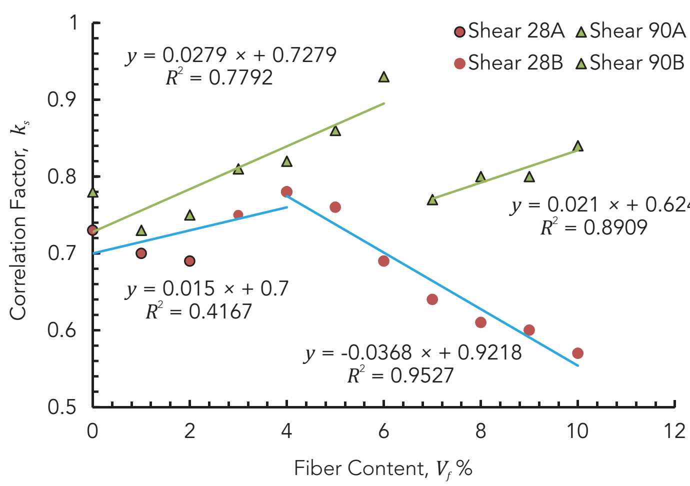

Figure 7: Variation of correlation factor with fiber content in shear

The regression analysis shows linear relationship with square root of compressive strength as given by equations 4(a), (b), (c), and (d).

3.4. Toughness

Toughness determined in terms of areas under the load-deformation and/or stress-strain curves is an indication of the energy absorption capability of the particular test specimen, and consequently, its magnitude depends directly on the geometrical characteristics of the test specimen and the loading system such as compression, flexure, and shear.

3.4.1 *Compressive toughness*

The compressive toughness is determined by calculating area under stress-strain curve in compression. Figures 3 are used to calculate this toughness at 28 days. Similar curves are used for 90 days toughness calculations. The results of the compressive toughness are presented in Table 3. The maximum value of compressive toughness is 1.60 kN mm and 1.64 kN mm for 8% fiber content at 28 days and 90 days, respectively. The improved toughness in compression, imparted by PMFRC, is useful in preventing sudden failure under static loading.

3.4.2 *Flexural toughness*

The flexural toughness is obtained by calculating area under load-deflection curve as shown in Figures 4. The results of the flexural toughness at 28 days are presented in Table 3. Flexural toughness increased continuously with increase in fiber content. The maximum value of flexural toughness is 36.83 kN mm and 37.48 kN mm for 10% fiber content at 28 days and 90 days, respectively. The substantial increase in flexural toughness values indicate the composite with plastic behavior after the post-peak crack due to increase in flexural deformation.

3.4.3 *Shear toughness*

The shear toughness in single shear is obtained by calculating area under shear load-shear deformation curve as shown in Figures 6. The results of the shear toughness at 28 days are presented in Table 3. Shear toughness increased continuously with increase in fiber contents. The maximum values of shear toughness are 11.39 kN mm and 12.34 kN mm for 10% and 9% fiber contents at 28 days and 90 days, respectively. The increase in shear toughness is due to increase in shear strain capacity of PMFRC specimens in post-peak range.

3.5 Number and Length of Fibers

Number and length of fibers are recorded with respect to fiber volume fraction on face of failed cross-section. The results of the number, average pull-out length, and critical length of fibers across the cross-section for beam under flexure and push-off specimen for single shear are presented in Table 4. The average effective length of fiber is calculated considering fibers on single cracked surface only. The critical length of fiber is found to be greater than the length of fiber which supports the assumption that the pull-out mostly occurs across a crack. The mean fiber pull-out length in flexural failure is 1.74 cm and in shear failure it is 1.91 cm, which is greater than 1.25 cm ($l_f/4$) to cause composite failure by fiber pull-out as given by Hannant [30].

Table 3: Toughnesses under compression, flexure, and shear of PMFRC

FIBER CONTENT (%)	COMPRESSIVE TOUGHNESS (kN mm)		FLEXURAL TOUGHNESS (kN mm)		SHEAR TOUGHNESS (kN mm)	
	28 DAYS	90 DAYS	28 DAYS	90 DAYS	28 DAYS	90 DAYS
0 (NC)	0.35	0.19	0.07	6.84	5.00	5.37
Mp (PMC)	0.92	0.47	0.08	7.56	4.07	4.21
1	0.36	0.57	7.48	10.51	5.11	5.21
2	0.56	0.57	8.16	9.93	5.38	5.50
3	0.98	1.01	17.09	20.44	6.58	7.14
4	0.65	0.69	9.94	17.90	6.90	8.67
5	1.51	1.56	14.89	24.38	9.54	10.76
6	0.97	1.03	17.93	18.55	10.86	11.91
7	1.31	1.36	15.88	17.19	9.31	9.47
8	**1.60**	**1.64**	19.50	22.18	8.27	8.19
9	0.67	0.69	26.06	26.31	10.30	**12.34**
10	0.98	1.10	**36.83**	**37.48**	**11.39**	9.96

Table 4. Number and average pull-out length of fibers on failure plane.

FIBER CONTENT V_f (%)	NO. OF FIBERS ON FAILURE PLANE		AVERAGE EFFECTIVE LENGTH OF FIBER (cm)		CRITICAL LENGTH OF FIBER $l_f \leq (l_c = 2\,l_e)$	
	FLEXURE BEAM	PUSH-OFF SHEAR	FLEXURE SPECI-MEN	SHEAR SPECI-MEN	FLEXURE SPECI-MEN	SHEAR SPECI-MEN
1	2	6	1.25	0.95	7.50	8.10
2	8	8	1.18	2.05	7.64	5.90
3	12	16	1.55	1.80	6.90	6.40
4	18	19	1.82	2.10	6.36	5.80
5	20	23	1.98	1.95	6.04	6.10
6	18	22	1.78	1.81	6.44	6.38
7	24	21	1.25	1.76	7.50	6.48
8	22	23	2.02	1.28	5.96	7.44
9	32	18	1.65	2.40	6.70	5.20
10	28	26	1.84	2.17	6.32	5.66

4. CONCLUSIONS

In this study, the combined effect of high fiber contents and constant dosage of polymer on properties of high strength concrete are investigated and discussed. The following conclusions are drawn from results and discussion:

1. Considerable increase in compressive strength is not achieved due to addition of steel fibers and polymer.
2. Significant increase in flexure and shear strength is achieved. It may be attributed to the increased fiber content and improved dispersion of fibers due to addition of polymer in the mix.
3. Significant improvement in compressive, flexural, and shear toughness is achieved due to synergistic effect of polymer and fibers in the concrete composites. The increase in the toughness values indicates the increase in the ductility of polymer-modified fiber-reinforced concrete.
4. Based on regression analysis, the equations for flexural and shear strengths are proposed in terms of compressive strength and fiber content.
5. All the specimens showed linear elastic behavior up to first crack and deformation softening in post-peak range under compression, flexure, and shear.
6. Stress-strain behavior of PMFRC under flexure and shear indicates strain hardening between first crack stress and peak crack stress.
7. The number and average pull-out length of fibers across the failure plane are obtained and critical length of fiber is calculated. The average pull-out length of fiber is found to be 25% of fiber length.

REFERENCES

[1] Ohama, Y. (1998). "Polymer-based admixtures", *Cement and Concrete Composites*, Vol. 20, No. 2, pp. 189-212.

[2] Ohama, Y. (2011). "Concrete-polymer composites – The past, present and future", *Key Engineering Materials*, Vol. 466, pp. 1-14.

[3] Kardon, J. B. (1997). "Polymer-modified concrete: Review", *Journal of Materials in Civil Engineering*, Vol. 9, No. 2, pp. 85-92.

[4] Beaudoin, J. J. (1990). "Handbook of fiber-reinforced concrete: Principles, properties, developments and applications", Noyes Publications, Park Ridge, NJ, USA.

[5] Li, G., Zhao, X., Rong, C., and Wang, Z. (2010). "Properties of polymer-modified steel fiber-reinforced cement concretes", *Construction and Building Materials*, Vol. 24, No. 7, pp. 1201-1206.

[6] Kalawane, U., Ghugal, Y., and Dahake, A. (2016a). "Shear strength of polymer-modified steel fiber-reinforced concrete", *The Indian Concrete Journal*, Vol. 90, pp. 54-63.

[7] Kalawane, U., Ghugal, Y., and Dahake, A. (2016b). "Toughness of polymer-modified steel fiber-reinforced concrete", *Open Journal of Civil Engineering*, Vol. 6, pp. 8-18.

[8] Lin, Y., Karadelis, J. N., and Xu, Y. (2013). "A new mix design method for steel fiber-reinforced, roller compacted and polymer-modified bonded concrete overlays", *Construction and Building Materials*, Vol. 48, pp. 333-341.

[9] Issa, M. A., Alhassan, M. A., and Shabila, H. (2008). "High-performance plain and fibrous latex-modified and microsilica concrete overlays", *Journal of Materials in Civil Engineering*, Vol. 20, No. 12, pp. 742-753.

[10] Chen, B. and Liu, J. (2007). "Mechanical properties of polymer-modified concretes containing expanded polystyrene beads", *Construction and Building Materials*, Vol. 21, No. 1, pp. 7-11.

[11] Wang, M., Wang, R., Yao, H., Farhan, S., Zheng, S., Wang, Z., Du, C., and Jiang, H. (2016). "Research on the mechanism of polymer latex modified cement", *Construction and Building Materials*, Vol. 111, pp. 710-718.

[12] Karadelis, J. N. and Lin, Y. (2015). "Flexural strengths and fiber efficiency of steel-fiber-reinforced, roller-compacted, polymer-modified concrete", *Construction and Building Materials*, Vol. 93, pp. 498-505.

[13] Xu, F., Zhou, M., Chen, J., and Ruan, S. (2014). "Mechanical performance evaluation of polyester fiber and SBR latex compound-modified cement concrete road overlay material", *Construction and Building Materials*, Vol. 63, pp. 142-149.

[14] Xu, F., Peng, C., Zhu, J., and Chen, J. (2016). "Design and evaluation of polyester fiber and SBR latex compound-modified perlite mortar with rubber powder", *Construction and Building Materials*, Vol. 127, pp. 751-761.

[15] Chakraborty, S., Kundu, S. P., Roy, A., Adhikari, B., and Majumder, S. B. (2013). "Polymer-modified jute fiber as reinforcing agent controlling the physical and mechanical characteristics of cement mortar", *Construction and Building Materials*, Vol. 49, pp. 214-222.

[16] Huang, B., Wu, H., Shu, X., and Burdette, E. G. (2010). "Laboratory evaluation of permeability and strength of polymer-modified pervious concrete", *Construction and Building Materials*, Vol. 24, No. 5, pp. 818-823.

[17] Ghugal, Y. (2016). "Performance of polymer-modified polypropylene fiber-reinforced concrete with low fiber volume fractions", *The Indian Concrete Journal*, Vol. 90, No. 3, pp. 44-52.

[18] Bijen, J. (1990). "Improved mechanical properties of glass fiber-reinforced cement by polymer modification", *Cement and Concrete Composites*, Vol. 12, No. 2, pp. 95-101.

[19] Meraj, T., Pandey, A. K., and Rao, B. K. (2014). "Flexural behavior of latex modified steel fiber-reinforced concrete", *Indian Journal of Engineering and Material Sciences,* Vol. 21, pp. 219-226.

[20] Bureau of Indian Standards. (2013). "IS 12269 (2013): Ordinary portland cement, 53 grade specifications", *BIS*, New Delhi, India.

[21] Bureau of Indian Standards. (1970). "IS 383 (1970): Specification for coarse and fine aggregates from natural sources for concrete", *BIS*, New Delhi, India.

[22] ASTM A820 / A820M. (2016). "Standard specification for steel fibers for fiber-reinforced concrete", ASTM International, West Conshohocken, PA, USA.

[23] Bureau of Indian Standards. (2009). "IS 10262 (2009) : Guidelines for concrete mix design proportioning", *BIS*, New Delhi, India.

[24] Bureau of Indian Standards. (1959). "IS 516 (1959): Method of tests for strength of concrete", *BIS*, New Delhi, India.

[25] Japan Society of Civil Engineers. (1999). "G553: Test method for shear strength of steel fiber-reinforced concrete. Standard specifications for concrete structures, test methods and specifications", *Japan Society of Civil Engineers*, Tokyo, Japan.

[26] Rao, G. A. and Rao, A. S. (2009). "Toughness indices of steel fiber-reinforced concrete under mode II loading", *Materials and Structures*, Vol. 42, No. 9, pp. 1173-1184.

[27] Khaloo, A. R. and Kim, N. (1997). "Influence of concrete and fiber characteristics on behavior of steel fiber-reinforced concrete under direct shear", *ACI Materials Journal*, Vol. 94, No. 6, pp. 592-601.

[28] Barr, B. (1987). "Compact shear test specimens for FRC materials", *Composites*, Vol. 18, No. 1, pp. 54-60.

[29] Tan, K. H. and Mansur, M. A. (1990). "Shear transfer in reinforced fiber concrete", *Journal of Materials in Civil Engineering*, Vol. 2, No. 4, pp. 202-214.

[30] Hannant, D. J. (1978). *Fiber cements and fiber concretes*, Wiley, Chichester; New York, USA.

NOMENCLATURE

A Loaded area of cube (mm^2) = (150 × 150) mm^2

A_s Shear plane area in direct shear (mm^2) = (150 × 150) mm^2

b Width of beam (mm)

d Depth of beam (mm)

f_{cr} Flexural strength (MPa)

f_{cu} Compressive strength (MPa)

k_{cr} Correlation constant between the flexural strength and compressive strength

k_s Correlation constant between the shear strength and compressive strength

L Span of the beam (mm)

P_c Failure load in compression (kN)

P_f Central load through two-point load system (kN)

P_s Failure load in direct shear (kN)

τ_s Shear strength of concrete in direct shear (MPa)

PRAPHULLA K. DESHPANDE holds an M.E. Degree from Shivaji University, Kolhapur. He is an Associate Professor in the Department of Applied Mechanics, Government College of Engineering, Karad, Maharashtra, and presently a research scholar at Structural Engineering Department, Veermata Jijabai Technological Institute, Mumbai, Maharashtra, India. His areas of research interest are: concrete technology, composite materials, concrete composites, and structural design. Email: pkdeshpande_p17@st.vjti.ac.in

KESHAV K. SANGLE holds a Ph.D. Degree from Indian Institute of Technology, Mumbai. He is a Professor in Structural Engineering Department, Veermata Jijabai Technological Institute, Mumbai, Maharashtra, India. He has research experience of 20 years and has published more than 52 research papers in international and national journals and conferences. His areas of research interest are: non-linear analysis, seismic and stability analysis, and progressive collapse of high rise structures. Email: kksangle@st.vjti.ac.in

YUWARAJ M. GHUGAL holds a Ph.D. Degree from Indian Institute of Technology, Mumbai. He is a Professor and Head of the Department of Applied Mechanics, Government College of Engineering, Karad, Maharashtra. He has research experience of 28 years and has published more than 173 research papers in international and national journals and conferences. His areas of research interest are: higher order theories of analysis of beams and plates, composite materials, and fiber-reinforced concrete.
Email: ymghugal@gmail.com

Cite this article: Deshpande, P. K., Sangle, K. K., Ghugal, Y. M. (2021). "Performance of polymer-modified fiber-reinforced high strength concrete", *The Indian Concrete Journal*, Vol. 95, No. 6, pp. 47-56.

ICJ THE INDIAN CONCRETE JOURNAL

www.icjonline.com

TAKE A CONCRETE DECISION. SUBSCRIBE TO ICJ TODAY.

Write to us at info@icjonline.com and order your copy now!

SUBSCRIPTION FORM [For Indian Nationals]

☐ Collector's Edition ☐ New subscriber ☐ Renewal *(Please tick one)*

Name: ______________________
(Please fill in block letters)

Address: ______________________

City: ______________________

State / Province: ______________________

Pin Code: ______________________
(PIN CODE IS COMPULSORY)

Date of birth: d d m m y y

Designation: ______________________
(Leave this blank if it is a residential address)

Company / Organisation: ______________________
(Leave this blank if it is a residential address)

Cell No.: ______________________
(MOBILE NUMBER IS COMPULSORY)

Email: ______________________
(EMAIL IS COMPULSORY)

Subscription Tariff, Rupees (Inclusive of Postage & Handling)	1 year
Collector's Edition	1000/-
Online E-Journal*	1200/-
Paper Edition	1800/-
Online E-Journal* & Paper Edition	2800/-

* In Online E-Journal, there will be no hard copy, subscribers can view the journal online at www.icjonline.com with username and password

Send this form or write to info@icjonline.com Website: www.icjonline.com

DETAILS OF OTHER PAYMENT OPTIONS AND GENERAL TERMS AND CONDITIONS

TERMS AND CONDITION:
1. Advance payment needed 2. We are currently only accepting online payments. Details for the transfer are given below:
Account Name - ACC LIMITED **Account Number** - 57500000308512 **Branch Address** - Fort, Mumbai **IFSC Code** - HDFC0000060
3. After completion of each transaction, kindly inform us of the amount, transaction date, senders name, and senders bank account number by email. 4. Payment once received will not be refunded or adjusted. 5. Please note that the subscription will be started / renewed from the next month of the receipt of the payment. We do not offer backdated subscriptions. 6. For any extra hard copy of the past 10 years, write to us for applicable charges, subject to availability, until stocks last. 7. ICJ is ordinarily posted to all subscribers by ordinary post on the 1st of every month from the Mumbai post office. If you do not receive your copy by the end of the month, you can email us for a free replacement copy in the next month. A free replacement copy will not be entertained thereafter. For example, a free replacement copy for the March 2019 issue will be entertained only in April 2019, neither earlier, nor later. A free replacement copy for the March 2019 issue will not be entertained after April 2019. 8. Only one replacement copy will be entertained per year (12 months). 9. ICJ is posted to all subscribers by ordinary post. If you want to opt for courier service / registered post parcel, kindly add Rs. 2400 per year to the final amount.

(Please note that we have no branches)

Postal Registration Number: THC/125/2018-2020 | RNI Number: 13986/57 | Total Pages: 58
Published and posted on 1st of every month. Posted at Patrika Channel Sorting Office, Mumbai 400 001